

Role of Fibrillation on Poisson's Ratio of Expanded Polytetrafluoroethylene (PTFE)

by

Dimitrios A. Vavlekas

BSc. National Technical University of Athens-Greece, (Chemical Engineering) 2003

MSc. Tulane University-USA, (Chemical & Biomolecular Engineering) 2008

MSc. (by Research) University of Birmingham-UK, (Biosciences) 2014

A THESIS SUBMITTED IN PARTIAL FULFILLMENT OF
THE REQUIREMENTS FOR THE DEGREE OF

DOCTOR OF PHILOSOPHY

in

The Faculty of Graduate and Postdoctoral Studies
(Chemical and Biological Engineering)

THE UNIVERSITY OF BRITISH COLUMBIA
(Vancouver)

July 2017

© Dimitrios A. Vavlekas, 2017

Abstract

The polytetrafluoroethylene (PTFE) paste extrusion was studied to elucidate the role of structure formation (fibrillation) on the Poisson's ratio of final products such as stents and other implants. In particular two types of PTFE have been studied in capillary extrusion using dies having different reduction ratios (RR) and die entrance angles. The extrudates collected at different processing conditions, were tested in uniaxial extension to assess their mechanical properties. The tensile modulus, yield stress and ultimate tensile strength of the obtained extrudates were found to be increasing functions of reduction ratio, although the opposite effect was found for the ultimate elongational strain. Moreover, a PTFE paste was extruded using a capillary rheometer at various temperatures through cylindrical dies of different reduction ratios (1-D structure samples). Uniaxial tensile experiments were performed on the collected extrudates using the SER at different temperatures and Hencky strain rates. A nonlinear viscoelastic model (Matsuoka) was used to model the transient tensile results. An empirical model was also developed to predict the tensile ultimate strength as a function of processing conditions such as temperature and die reduction ratio, as well as, the testing operating conditions i.e., temperature and Hencky strain rate. PTFE flat profiles were extruded using slit dies, which promoted orientation of fibrils in two directions (2-D structure samples). Uniaxial tensile experiments were performed on the collected extrudates using the SER at different temperatures and Hencky strain rates to determine mechanical properties. Poisson's ratio was determined using image analysis and the results were compared using data from the 1-D structure samples. Polarized Raman spectroscopy was used to gain additional information on the degree of fibril orientation at different locations along and across the width and length of the extrudates. Finally, a simple model was derived for the density change in tensile deformation by taking into the account the Poisson's ratio and the strain recovery. Results of the Raman spectra and the strain recovery coefficient from density changes, were found to be in agreement with the fibril structure/morphology obtained from SEM micrographs.

Lay Summary

In this PhD thesis the role of fibrillation on Poisson's ratio of PTFE was studied. For that reason a novel steady-state phenomenological tensile stress model was developed to predict the ultimate strength as a function of different processing and testing parameters. The transient tensile results were presented to be described by a theoretical model developed by Matsuoka, with resulting parameters similar to 1-D and 2-D samples tested in the direction that fibrils orient. The Poisson's ratio of the material was determined based on uniaxial extension studies. Moreover, it was found that the relative density of the PTFE extrudates decreases in uniaxial extension due to its compressibility in a controlled way, leading to the manufacture of a product with desired porosity. This relative density prediction again is of great interest since PTFE has been used for years in the production of filter membranes.

Preface

This thesis entitled "Role of Fibrillation on Poisson's ratio of expanded Polytetrafluoroethylene" presents the research the author performed during his PhD study under the supervision of Professor Savvas G. Hatzikiriakos. The following journal papers have been published from the research work presented in this dissertation.

Journal Papers

M. Ansari, D. Vavlekas, J.L. McCoy, S.G. Hatzikiriakos, "Paste Extrusion and Mechanical Properties of PTFE", *International Polymer Processing*, XXX, 603-614 (2015). (This paper is based on the data presented in Chapter 5 of this thesis).

D. Vavlekas, M. Ansari, H. Hao, F. Fremmy, J.L. McCoy, S.G. Hatzikiriakos, "Zero Poisson's Ratio PTFE in Uniaxial Extension", *Polymer Testing*, 55, 143-151, (2016). (This paper is based on the data presented in Chapter 7 of this thesis).

D. Vavlekas, L. Melo, M. Ansari, E. Grant, F. Fremy, J. L. McCoy, S. G. Hatzikiriakos, " Role of PTFE Paste Fibrillation on Poisson's ratio", *Polymer Testing*, 61, 65-73, (2017). (This paper is based on the data presented in Chapter 8 of this thesis).

Conference Presentations

D. Vavlekas, M. Ansari, F. Fremmy, M.K. Martin, S.G. Hatzikiriakos, "Tensile Yield Stress Modelling of PTFE paste extrudates: Effect of Processing Conditions", ANTEC 2016 proceeding and oral Presentation, Indianapolis, USA, May 2016.

Table Of Contents

Abstract.....	ii
Lay Summary	iii
Preface	iv
Table Of Contents.....	v
List Of Tables	viii
List Of Figures.....	x
List Of Symbols.....	xvii
List Of Abbreviations	xviii
Acknowledgments	xix
Dedications	xx
CHAPTER 1:Applications Of Polytetrafluoroethylene And Problem Definition	1
1.1 Chemistry And Properties	1
1.2 Applications Of PTFE	4
CHAPTER 2:PTFE Paste Extrusion And Poisson’s Ratio: Literature Review	8
2.1 Introduction	8
2.2 PTFE Paste Preforming And Extrusion.....	8
2.3 PTFE Paste Extrusion.....	11
2.4 Previously Proposed Mathematical Models For PTFE Extrusion-Constitutive Equations For Pressure Drop Prediction In Capillary Die	13
2.4.1 Snelling And Lontz Model	13
2.4.2 Ariawan Model.....	15
2.4.3 Anvari Model.....	15
2.5 Definition Of Poisson’s Ratio And Its Physical Significance	17
2.6 Mechanism For Expanded PTFE Negative Poisson’s Ratio	19
2.7 Tensile Properties Of PTFE And Modelling	22
CHAPTER 3:Scope Of The Work.....	24
3.1 Introduction	24
3.2 Thesis Objectives.....	24
3.3 Thesis Organization.....	25
CHAPTER 4:Materials And Experimental Equipment.....	27
4.1 Introduction	27
4.2 Materials	27
4.2.1 PTFE Fine Powder Resins.....	27
4.2.2 Lubricant (Isopar H).....	27
4.3 Methods And Experimental Equipment	28
4.3.1 Paste Preparation	28
4.3.2 Preforming Of Paste:	28

4.3.3	Capillary Extrusion.....	29
4.3.4	Mechanical Property Characterization Of Samples.....	31
4.3.4.1	Sentmanat Extensional Rheometer (SER).....	31
4.3.4.2	Compression And Tensile Testing (Com-Ten)	33
4.3.5	Determination Of Poisson's Ratio	34
4.3.6	Densitometer.....	35
4.3.7	Field Emission-Scanning Electron Microscopy	36
4.3.8	Raman spectroscopy	36
CHAPTER 5: Paste Extrusion and Mechanical Properties of PTFE.....		38
5.1	Introduction	38
5.2	Extrusion Process	39
5.3	Tensile Mechanical Properties	44
5.4	Densitometry	50
5.5	Summary.....	54
CHAPTER 6: ...Effect Of Extrusion Mode On PTFE Extrudates: Flow Rate Control Vs. Load Control.....		56
6.1	Introduction	56
6.2	Extrusion Under Flow Rate Control Mode.....	56
6.3	Extrusion Under Load Control (Pressure Drop) Mode	60
6.4	Summary.....	70
CHAPTER 7: Zero Poisson's Ratio PTFE In Uniaxial Extension.....		71
7.1	Introduction	71
7.2	Transient Tensile Stress.....	72
7.3	Ultimate Strength.....	76
7.4	Densitometry	81
7.5	SEM Micrographs	83
7.6	Summary.....	84
CHAPTER 8: Role Of PTFE Paste Fibrillation On Poisson's Ratio		86
8.1	Introduction	86
8.2	Effect Of Hencky Strain Rate And Testing Temperature (Tt) On Poisson's Ratio ...	87
8.3	Transient Tensile Stress.....	88
8.4	Raman spectroscopy Analysis.....	91
8.5	SEM Imaging.....	96
8.6	Densitometry	97
8.7	Summary.....	99
CHAPTER 9: . Conclusions, Contributions To Knowledge And Recommendations For Future Work.....		101
9.1	Conclusions	101
9.1	Contributions To Knowledge	103
9.1.1	Ultimate Strength As A Function Of Processing And Testing Conditions	103
9.1.2	Ultimate Strength Correlated With Poisson's Ratio For 1-D And 2-D Samples.....	104
9.1.3	Relative Density Of A Compressible Material In Uniaxial Extension.....	104

9.2 Recommendations For Future Work	104
Bibliography	106

List Of Tables

<i>Table 2.1: Changes in the lower limit of the integral of Eq.2.5, by two different researchers</i>	<i>16</i>
<i>Table 4.1: Physical properties of PTFE resins provided by Saint Gobain</i>	<i>27</i>
<i>Table 4.2: Physical properties of PTFE resins provided by DAIKIN.....</i>	<i>27</i>
<i>Table 4.3: Physical properties of Isopar H supplied by ExxonMobil</i>	<i>28</i>
<i>Table 4.4: Characteristics of capillary dies used in the study of process of PTFE paste extrusion (Objective 1).</i>	<i>30</i>
<i>Table 4.5: Extrusion & SER characteristics of the experimental study in Chapter 7.....</i>	<i>33</i>
<i>Table 4.6: Extrusion & SER characteristics of the experimental study in Chapter 7.....</i>	<i>33</i>
<i>Table 5.1: Radial flow model parameters (Equation 2.6).....</i>	<i>40</i>
<i>Table 6.1: Average diameter and specific gravity of wet extrudates produced from die with RR=56 under flow rate control (shear rate) mode.....</i>	<i>60</i>
<i>Table 6.2: Average diameter and specific gravity of dry extrudates produced from die with RR=56 under flow rate control (shear rate) mode.....</i>	<i>60</i>
<i>Table 6.3: Average diameter and specific gravity of wet extrudates produced from die with RR=56 under load control (Pressure).....</i>	<i>65</i>
<i>Table 6.4: Average diameter and specific gravity of dry extrudates produced from die with RR=56 under load control (Pressure).....</i>	<i>65</i>
<i>Table 6.5: Values of the flow curve for both modes of operation under different runs</i>	<i>66</i>
<i>Table 6.6: Values of the flow curve for both modes of operation under same runs.....</i>	<i>66</i>
<i>Table 6.7: Values of the flow curve for both modes of operation under same runs for HDPE</i>	<i>68</i>
<i>Table 6.8: Average diameter and specific gravity of wet extrudates for PTFE (F104 HMW H-PTFE) tested under different lube concentrations, dies with different RR values for both modes of operation</i>	<i>70</i>
<i>Table 6.9: Average diameter and specific gravity of dry extrudates PTFE (F104 HMW H-PTFE) tested under different lube concentrations, dies with different RR values for both modes of operation</i>	<i>70</i>

Table 7.1: List of fitting parameters of Eq. 2.8 at various temperatures.73

Table 7.2: List of fitting parameters of Eq.2.8 at different Hencky strain rates.75

Table 7.3: List of the values of parameters of Eq.7. 7.....79

Table 8.1: List of fitting parameters of Matsuoka Eq. (2.8) at various temperatures.....89

Table 8.2: List of fitting parameters of Eq. 2.8 at different Hencky strain rates90

Table 8.3: List of fitting parameters of Eq. 2.8 for samples with different fibrillation.....90

List Of Figures

<i>Figure 1.1: Chemical structure of Polytetrafluoroethylene (PTFE) (Wikol, et al. visited on 25/10/2014).....</i>	<i>1</i>
<i>Figure 1.2: Partial phase diagram of PTFE (Sperati, 1989).....</i>	<i>3</i>
<i>Figure 1.3: Schematic diagram of previously proposed mechanism of fibrillation, (a) Compacted powder is about to enter the conical zone of the die, (b) Particles are highly compressed within the conical part resulting in mechanical locking of crystallites and (c) Particles exiting the die where they return to their initial spherical shape, whereas the crystallites get unwound and create fibrils, which connect the particles. (Image reproduced from Ariawan 2001, PhD Thesis).....</i>	<i>5</i>
<i>Figure 2.1: Schematic representation of a capillary die.....</i>	<i>9</i>
<i>Figure 2.2: Typical SEM images of PTFE paste: (a) before extrusion, and (b) after extrusion using a capillary die. Images taken by Ardakani H.A. PhD Thesis (2014).....</i>	<i>10</i>
<i>Figure 2.3: Schematic picture of the paste extrusion (DuPont, 1994).....</i>	<i>12</i>
<i>Figure 2.4: Typical behavior of pressure transient during PTFE paste extrusion (Ariawan, PhD Thesis, 2001)</i>	<i>13</i>
<i>Figure 2.5: (a) Schematic of a tapered orifice die showing the various characteristic dimensions and (b) schematic of a tapered die that includes a certain length of die land L..</i>	<i>14</i>
<i>Figure 2.6: Schematic representation of the difference between the two mathematical models proposed by Ariawan et al.2001 and Anvari et al.2013</i>	<i>16</i>
<i>Figure 2.7: Schematic representation of behaviour of a material possessing a) a positive Poisson's ratio and b) negative Poisson's ratio.....</i>	<i>17</i>
<i>Figure 2.8: Numerical region of Poisson's ratio for a range of isotropic materials. For gases $\nu=0$, metals, polymers and ceramics, lies between the area (0.25, 0.35), while materials in which stress can cause a shape change (weakly compressible materials, liquids, rubbers), ν approaches $\frac{1}{2}$ (Image reproduced by Greaves, et al. 2011).</i>	<i>18</i>
<i>Figure 2.9: a) Conventional hexagonal honey-comb system, which gives a positive Poisson's ratio, b) System with a negative Poisson's ratio (Lakes, 2001)</i>	<i>19</i>
<i>Figure 2.10: Microstructural changes of ePTFE under tensile loading: a)Initial packed microstructure b) lateral expansion of nodes and fibrils, c) Further lateral expansion causing rotation of nodes,d) final fully expanded condition.Image taken by Caddock & Evans, 1989).....</i>	<i>20</i>
<i>Figure 2.11: Poisson's ratio and young modulus plotted against the engineering strain shows three different areas of the material behaviour (Caddock & Evans, 1989).....</i>	<i>21</i>

Figure 2.12: Examples of ePTFE a) partial uniaxial ,b)partial biaxial ,c) complete biaxial drawings, d)SEM image of ePTFE showing nodal particles interconnected with fibres, proving the biaxial drawing suggested earlier.According to the same hypothesis, at high elongations the material fully expands and the parallel lying fibres are undergoing a micro-rotation in the x-direction, during various stages of tensile deformation. Interestingly, no broken fibrils were detected and they were considered to act like elastic springs.All experiments were conducted at room temperature (Caddock & Evans, 1989).21

Figure 2.13: Typical tensile graph of PTFE sample. The diameter of the sample (0.76 mm) remains unchanged during uniaxial extension for all cases as seen by the images \blacklozenge) $\epsilon_E=0$ \blacksquare) $\epsilon_E=0.5$ \blacktriangledown) $\epsilon_E=5.0$ \bullet) $\epsilon_E=12.5$, leading to a Poisson's ratio of the sample very close to zero.22

Figure 4.1: Two different dies which were used for the study of mechanical properties of the extrudates. Left die (a) is the cylindrical one, while on the right (b) the slit die can be seen. In both dies the fibrils were oriented in one dimension (1-D), due to the nature of the flow.....29

Figure 4.2: a) Schematic of flat die used, b) schematic of the flat extrudates produced and c) preparation of the sample pieces for uniaxial extension testing and Raman spectroscopy....31

Figure 4.3: Schematic representation of SER fixture.....32

Figure 4.4: Test system overview of the Com-Ten fixture.....34

Figure 4.5: a) Schematic of a cylindrical (1-D) sample extended in the longitudinal direction and the change in the width of the sample presented and b) schematic of a flat extrudate (2-D), where all the dimensions of interest are shown, for evaluating the Poisson's ratio.....34

Figure 4.6: Schematic of the experimental setup of Raman spectroscopy (Christy, et al. 2015)37

Figure 5.1: Effect of reservoir/die reduction ratio on transient extrusion pressure drop for the paste of C-PTFE+18 wt. % Isopar-H at room temperature41

Figure 5.2: Effect of reservoir/die reduction ratio on steady state extrusion pressure drop for the paste of C-PTFE+18 wt. % Isopar-H at room temperature.....42

Figure 5.3: The effect of die contraction angle on the steady state extrusion pressure for the paste of C-PTFE+18 wt. % Isopar-H at room temperature42

Figure 5.4: The effect of type of PTFE resin on the steady state extrusion pressure for the paste of PTFE+18 wt. % Isopar-H at room temperature.....43

Figure 5.5: The effect of processing temperature on the steady state extrusion pressure drop for the paste of H-PTFE+18 wt. % Isopar-H.....44

<i>Figure 5.6: The definition of 5 extrusion zones for a typical transient pressure extrusion curve</i>	45
<i>Figure 5.7: Typical tensile experiment (stress-strain curve) to illustrate the definition of four mechanical properties considered in this study</i>	45
<i>Figure 5.8: The effect of the reduction ratio and extrusion zone on (a) elastic modulus, (b) yield stress @ 1% offset, (c) ultimate tensile strength and (d) ultimate elongational strain for C-PTFE+18 wt. % Isopar-H extrudates</i>	46
<i>Figure 5.9: The effect of apparent shear rate on (a) elastic modulus, (b) yield stress @ 1% offset, (c) ultimate tensile strength and (d) ultimate elongational strain for C-PTFE+18 wt.% Isopar-H extrudates for dies with reduction ratios of 56 and 351</i>	47
<i>Figure 5.10: The effect of PTFE resin type on (a) elastic modulus, (b) yield stress @ 1% offset, (c) ultimate tensile strength and (d) ultimate elongational strain for dies different reduction ratio</i>	48
<i>Figure 5.11: Effect of contraction angle on (a) elastic modulus, (b) yield stress @ 1% offset, (c) ultimate tensile strength and (d) ultimate elongational strain for C-PTFE+18 wt. % Isopar-H extrudates</i>	49
<i>Figure 5.12: The effect of extensional strain on the specific gravity of the PTFE extrudates</i>	51
<i>Figure 5.13: SEM micrographs of H-PTFE extrudates processed from die with RR=56 at extensional strain levels of (a) 0, (b) 23.8%, (c) 142%, (d) 237% & (e) 300%. The samples were extruded and extended in the horizontal direction</i>	52
<i>Figure 5.14: The recovered strain versus time for different extensional strains for C-PTFE+18 wt. % Isopar-H extruded from die with reduction ratio of 56</i>	53
<i>Figure 5.15: The strain recovery coefficient κ as a function of reduction ratio for C-PTFE+18 wt. % Isopar-H extrudates</i>	54
<i>Figure 6.1: Average diameter of wet and dry extrudates produced at a capillary extrusion of PTFE paste (F104 HMW H-PTFE) at the shear rate of 74 s^{-1}</i>	57
<i>Figure 6.2: Average specific gravity of wet and dry extrudates produced at a capillary extrusion of PTFE paste (F104 HMW H-PTFE) at the shear rate of 74 s^{-1}</i>	58
<i>Figure 6.3: Average diameter and specific gravity of dry extrudates produced at a capillary extrusion of PTFE paste (F104 HMW H-PTFE) at the shear rate of 74 s^{-1}</i>	59
<i>Figure 6.4: Average diameter of wet and dry extrudates produced at a capillary extrusion of PTFE paste (F104 HMW H-PTFE) at the shear rate of 1109 s^{-1}</i>	59

<i>Figure 6.5: Average specific gravity of wet and dry extrudates produced at a capillary extrusion of PTFE paste (F104 HMW H-PTFE) at the shear rate of 1109 s^{-1}.....</i>	<i>60</i>
<i>Figure 6.6: Average diameter of wet and dry extrudates produced under load control mode (11.1 MPa).....</i>	<i>61</i>
<i>Figure 6.7: Average specific gravity of wet and dry extrudates produced under load control mode (11.1 MPa).....</i>	<i>62</i>
<i>Figure 6.8: Average diameter and specific gravity of dry extrudates produced under load control mode (11.1 MPa)</i>	<i>62</i>
<i>Figure 6.9: Average diameter of wet and dry extrudates produced under load control mode (18.6MPa).....</i>	<i>63</i>
<i>Figure 6.10: Average specific gravity of wet and dry extrudates produced under load control mode (18.6 MPa).....</i>	<i>64</i>
<i>Figure 6.11: Average diameter and specific gravity of dry extrudates produced under load control mode (18.6 MPa)</i>	<i>64</i>
<i>Figure 6.12: Flow curve of PTFE (F104 HMW H-PTFE) paste obtained for both modes of operation using a die having $RR=56$.....</i>	<i>66</i>
<i>Figure 6.13: Both modes of operation during the same experimental run. The run started with constant flow rate control (221s^{-1}) and switched to constant load control (pressure drop of 12.5 MPa) once steady state was reached.....</i>	<i>67</i>
<i>Figure 6.14: Both modes of operation during the same experimental run. The run started with constant flow rate control (1109s^{-1}) and switched to constant load control (pressure drop of 15.95 MPa) once steady state was reached.....</i>	<i>67</i>
<i>Figure 6.15: Flow curve of HDPE (BCT132714) obtained for both modes of operation using a die having $RR=156$.....</i>	<i>68</i>
<i>Figure 6.16: Flow curve of PTFE (F104 HMW H-PTFE) paste obtained for both modes of operation using a die having $RR=156$.....</i>	<i>69</i>
<i>Figure 6.17: Flow curve of PTFE (F104 HMW H-PTFE) paste obtained for both modes of operation using a die having $RR=56$ and decreased lube concentration (15.25 wt. %).</i>	<i>69</i>
<i>Figure 7.1: Tensile results at $\dot{\epsilon}_H=0.6\text{ s}^{-1}$ at four different temperatures for PTFE samples extruded at $T_p=25^\circ\text{C}$ through a capillary die with reduction ratio of 156. The dash-lines are best fitting of Eq. 2.8 (Matsuoka Eq.).....</i>	<i>73</i>

Figure 7.2: Elastic Modulus E_0 versus testing temperature, T_t , for PTFE samples extruded at $T_p=25^\circ\text{C}$ through a capillary die with reduction ratio of 156. The slope results in an activation energy of 11.7 kJ/mol..... 74

Figure 7.3: Tensile results at four different Hencky strain rates tested at $T_t=50^\circ\text{C}$ for PTFE samples extruded at $T_p=25^\circ\text{C}$ through a capillary die with reduction ratio of 156. The dash-lines are best fitting of Eq. 2.8..... 75

Figure 7.4: Ultimate strength as a function of Hencky strain rate at four different tensile temperatures for PTFE samples extruded at $T_p=50^\circ\text{C}$ through a die with reduction ratio of 156. 76

Figure 7.5: $\sigma_u - \dot{\epsilon}_H$ power-law prefactor (K_σ) as a function of tensile temperature for PTFE samples extruded at different extrusion temperatures through dies with various reduction ratios. The dash-lines are the fitting of Arrhenius equation with a constant slope..... 77

Figure 7.6: $K_\sigma - T_t$ Arrhenius prefactor ($K_{\sigma,t}$) as a function of processing temperature for PTFE samples extruded through dies with various reduction ratios. The dash-lines are the fitting of Arrhenius equations. 78

Figure 7.7: $K_{\sigma,t} - T_p$ Arrhenius (a) activation energy (E_p) and (b) prefactor ($K_{\sigma,p}$) as a function of die reduction ratio. The dash-lines are the fittings of the specified equations in each figure. 80

Figure 7.8: The predictions of Eq. 7.7 for ultimate strength as a function of Hencky strain rate as dash-lines for (a) different die reduction ratio at T_t and $T_p=50^\circ\text{C}$, (b) different tensile temperatures for $RR=56$ and $T_p=150^\circ\text{C}$, (c) different processing temperatures for $RR=156$ and $T_t=100^\circ\text{C}$ and (d) different tensile temperatures for $RR=100$ and $T_p=50^\circ\text{C}$ 80

Figure 7.9: The relative density as a function of Hencky strain for extrudates collected at processing temperatures of 25°C (closed symbols) and 50°C (open symbols) extruded through dies with a) $RR=56$, b) $RR=100$ and c) $R=156$. The dash lines are the fitting of Eq.7.8. 82

Figure 7.10: The strain recovery coefficient as a function of reduction ratio. The closed symbols are collected from our previous study (Ansari, et al.2015)..... 83

Figure 7.11: SEM micrographs for PTFE extrudates illustrating their differences in fibrillated structure. Images (a) & (b) show the differences in fibrils when using dies with different RR (the larger the RR the more the fibrils), and (c) & (d) show the difference in fibrils when extruding at different extrusion temperature. The higher the extrusion temperature the higher the fibrillation. The arrows represent the extrusion direction 84

Figure 8.1: Typical graph that shows the change of the width of the sample during uniaxial extension as a function of Hencky strain and the corresponding Poisson's ratio values 87

Figure 8.2: Poisson's ratio values in a) width and b) thickness directions of PTFE 2-D extrudates at three different Hencky strain rates and three different testing temperatures....88

Figure 8.3: Tensile results at $\epsilon_H = 0.6 \text{ s}^{-1}$ at four different temperatures for PTFE samples extruded at $T_p = 25^\circ\text{C}$ through a specially designed die. The dash lines are best fitting of Eq. 2.8.....89

Figure 8.4: Tensile results at three different Hencky strain rates tested at $T_t = 25^\circ\text{C}$ for PTFE samples extruded at $T_p = 25^\circ\text{C}$ through the 2-D die. The dash-lines are best fitting of Eq. 2.8.....90

Figure 8.5: Typical PTFE Raman Spectrum. Prominent vibrational modes of interest range from $700 - 1500 \text{ cm}^{-1}$, with the C-C symmetrical stretch at 1407 cm^{-1} being of primary interest92

Figure 8.6: Typical depolarized PTFE Raman spectra for a) cylindrical 1-D sample and b) flat 1-D sample extruded from a slit die. The shape of the dies and the corresponding extrudates can be seen in each image93

Figure 8.7: PTFE sample cut from the extrudate perpendicular to machine direction (as depicted in Fig 1c), prior to Raman examination on five different spots. X is the transverse direction, Y is the machine (extrusion) direction, and Z is the extrudate's thickness axis. Fibrils are primarily oriented in the transverse direction (along the X-axis) with some oriented in the machine direction (along the Y-axis). Dots in the XZ and YZ planes represent the fibril ends oriented normal to their respective surface.....93

Figure 8.8: Depolarized PTFE Raman spectrum for point (a) on the extrudate.....95

Figure 8.9: Preferred orientation of the extrudates according to depolarized Raman spectroscopy95

Figure 8.10: a) Raman relative intensity changes for two different levels of strains for the points (β) shown as circles and (ϵ) shown as squares on the 2-D extrudate. Hollow symbols show intensity changes when the laser beam is parallel to fibrillation, while closed symbols for perpendicular to fibrillation b) Typical stress- strain curve justifying the choice of the strains 0.7 and 1.5 correspondingly.....96

Figure 8.11: SEM micrograph for point beta (β) showing that most of the fibrillation occurs perpendicular to the extrusion direction97

Figure 8.12: The relative density as a function of Hencky strain for extrudates collected at $T_p=25^\circ\text{C}$. The samples were extruded at identical RR dies and a) shows 1-D structure cylindrical sample, while b) shows 2-D structure sample. The fitting of Eq.8.3 is shown as dashed lines98

Figure 8.13: Results for cylindrical 1-D structure samples: a) Tensile results at $\dot{\epsilon}_H = 0.3 \text{ s}^{-1}$ and $T_t = 50 \text{ }^\circ\text{C}$ for PTFE samples extruded at $T_p = 100 \text{ }^\circ\text{C}$, through dies with different RR values and b) Overall trend of the ultimate strain versus RR100

List of Symbols

Δl	Extrudate length change (mm)	$\dot{\gamma}_A$	Apparent shear rate (1/s)
l_r	Extrudate lengths after removing tensile stress (mm)	γ_0	Initial specific gravity
r_a	Die radius (mm)	γ	Specific gravity
r_b	Reservoir radius (mm)	σ	Total stress (MPa)
ΔP	Extrusion pressure (MPa)	γ_{\max}	Maximum strain
C'	Elastic proportionality constant (kPa)	$\dot{\gamma}_{\max}$	Maximum strain rate (1/s)
D_b	Reservoir diameter (cm)	RR	Reduction ratio
D	Die diameter (mm)	Q	Volumetric flow rate (in ³ /min)
E	Young's modulus (MPa)	ϵ_u	Ultimate elongation
f	Friction coefficient	σ_u	Ultimate tensile strength (MPa)
K	Viscous proportionality constant (kPa s ^m)	σ_y	Yield stress @ %1 strain offset (MPa)
L	Die length (mm)	2α	Die entrance angle (°)
l_0	Extrudate initial length (mm)	n	Elastic power-law index
m	Viscous power-law index	R	Ideal gas universal constant (kJ/mol K)
C	Yielding coefficient in Matsuoka Eq.	ϵ_E	Engineering strain
E_0	Elastic modulus in Matsuoka Eq.(MPa)	$\dot{\epsilon}_E$	Engineering strain rate (1/s)
E_t	Arrhenius activation energy (kJ/mol)	ϵ_H	Hencky strain
T_t	Tensile temperature (°C)	$\dot{\epsilon}_H$	Hencky strain rate (1/s)
$T_{t,ref}$	Tensile reference temperature (°C)	ϵ_r	Recovered strain
RD	Relative density	κ	Strain recovery coefficient
RD_0	Initial relative density	λ	Relaxation time in Matsuoka Eq.(s)
T_p	Processing (Extrusion) temperature (°C)	σ_E	Engineering stress (MPa)
n	Relaxation exponent in Matsuoka Eq.	ν	Poisson's ratio

List of Abbreviations

PTFE	Polytetrafluoroethylene
H-PTFE	Homopolymer PTFE
C-PTFE	Copolymer PTFE
ePTFE	Expanded PTFE
NPR	Negative Poisson's Ratio
ZPR	Zero Poisson's Ratio
RR	Reduction Ratio
SER	Sentmanat Extensional Rheometer
SEM	Scanning Electron Microscopy
HeNe	Helium-Neon
LPF	Long-pass filter
ROI	Region of interest
DWT	Discrete wavelet transform
Com-Ten	Compression -Tensile
iSCAT	Interferometric Scattering Microscopy
DFT	Density functional theory

Acknowledgments

Completing a thesis is a challenge and thanking all those who contributed to it is an even greater one. Due to the nature of my study, many people were involved in it, in one or another way, thus, I would like here to express my warmest thanks to all of them.

My sincere gratitude belongs to my supervisor Professor Savvas G. Hatzikiriakos for offering guidance to my studies throughout these years to achieve the best possible result. Special thanks are also owed to the post-doctoral fellow Dr. Mahmoud Ansari for the valuable discussions and suggestions.

Many thanks must also go out to all the members of my committee Professors Dana Grecov, James Feng, Dr. Mahmoud Ansari and the Chair of my committee Bhushan Gopaluni. Thanks I must also address to the rest of my colleagues of Prof. Hatzikiriakos's group, all the PhD students Marzieh, Vinod, Salma, Tanja, Vasili, Tannaz for their friendly environment and collaboration throughout these years within and outside the University, as well as colleagues and students who contributed to the success of this project (Thanasi, Yann, Han, Dr. Liu). Members from the Saint Gobain in Boston Drs. Mike Martin, Jessica L. McCoy, Julia DiCorleto, Flavien Fremmy and from the UBC Chemistry department Professor Edward Grant and his student Luke Melo.

But my greatest debt has been to my family, my parents Apostolos and Joanna Vavleka and my siblings, sister Georgia and brothers Nikolaos and Stavros, who supported me mostly emotionally in all my efforts throughout these years until my last academic step, to fulfill my PhD at an esteemed University in Canada, The University of British Columbia.

Vancouver, July 2017

Dimitrios A.Vavlekas

Dedications

To my Parents...

CHAPTER 1: Applications Of Polytetrafluoroethylene And Problem Definition

1.1 Chemistry And Properties

The discovery of the polymerization of tetrafluoroethylene by DuPont's Roy Plunkett in 1938, was followed by a wide range of applications for this material, once its physical and chemical properties were disclosed. Polytetrafluoroethylene (PTFE), is composed of only carbon and fluorine elements, in which a long straight carbon backbone is surrounded by the fluorine atoms as seen by Fig. 1.1.

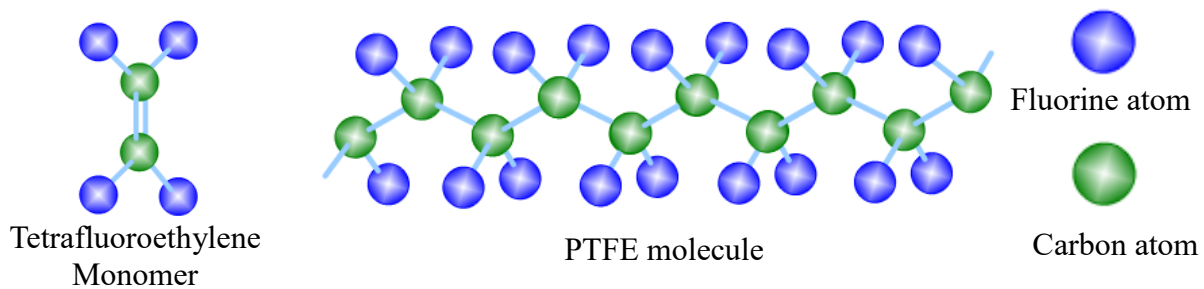


Figure 1.1: Chemical structure of Polytetrafluoroethylene (PTFE) (www.subtech.com visited on 25/10/2014).

The distribution of fluorine atoms is even, which makes them nonpolar and nonreactive. The bonds between carbon-carbon and carbon-fluorine are both very strong (Cotrell, 1958; Sheppard & Shards, 1969). This latter, along with the protective cover and the nonpolarity of the material, makes PTFE a material of good thermal stability and compatibility with many corrosive processing fluids used in the industries (concentrated acids, bases, solvents). Moreover, it is not affected by UV-radiation, it is biocompatible and has a very low coefficient of friction (Clough N.E. visited on 30/09/2014).

From the periodic table, fluorine is the most electronegative element, meaning that it doesn't share electrons with the neighboring fluorine atoms, resulting in a low surface free energy for PTFE. That property explains the low wettability of PTFE. Because of this chemical structure, PTFE appears to have not only a range of good chemical properties (e.g. chemical resistance to corrosive reagents, insolubility, long-term weatherability, non-adhesiveness and inflammability), but also good electrical (e.g. low dielectric constant, high surface resistivity and high volume resistivity) and mechanical properties as well, such as flexibility at low temperatures, low friction coefficient and stability at high temperatures (DuPont visited on

30/12/ 2014). Along with all its other properties, it has become the ideal polymer for applications such as in the pharmaceutical field, membrane technology, wire and cable industries and many others.

First time melting takes place at 342°C, whereas thereafter at 327 °C (Sperati, 1989) meaning that cooling does not re-crystallize the molecule chains back to the original configuration. PTFE melt viscosity is relatively high and stable, even at 380°C, at approximately 10 GPa·s. Due to its high melt viscosity and melting temperature, it is not possible to process PTFE resin using the traditional polymer processing methods (Gangal & Kroschwitz, 1994; Gangal, *et al.* 1989; Ebnesajjad, 2000; Li, *et al.* 2012). Instead, paste extrusion and cold pressing techniques are being used, since it is almost impossible to melt process that material.

Apart from the melting temperature, PTFE appears to have two more particularly important temperatures known in the literature as transition temperatures, which can be seen in the phase diagram of Fig. 1.2 (Sperati, 1989). The first one is at 19°C at which the PTFE molecular chain segments, change from a three dimensional order to a less ordered structure, by undergoing a slight untwisting from 180° twist per 13 CF₂ groups to 180° twist per 15 CF₂ groups (particles become more flexible). That chain change causes a volume increase in the material of about 1.3%. The second transition appears to be at 30°C (Rae & Dattelbaum, 2004), at which the number of CF₂ per 180° twist remains the same at 15, whereas the degree of disorder of the rotational orientation of molecules around their long axis increases. For increasing the temperature from below 19°C to above 30°C the total volume increase is 1.8% (Blanchet, 1997; Clark, 1962).

Shearing of the particles below 19°C will cause the particles to slide past each other retaining their identity as they are nearly undeformable. However, above 19°C, shearing of the particles will cause the unwinding of crystallites, which will appear as fibrils interconnecting the neighboring particles altogether (fibrillation). Therefore, for successful paste extrusion the temperature has to be at least above 19°C, while above the second transition temperature (30°C) the degree of fibrillation increases leading to products of higher dimensional stability (Ardakani, PhD Thesis, 2014; Ariawan, PhD Thesis, 2001; Ochoa, PhD Thesis, 2006).

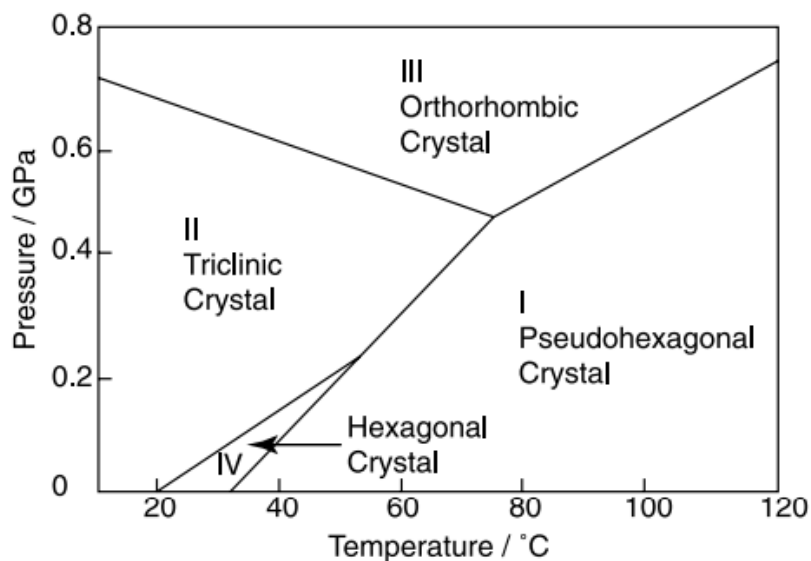


Figure 1.2: Partial phase diagram of PTFE (Sperati, 1989)

Nowadays PTFE is manufactured and sold in three forms: as an aqueous dispersion, fine powder or granular (Chandler-Temple, 2008). PTFE is formed as an aqueous dispersion of particles (with size range 0.2-0.3 μm), involving either one of two procedures mentioned below, by an addition reaction and the final polymer has a very high molecular weight $3 \cdot 10^6$ g/mol (O’Leary & Geil, 1967). Both techniques have been described in detail by (Ariawan, PhD Thesis, 2001; Ochoa, PhD Thesis, 2006). The first procedure, known as *suspension polymerization*, is the route to produce a dried polymer, known as granular resin and it is processed as molding powder. The second technique is known as *emulsion* or *dispersion* polymerization, through which dispersion and fine powder PTFE products are manufactured. The obtained powder is susceptible to mechanical damage and therefore shearing of the particles is avoided during transportation, handling and storage (by keeping it in low temperatures), which would create premature coagulation (Gangal & Kroschwitz, 1994).

This work focuses on the powder resin, which is typically processed through paste extrusion. The resin initially is mixed with a lubricant (ideally a hydrocarbon of low surface tension below 18 mN/m- Gangal & Kroschwitz, 1994) at a specific concentration, which may vary from 16-25 wt.% (Daikin Technical Bulletin, 2003; Ebnesajjad, 2000). The powder-lubricant mixture is known as paste and is mixed in a shear-free mixing environment, by simply rotating the container at a temperature below the first transition temperature of the

polymer (19 C°), to avoid premature coagulation through fibrillation as explained above. The main role of the lubricant is to eliminate the mechanical damage, which might occur to the particles during the extrusion process (Mazur, 2005). The paste is then left to age within a fridge overnight, to ensure complete wetting of the particles, prior to the extrusion process. The extrusion takes place using dies of different geometrical characteristics (depending on the desired shape of the final product) and different temperatures and the final product known as extrudate is placed in the oven for ease removal of the lubricant (low boiling point), overnight.

The rheology of the material for pastes like the PTFE paste constantly changes as it flows through contractions, while the structure of PTFE is irreversible. Paste starts as a two-phase fluid-like system (liquid along with PTFE solid fine particles) and it ends in a fibrillated solid-like phase. This complicates the physical understanding of the paste extrusion (Patil, *et al.* 2006).

During the extrusion process, as the resin particles enter the die zone, they get highly compressed (Fig. 1.3 a). Upon entering the conical part of the die, the particles squeeze and rub against each other, under the application of high pressure due to the reduction of the flow cross-sectional area in the direction of flow. Due to the neighboring shearing of the particles the PTFE crystallites begin to mechanically interlock, which results into the interconnection of adjacent particles (Fig. 1.3b). As the particles flow towards the exit of the die, they experience an elongational (accelerated) flow, during which the mechanically locked crystallites are unwound, creating fibrils (Fig. 1.3c) (Ariawan, *et al.* 2002a; Ariawan, *et al.* 2002b).

1.2 Applications Of PTFE

Initially PTFE was used in small quantities for products such as sheets, tapes gaskets, electrical insulators. Very quickly its usefulness was acknowledged and a production in large scale has started in aerospace technologies and nuclear power industries telecommunication and electronics, chemical processes, automotive products, non-stick cookware (Clough N.E. visited on 30/09/2014). A key process discovered by Wilbert and Robert Gore transformed this versatile material into an expanded version known as ePTFE. Its use today in many *in vivo* dental and biomedical applications is vast, such as: vascular grafts, surgical sutures, cardiovascular and soft tissue patches, endovascular prostheses, facial (chin, cheek, lips,

nasolabial furrows, glabellar creases) and orthopaedic joint implants, knee pads and vocal cord defects (Chandler-Temple, 2008; Lakes, 2001; DermNet NZ visited on 13/06/2014).

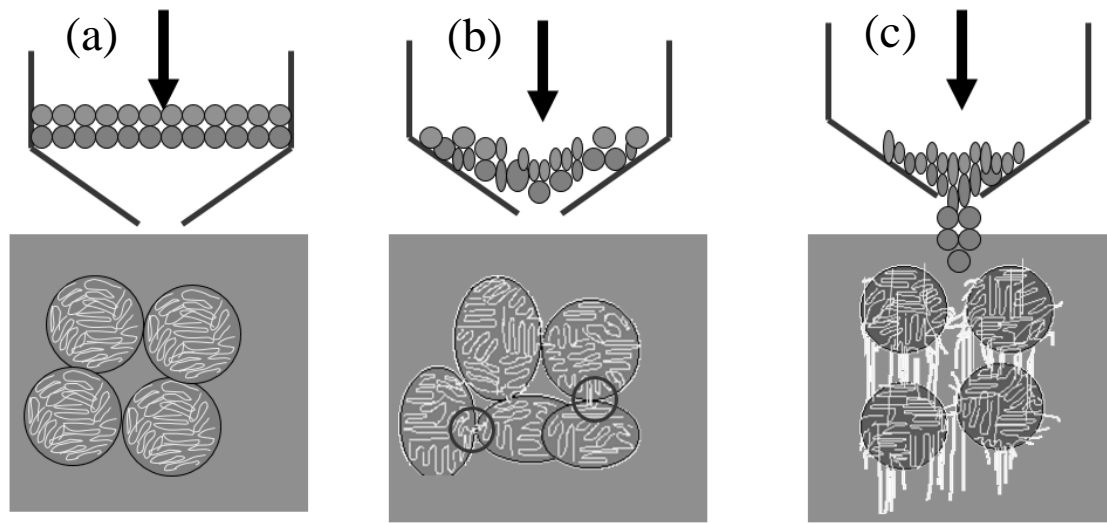


Figure 1.3: Schematic diagram of previously proposed mechanism of fibrillation, (a) Compacted powder is about to enter the conical zone of the die, (b) Particles are highly compressed within the conical part resulting in mechanical locking of crystallites and (c) Particles exiting the die where they return to their initial spherical shape, whereas the crystallites get unwound and create fibrils, which connect the particles. (Image reproduced from Ariawan 2001, PhD Thesis).

Another important application of PTFE can be found in clothing. According to literature, clothing should support both elastic recovery and thermoregulation procedures of the human body. The thermoregulation equilibrium should be maintained in the human body as it is considered to be one of the most important mechanisms of the human skin, (also known as the "cooling effect"), produced by the evaporation of sweat. Moisture when remains under clothing is an unpleasant feeling and may also lead to unhealthy conditions. Moreover, elastic recovery plays another role since its reduction may lead to less conformable outfits. For that reason microporous PTFE membrane can be used for clothing and shoes, which can transfer sweat from inside to outside and is water vapour permeable (Huang, *et al.* 2004).

The expanded version of this polymer, was discovered in 1969. This means that fast stretching techniques at high temperatures can be applied to extruded sheets of PTFE to expand its volume and increase its porosity in a controlled manner. The material can be stretched biaxially into various extension rates achieving different amount of porosities each time, desired in various applications. The stretching of PTFE is made above its lowest crystalline melting point, which causes an increase in disorder and in the amorphous content of the

material. That was characterised as a "locking step" for the fibrils and crystallites, in which both the creep resistance and the material's strength was improved (US PATENTS: 3.953.566-3.962.153).

In 1995 various ePTFE structures were tested for their elastic properties as artificial arterial prostheses materials. It was shown overall highly strain dependent properties and for the case of ePTFE, it was found to have negative Poisson's ratio values as low as -14 at certain strains and temperatures (Caddock & Evans, 1995).

Since the discovery of the expanded material, ePTFE found additional numerous applications. As a membrane it could separate wetting and not wetting liquids, solids from corrosive liquids and vice versa, seat cushions or air filters, which can be easily tuned or cleaned (Chandler-Temple, 2008; Lakes, 2001). It demonstrated improved water resistance and due to the lower density, it also showed lower dielectric constant (better candidate for use of finer wires and cables). Expanded PTFE also appeared to bond to itself and other materials more readily than the unexpanded form. It also appeared to have increase in final length 1760 times, without diminishing the thickness of the final product (Chandler-Temple, 2008). PTFE (& ePTFE) is non-toxic, so the rejection by the body of that material is very rare. Moreover, due to its high porosity, the body's tissue can network and grow into an ePTFE implant (DermNet NZ visited on 13/06/2014). By 1984, ePTFE tubes were used as vascular prostheses and tissue ingrowth could occur in the internodal area after implantation (Cumming, *et al.* 1983; Heydorn, *et al.* 1977). Other applications required thicker materials, such as soft tissue replacement so therefore multiple layers of unsintered lubricated PTFE were constructed and once the desired thickness was reached the material was expanded either uni-, bi- or multiaxially in a specific rate, below the crystalline melting point of PTFE (Chandler-Temple, 2008).

As seen above, there are many applications of PTFE and the unique products which can be made are typically made empirically by using trial-and-error most of the times. Fibrillation is a unique feature of this polymer, which can be formed through the process of paste extrusion and it is due to this, that unique products can be designed and fabricated. To increase this and further optimize those properties a thorough understanding of this phenomenon is required and furthermore how this, affects mechanical properties, density and porosity.

In this PhD study, the role of fibrillation on the PTFE expansion and its relation to the Poisson's ratio of the material will be elucidated. Furthermore, its mechanical (tensile) and

physical properties (density) upon stretching and the parameters that influence these properties will be studied in detail. It is hoped that ways of controlling the expansion of PTFE will be identified i.e., ePTFE expansion (Poisson's ratio) as a function of temperature, strain and strain rate, as well as degree of fibrillation.

CHAPTER 2: PTFE Paste Extrusion And Poisson's Ratio: Literature Review

2.1 *Introduction*

The term expanded was first introduced in 1972, referring to a material that had quite lower specific gravity than solid PTFE after applying certain post-processing conditions (US PATENT 3.664.915-Gore W.L.1972). Wilbert Gore in 1958 started producing PTFE sheets, which were heated and stretched through rollers and he developed a method to form biaxially expanded fibrillated sheets of high porosity. In this section the literature relevant to paste extrusion, expansion of PTFE samples and how their morphological and mechanical properties are affected by stretching, are reviewed.

2.2 *PTFE Paste Preforming And Extrusion*

Paste extrusion is a process broadly used in many industries including pharmaceutical, chemical, and food processing. Generally speaking, paste is a blend of solid and liquid, mixed in concentrations such that the resulting material can be sufficiently moulded and extruded (Benbow & Bridgwater, 1993). PTFE can be processed by extrusion at room temperature as a paste. It is first mixed with a lubricant (an inert liquid hydrocarbon) and then is converted into preform of specified shape and dimensions using a relatively low compressive load (Ochoa, PhD Thesis, 2006). The lubricant concentration should be as low as possible, but at the same time above a certain level to avoid excessively high extrusion pressure. The optimum range was found to be between 15-25wt. % (Benbow & Bridgwater, 1993; Mazur, 1995). The viscosity of the liquid was also found to have a large effect on the quality of the paste, since an increased viscosity liquid results in: i) a less uniform mixture, ii) the extrusion pressure becomes high and iii) during the drying process many microcracks appear in the extrudates (Ebnesajjad, 2000; Ochoa & Hatzikiriakos, 2005). It was also noticed that the nature of the fibrils was dependent on the nature of the lubricant used (initially naphtha, kerosene, glycol) (Ochoa, PhD Thesis, 2006).

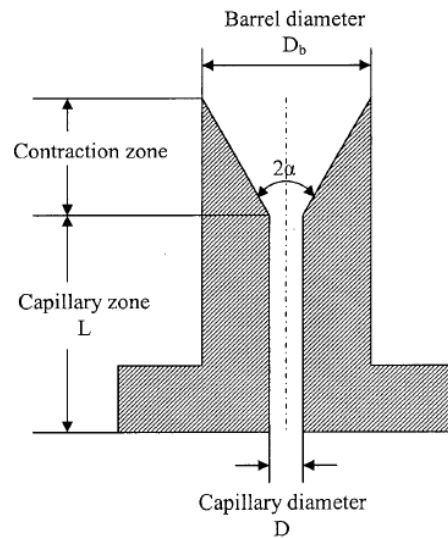


Figure 2.1: Schematic representation of a capillary die

For the extrusion process a mixture of PTFE powder and the lubricant is inserted into a chamber and compressed at a specific load and time to create a preform (Mazur, 1995). Then, it is extruded through dies of various shapes depending on the product. The most important geometrical parameters in paste extrusion using a cylindrical die can be seen in Fig. 2.1. These are the capillary diameter D , the length-to-diameter (L/D) ratio, entrance angle (2α) and the die reduction ratio defined as the ratio of cross sectional area of barrel to cross sectional area of die at the exit, that is ($RR \equiv D_b^2 / D^2$), where D_b is the barrel diameter and D is the die land diameter .

Previous studies have shown that there are optimum values for the L/D ratios, entrance angle, lubricant concentration and viscosity to obtain the optimum extrudate properties (Ochoa & Hatzikiriakos, 2005; Ochoa, PhD Thesis, 2006). As mentioned earlier, a very interesting phenomenon that takes place during extrusion and which contributes to the mechanical strength of the extrudates is fibrillation. During flow, fibrils are formed especially during the flow in the contraction zone (Fig. 2.1), which interconnect the particles and give dimensional stability to the extruded product. Fig. 2.2 shows the difference in structure of PTFE before and after extrusion process and the creation of fibrils which essentially orient in the direction of flow in axisymmetric flows. The degree of fibrillation can be affected by different parameters such as the processing temperature (Ochoa, *et al.* 2006; McGee & Collier, 1986;) and flow rate (McGee & Collier, 1986; Ochoa PhD Thesis, 2006), the type

and the amount of the lubricant used (Ebnesajjad, 2000; Mazur, 1995; Ochoa & Hatzikiriakos, 2004; Ochoa & Hatzikiriakos, CDRM 2003) the type of PTFE (Dominghaus, 1993; Wlochowich & Scigala, 1989; Frick, *et al.* 2013) and the geometrical characteristics of the die (Ochoa & Hatzikiriakos, 2005; Ariawan, *et al.* 2002b; Coleman, 1978).

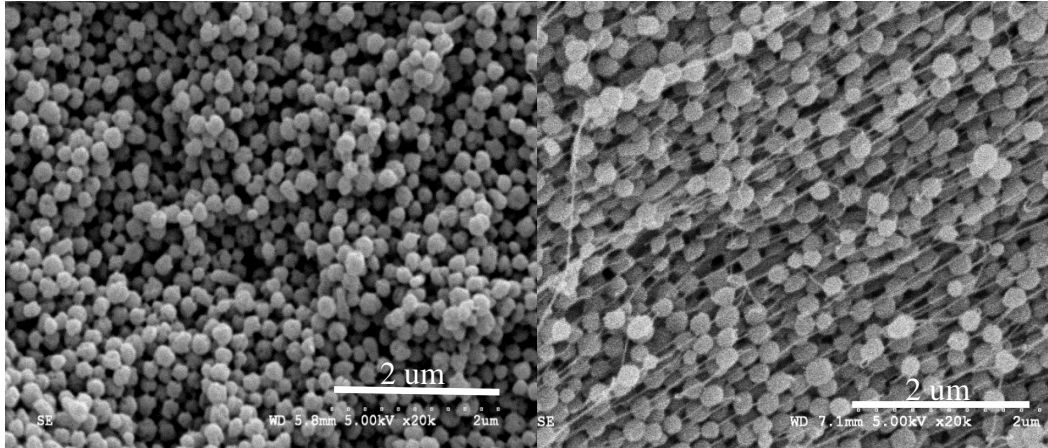


Figure 2.2: Typical SEM images of PTFE paste: (a) before extrusion, and (b) after extrusion using a capillary die. Images taken by Ardakani H.A. PhD Thesis (2014).

Previous researchers (Ariawan, *et al.* 2002b, Ochoa & Hatzikiriakos, 2005) have done detailed studies to show the effect of different parameters (die entrance angle, die reduction ratio and the physical properties of lubricants), affecting the extrusion pressure of PTFE. Few of their results are discussed in the next paragraphs. Regarding the lubricant concentration it was found that a relatively low lubricant concentration results in a higher extrusion pressure, due to insufficient lubrication of the flow and in some cases the extrusion appears to be discontinuous. On the other hand, a higher than normal concentration leads in a flow that does not produce enough pressure for fibril formation. Consequently, there is an optimum lubricant concentration for optimizing the mechanical properties of the extrudate. Based on industrial experience, similar results were reported (Mazur, 1995).

Very important parameters that influence the extrusion pressure are the geometrical characteristics of the die, mentioned earlier. An increase in the reduction ratio results in an increase of extrusion pressure with a concavity downwards. Moreover, as the reduction ratio increases, the extrusion pressure increases as well, with increase in the length-to diameter ratio, L/D . The contraction angle plays also a significant contribution to pressure, since the majority of the fibrils are formed within the contraction zone, where the flow is mainly extensional. The extrusion pressure changes non-monotonically with the entrance angle of the conical die α and

it reaches a minimum for an entrance angle value of about 20°. Previous studies have shown that the rheological behavior of PTFE paste during the extrusion, strongly depends on the number of fibrils created, between the PTFE particles. (Ochoa, PhD Thesis, 2006).

For small entrance angles the PTFE paste behaves mostly as a shear-thinning fluid with little fibrillation to occur, which results in a decrease in the extrusion pressure. For entrance angle values above a critical one, the extrusion pressure increases with increasing contraction angle, also observed in the extrusion of elastic solids. Examples can be found in previous studies (Horrobin & Nedderman, 1998). The more fibrils are created, the more the paste gains elastic extensional properties that lead to higher extrusion pressures.

Ochoa *et al.* (2006) studied the steady-state extrusion pressure as a function of apparent shear rate, for temperatures ranging from 15 to 65°C. At temperatures below the first transition temperature (19°C), there is limited fibril formation and therefore the extrusion pressure is low. This has to do with the fact that below 19°C, the PTFE particles are strong enough to resist the deformation from an applied load and therefore shearing between the particles does lead to limited formation of fibrils. Thus, the extrudates appear very weak, also confirmed by tensile strength experiments. For temperatures higher than the two transition temperatures, there is an increase in both the extrusion pressure and the degree of fibrillation and therefore the extrudates become stronger. Ochoa *et al.* (2006) also found that the extrusion pressure experiences a decrease for temperatures beyond 45°C, while for temperatures 55°C and 65°C, there is no significant difference in the extrusion pressure. This might be attributed to the effect of temperature on the viscosity of the lubricant, whereas fibrillation remains the same. It was suggested at that point that, since the surface tension and the viscosity are both functions of temperature, the lubricant cannot wet the PTFE particles, neither can move freely within the paste for temperatures below the first transition temperature and therefore its distribution within the paste is expected to be poor.

2.3 PTFE Paste Extrusion

Fig. 2.3 shows the four main stages during the paste extrusion, which are the paste preparation, preforming, paste extrusion and sintering.

During the first step an amount of solid particles is mixed with a specific concentration of liquid. Mixing is performed using different methods such as stirring or a motorized roll. The

mixture is then aged for certain period of time to ensure proper dispersion of the liquid among the solid particles (Ebnesajjad, 2000).

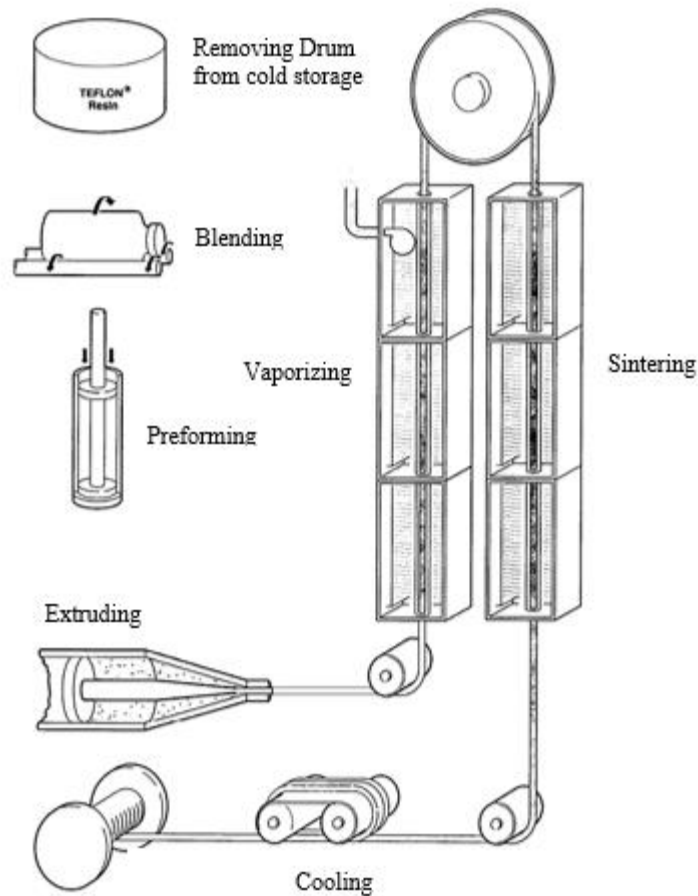


Figure 2.3: Schematic picture of the paste extrusion (DuPont, 1994)

The next step is to remove the air from the mixture, to avoid the creation of voids in the final products. To achieve that, the paste is compressed into a cylindrical billet within a cylinder (extrusion barrel) under the application of a specific load and a certain time (Ebnesajjad, 2000; Mazur, 1995). The application of stress has to have a specific value (2MPa), since it might cause the liquid to move in the solid matrix in a way that it might cause maldistribution throughout the paste (Yu, *et al.* 1999). The preformed billet is then forced through the extrusion die by means of a piston (plunger). After the extrudate comes out of the die, it is placed in an oven for evaporating the lubricant and then it can either be used the way it is or processed even further by doing sintering, which is essentially heating of the polymer in a temperature close to its melting point (Hooper, *et al.* 2000; Ochoa, PhD Thesis, 2006).

Fig. 2.4 shows a typical pressure transient, acquired during PTFE paste extrusion by using a capillary rheometer (Ariawan, PhD Thesis, 2001). The graph can be divided into three zones. For zone I the increase in pressure is due to jamming of the paste within the die. An immobile system of PTFE particles is created within the barrel and a critical pressure known in the literature as yield pressure is required to break this system of particles to have initiation of flow. Zone II corresponds to the steady-state paste flow, while in zone III one can see a small increase in the pressure, which is due to the extrusion of a gradually drier paste during the final stages of the process. Several models were developed so far for paste flow and more specifically for PTFE paste. Some of these are described in the next paragraph.

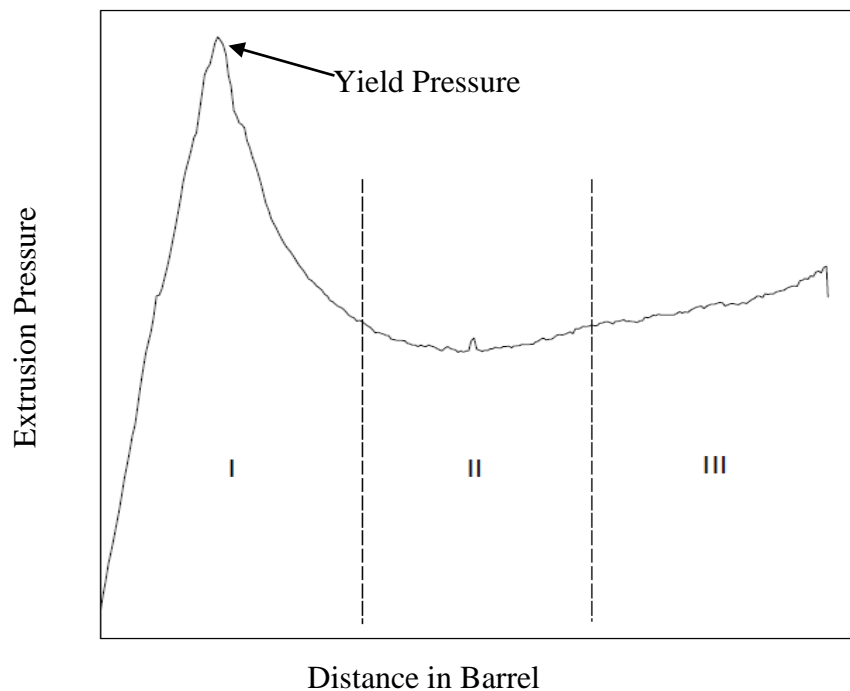


Figure 2.4: Typical behavior of pressure transient during PTFE paste extrusion (Ariawan, PhD Thesis, 2001)

2.4 Previously Proposed Mathematical Models For PTFE Extrusion-Constitutive Equations For Pressure Drop Prediction In Capillary Die

2.4.1 Snelling And Lontz Model

Snelling-Lontz (1960) assumed that paste is a visco-elastic solid with total slip on the wall. They approached the problem by considering a constitutive equation that includes an elastic term (strain-hardening) and a viscous one (shear-thinning). Furthermore, they

determined experimentally the velocity field within the die entry region, by following during an extrusion procedure, the spreading of pigmented paste within the die. These authors by using the rheological model:

$$\tau = C'\gamma^n + \eta \left(\frac{d\gamma}{dt}\right)^m \quad (2.1)$$

and assuming steady state flow through an *orifice* die ($L/D = 0$) of conical entry angle 2α , derived the following relationship for the total pressure drop:

$$\Delta p = \frac{4C'}{3(n+1)} \left[3 \ln \left(\frac{D_b}{D} \right) \right]^{n+1} + \frac{4\eta}{3m} \left[\frac{12Q \sin^3 \alpha}{\pi(1-\cos \alpha)D^3} \right] \quad (2.2)$$

where C' , n , η , and m are constants estimated experimentally, $(D_b/D)^2$ is the reduction ratio and Q is the volumetric flow rate. This equation is based on the “radial flow” hypothesis that simplifies its derivation. According to this hypothesis the particles of the paste which are at the same radial distance from the virtual apex of the conical zone of the die (see Fig. 2.5), have the same velocity. This can be expressed by the following relationship in terms of the r-spherical coordinate:

$$\frac{dr}{dt} = -\frac{Q}{2\pi(1-\cos \alpha)r^2} \quad (2.3)$$

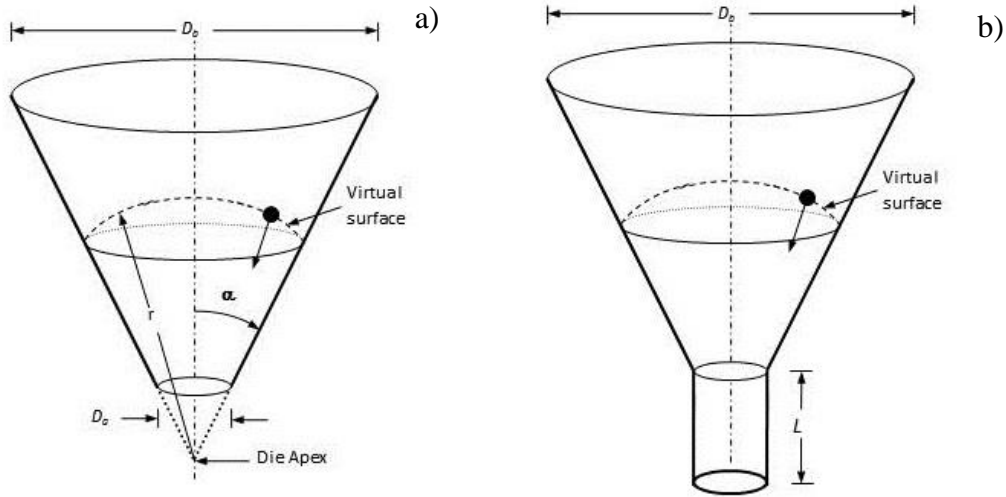


Figure 2.5: (a) Schematic of a tapered orifice die showing the various characteristic dimensions and (b) schematic of a tapered die that includes a certain length of die land L

2.4.2 Ariawan Model

Ariawan in 2002a used the radial flow hypothesis suggested by Snelling and Lontz (1960), to find a one-dimensional mathematical model, which could calculate the extrusion pressure. He ended up with a one-dimensional mathematical model capable to describe the effect of extrusion conditions for PTFE paste. By considering the paste as visco-elastic solid, the material exhibits during flow both strain hardening and viscous resistance effects. Hence, he used the following constitutive equation, by using a power-law modified Kelvin's stress-strain:

$$\sigma_{\theta} - \sigma_r = C' \gamma_{\max}^n + \eta \dot{\gamma}_{\max}^m \quad (2.4)$$

where σ_{θ} and σ_r are the principal stresses in θ and r directions, respectively, γ_{\max} is the maximum value of the strain and $\dot{\gamma}_{\max}$ the maximum value of the strain rate. Within the conical zone the extrusion pressure was found to be:

$$P_{extrusion} = \sigma_{rb} = \sigma_{ra} RR^B + 2(1+B) \left\{ C' \left(\frac{D_b}{2s \sin \alpha} \right)^{2B} \int_{r_a = \frac{D_b}{\sqrt{RR} s \sin \alpha}}^{r_b = \frac{D_b}{2s \sin \alpha}} \frac{(3 \ln(\frac{r_b}{r}))^n}{r^{2b+1}} dr + \left(\frac{\eta}{(3m+2B)} \left(\frac{12Q \sin^3 \alpha}{\pi(1-\cos \alpha) D_b^3} \right)^q (RR^{B+\frac{3m}{2}} - 1) \right) \right\} \quad (2.5)$$

where σ_{ra} is the stress at the die exit, RR is the reduction ratio, C' , η , m , n and f are material constants which are determined experimentally. This model was found to describe adequately well most experimental observations, such as the effects of reduction ratio, die entrance angle, pressure, L/D ratio of the die. While the above models predict the extrusion pressure, they provide no information on the effect of the degree of fibrillation of the paste.

2.4.3 Anvari Model

In 2013 Anvari, *et al.* proposed the modification of the lower limit of the integral hypothesizing that at the cylindrical part of the die, the particles do not follow the radial flow. Anvari *et al.* tried to modify the above equations to have a better prediction for their experimental results obtained at different processing conditions (several temperatures, die entrance angles, die length, diameters and extruder reservoir sizes). They have discussed that

this is fairly possible by changing the boundary conditions for above equations. As it is illustrated in Fig. 2.6, Anvari assumed that the iso-strain radial flow path starts from the conical channel exit, while Ariawan takes it from a radial arc to maintain radial flow hypothesis valid. This leads to changes for a boundary condition, which is summarized in the following table for the lower limit of the integral:

Table 2.1: Changes in the lower limit of the integral of Eq.2.5, by two different researchers

Ariawan	Anvari
$r_a = D_a/2 \sin \alpha$	$r_a = D_a/2 \tan \alpha$

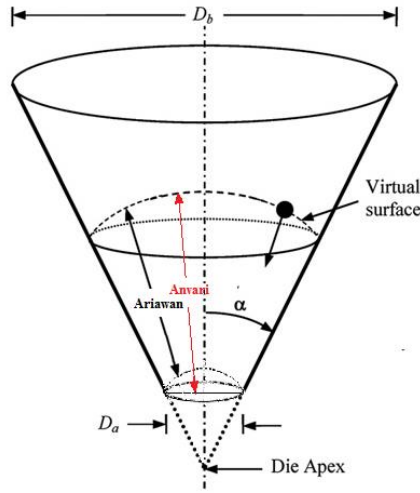


Figure 2.6: Schematic representation of the difference between the two mathematical models proposed by Ariawan et al.2001 and Anvari et al.2013

And the extrusion pressure is being given by the equation:

$$P_{extrusion} = \sigma_{ra} (RR)^B \quad (2.6)$$

$$+ 2(1+B) \left\{ C' \left(\frac{D_b}{2 \sin \alpha} \right)^{2B} \int_{r_a = \frac{D_b}{2 \tan \alpha \sqrt{RR}}}^{r_a = \frac{D_b}{2 \sin \alpha}} \frac{\left[3 \ln \left(\frac{r_b}{r} \right) \right]^n}{r^{2B+1}} dr + \frac{K}{(3m+2B)} \left[\frac{12Q \tan^3 \alpha}{\pi(1-\cos \alpha) D_b^3} \right]^m (RR^{B+3m/2} - 1) \right\}$$

where,

$$\sigma_{ra} = \left\{ C' \left(\frac{3}{2} \ln(RR) \right)^n + K \left(\frac{12Q \tan^3 \alpha RR^{\frac{3}{2}}}{\pi(1-\cos \alpha) D_b^3} \right)^m \right\} \left[1 - e^{\left(\frac{4fL}{D_a} \right)} \right]$$

$$\text{and } B = f \sin \alpha / [2(1-\cos \alpha)]$$

2.5 Definition Of Poisson's Ratio And Its Physical Significance

As discussed above, the Poisson's ratio is an important parameter for ePTFE as it characterizes its density, porosity and thus its mechanical properties. Poisson's ratio (ν), has been used to characterise the mechanical properties of isotropic materials from the hardest incompressible material, to the softest most extendable one, whether being homogeneous or not. As seen from Fig. 2.2. PTFE extrudates are frequently nonisotropic materials depending on the orientation of fibrils. Therefore, the Poisson ratio of the material might be depended on the direction at which is stretched and therefore should be defined carefully.

To define the Poisson's ratio consider Fig. 2.7 where the transverse strain (e_t) and the longitudinal strain (e_l) are also considered . Then the Poisson's ratio can be defined by Eq.2.7.

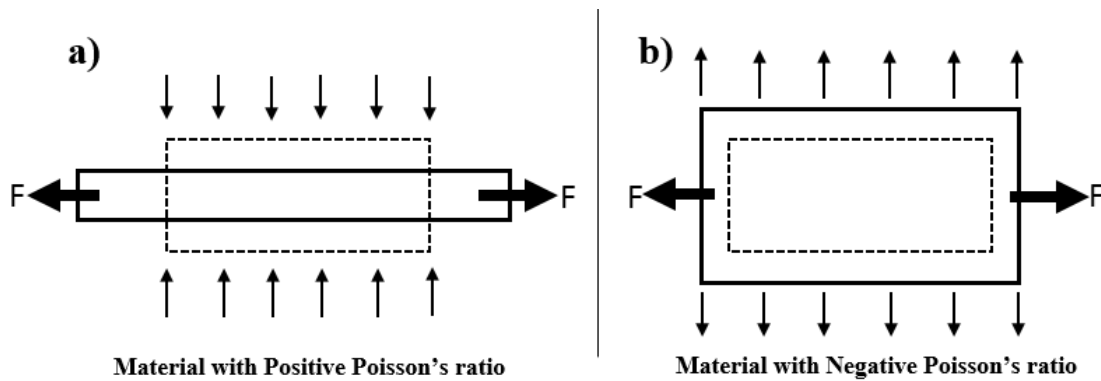


Figure 2.7: Schematic representation of behaviour of a material possessing a) a positive Poisson's ratio and b) negative Poisson's ratio.

$$\nu = - \frac{\text{Lateral strain}}{\text{Longitudinal strain}} \quad (2.7)$$

Therefore, Poisson's ratio is a measure of the resistance of a material to volume change (B), well-adjusted against the opposition of shape change (G). The latter can be expressed by:

i) the isothermal bulk modulus $B = -VdP/dV = 1/k$ (k : isothermal compressibility), that is volume change,

ii) the shear modulus $G = \sigma_t / (2e_t)$ a measure of stiffness of the material.

Thus, plotting ν as a function of B/G a relation should exist and this appears in Fig. 2.8. (Greaves, *et al.* 2011). Poisson's ratio for isotropic materials lies in the region of $[-1, 1/2]$ (Greaves, *et al.* 2011; Evans, *et al.* 1991; Evans, 1990).

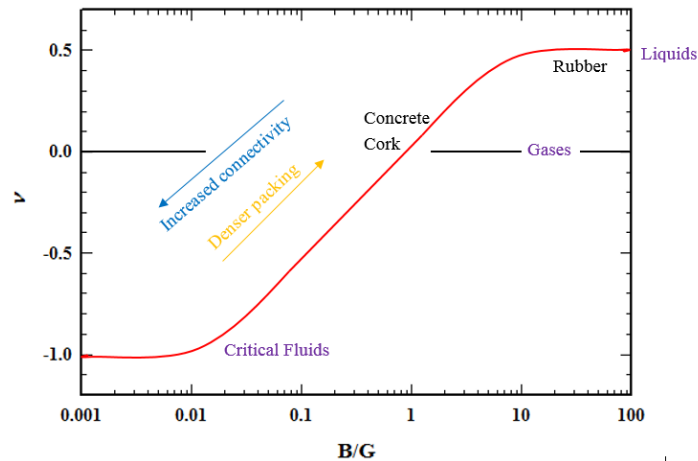


Figure 2.8: Numerical region of Poisson's ratio for a range of isotropic materials. For gases $\nu=0$, metals, polymers and ceramics, lies between the area (0.25, 0.35), while materials in which stress can cause a shape change (weakly compressible materials, liquids, rubbers), ν approaches $\frac{1}{2}$ (Image reproduced by Greaves, *et al.* 2011).

Materials with Poisson's ratio less than zero (negative) are called auxetic (Lakes, 2001). The word auxetic which is derived from the Greek auxetos was introduced in 1991 to avoid the cumbersome phrase "negative Poisson's ratio (NPR) materials" and to characterise the materials that their width and volume increase when stretched (Evans, *et al.* 1991). On the other hand, rubbery materials cannot easily change their volume (incompressible) (US PATENT 3.664.915-GORE W.L.1972). Auxetic materials can have improved mechanical properties such as enhanced shear moduli, plain strain fracture toughness or elastic indentation resistance (Lakes, 1987; Evans, 1990; Liu, visited on 12/01/2016).

Materials that have been fabricated with negative Poisson's ratio (NPR) can possess different types of structures including two-dimensional honeycombs (Gibson & Ashby, 1988), three dimensional foams with "inwardly bulging" cells ((Lakes, 1987; Friis, *et al.* 1988), microporous polymers (Evans & Caddock, 1989; Evans, *et al.* 1991; Caddock & Evans, 1989) or metals and minerals (Grima, *et al.* 2005; Baughman, *et al.* 1998; Alderson, *et al.* 2009; Sanchez-Valle, *et al.* 2005).

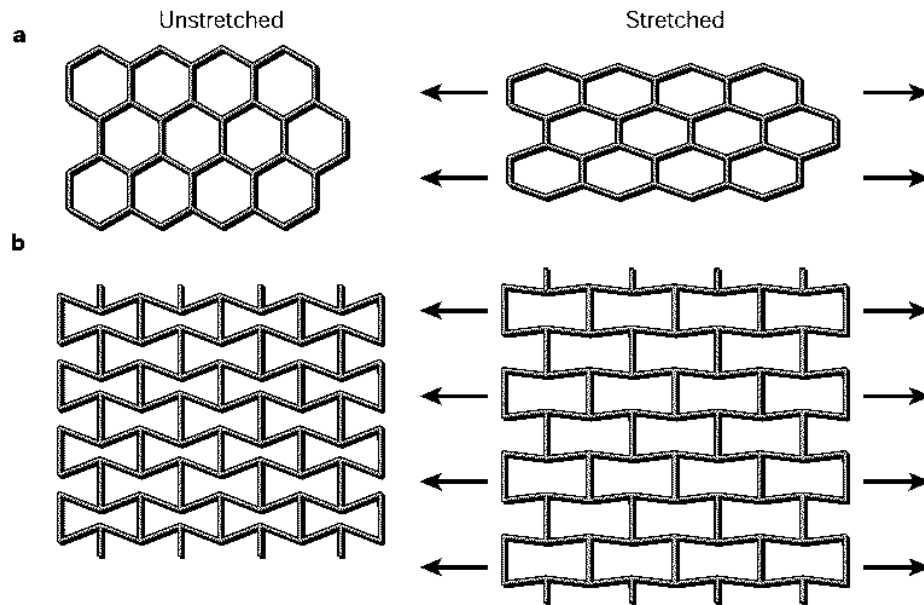


Figure 2.9: a) Conventional hexagonal honey-comb system, which gives a positive Poisson's ratio, b) System with a negative Poisson's ratio (Lakes, 2001)

Bowick *et al.* (2001), assumed that structures which take place during deformation as the ones seen in Fig.2.9 a) are known as "fixed connectivity" and occur in biological and synthetic systems (Bowick, *et al.* 2001).

Compared to the NPR materials, there are some materials having Zero Poisson's Ratio (ZPR), which their lateral dimension remains unchanged during uniaxial extensional deformation. Some examples of these materials are the membrane of the beetle's wings (Jin, *et al.* 2009), rectangular and scaffold type cellular structures and biological tissues (i.e., cartilage, ligament, corneal, brain), (Olympio, *et al.* 2007; Lira, *et al.* 2009; Soman, *et al.* 2012), or polymer gels (Geissler, *et al.* 1980). These materials are also compressible, since their volume increases upon stretching and they have been significantly ignored (this property cannot be easily achieved). However, they were found to be considerably useful in the production of cylindrical surfaces (Grima, *et al.* 2011).

2.6 Mechanism For Expanded PTFE Negative Poisson's Ratio

The negative Poisson's ratio observed for ePTFE has to do with the microstructure of the material, which undergoes significant changes during extension or compression, such as fibre stretching and shrinkage, aggregate rotation and node reaggregation. For example various hypotheses were made in the past, in which the microstructure of ePTFE consists of granular nodes and fibres, which can either form a uniaxial network or a biaxially drawn array. During

extension both these networks can break up their granular aggregates (nodes), until they finally form a network of fibrilly connected dispersion particles. According to the same hypothesis, at high elongations the material fully expands and the parallel lying fibres are undergoing a micro-rotation in the x-direction, during various stages of tensile deformation (Fig.2.10) (Caddock & Evans, 1989).

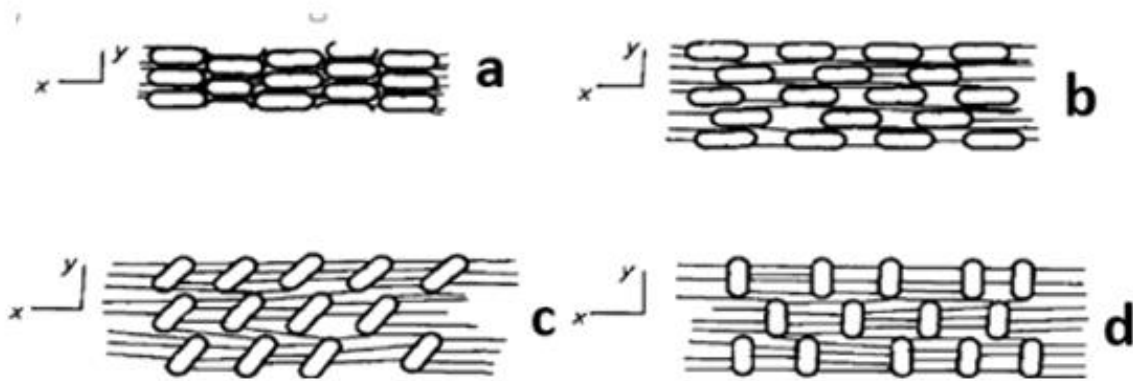


Figure 2.10: Microstructural changes of ePTFE under tensile loading: a)Initial packed microstructure b) lateral expansion of nodes and fibrils, c) Further lateral expansion causing rotation of nodes,d) final fully expanded condition.Image taken by Caddock & Evans, 1989).

Plots of Poisson's ratio and Young modulus plotted against the engineering strain shows three different areas of the material behaviour as shown in Fig. 2.11. In the first region the material undergoes a deformation of large strain and low modulus. During this stage the material succeeds the highest negative Poisson's ratio. In this stage the material is considered inelastic and the fibrils are behaving like inextensible springs, while the majority of the deformation is due to particle movement. In the second region the material behaves linearly elastic and its modulus increases and on continuing deformation the material behaves plastically.

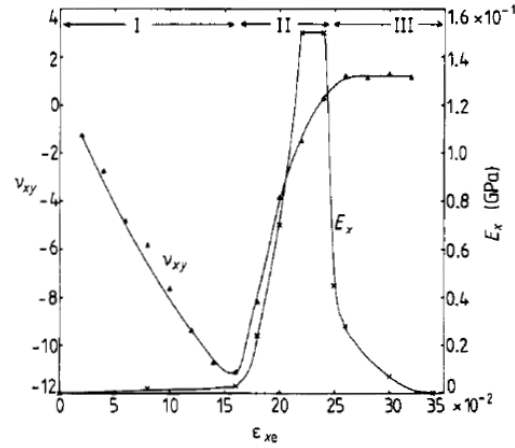


Figure 2.11: Poisson's ratio and young modulus plotted against the engineering strain shows three different areas of the material behaviour (Caddock & Evans, 1989).

ePTFE was found to have a range of various microstructures, which leads to a complex interaction between longitudinal and transverse strains and therefore to a high negative value of Poisson ratio (for the specific microstructure it reached -12), while plasticity effects can diminish this value by producing larger strains (Caddock & Evans, 1989).

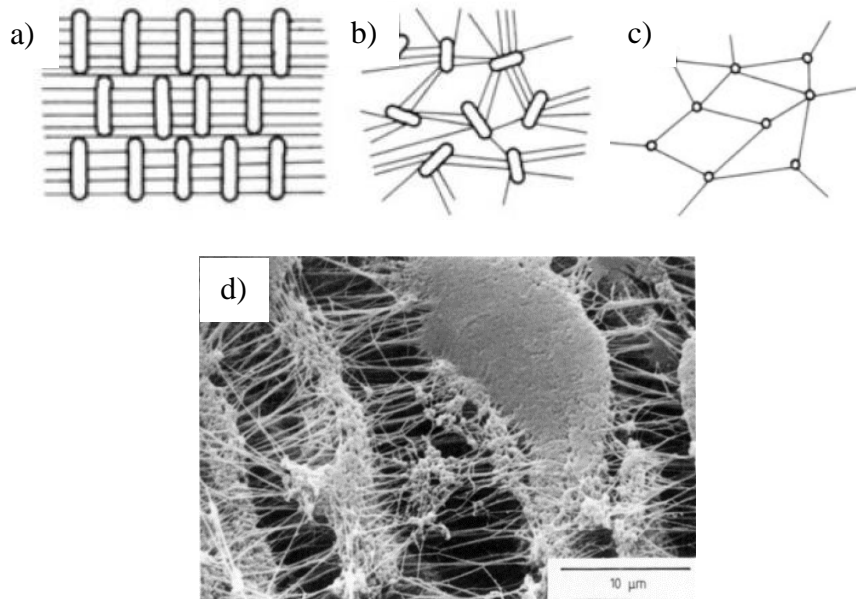


Figure 2.12: Examples of ePTFE a) partial uniaxial ,b)partial biaxial ,c) complete biaxial drawings, d)SEM image of ePTFE showing nodal particles interconnectd with fibres, proving the biaxial drawing suggested earlier.According to the same hypothesis, at high elongations the material fully expands and the parallel lying fibres are undergoing a micro-rotation in the x-direction, during various stages of tensile deformation. Interestingly, no broken fibrils were detected and they were considered to act like elastic springs.All experiments were conducted at room temperature (Caddock & Evans, 1989).

2.7 Tensile Properties Of PTFE And Modelling

A typical tensile result for a cylindrical PTFE sample is shown in Fig. 2.13 (Vavlekas, *et al.* 2016). The tensile results were acquired using the fixture SER (described in more detail in section 4.2) at $T_t=150^\circ\text{C}$ (tensile testing temperature) and Hencky strain rate of 0.6 s^{-1} for a sample extruded at $T_p=25^\circ\text{C}$ (extrusion temperature) through a die with reduction ratio of 156.

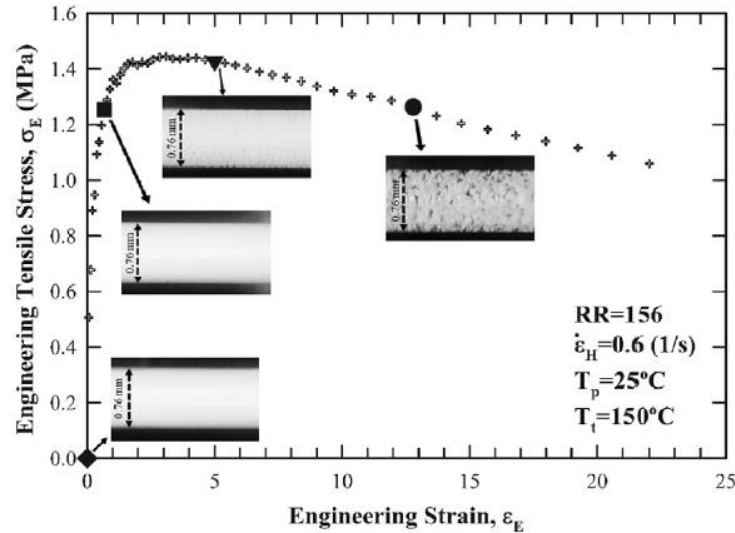


Figure 2.13: Typical tensile graph of PTFE sample. The diameter of the sample (0.76 mm) remains unchanged during uniaxial extension for all cases as seen by the images \blacklozenge $\epsilon_E=0$ \blacksquare $\epsilon_E=0.5$ \blacktriangledown $\epsilon_E=5.0$ \bullet $\epsilon_E=12.5$, leading to a Poisson's ratio of the sample very close to zero.

The results show a monotonic increase up to a maximum point, which is known as "ultimate strength" followed by a drop in engineering stress until sample's failure. The shape of the curve represents a ductile failure which can be seen for other semi-crystalline polymers like HDPE (Reis, *et al.* 2013). Ochoa (PhD Thesis, 2006) measured the tensile mechanical properties of some PTFE extrudates using SER fixture and he observed the same trend as the one presented in this work. The images of the extrudate at four different strain levels for this set of tensile experiment are also shown in Fig. 2.13. As it is clear from these images, the bulk of the extrudate becomes porous during stretching. In other words, the *micro-porous* structure (fibrillated) of PTFE extrudate is expanding during stretching toward a visible *macro-porous* one, at engineering strains as high as 12. However, the diameter of the sample remains unchanged, which is an indication of the material compressibility.

Matsuoka *et al.* (1986) proposed a nonlinear viscoelastic model for soft solids which accounts for the effect of uniaxial strain rate (Eq. 2.8) and Poisson's ratio. This will be used in

the present work for modelling of PTFE extrudates and to understand how the Poisson's ratio affects the tensile properties of the material:

$$\sigma_E = E_0 \varepsilon_E (1 + \varepsilon_E)^{-2\nu} \exp(-C\varepsilon_E) \exp\left[-(\varepsilon_E/\dot{\varepsilon}_E \lambda)^n\right] \quad (2.8)$$

where " ν " is the Poisson's ratio and " E_0 ", " λ ", " C " and " n " are parameters which represent the elastic modulus, relaxation time, yielding coefficient and relaxation exponent, respectively.

Considering Eq. 2.8, Matsuoka *et al.* (1986) has shown power-law trend for the ultimate strength as a function of engineering strain rate. Wang, *et al.* (2002) also found a power-law relationship for the elastic modulus (E) and tensile strength (σ_b) with strain rate for short fibre reinforcement Polyamide-6. They noticed that both E and σ_b , decrease with increasing temperature and increase with increasing strain rate. Moreover, a careful analysis of Ochoa's, (2006) data interestingly exhibit the power-law exponent of 0.16 for certain PTFE extrudates.

As discussed above the main goal of this PhD study is to understand the mechanisms of expansion of PTFE upon stretching. In other words to identify the parameters that affect its expansion upon stretching, such as the degree of fibrillation (that is affected by the paste extrusion parameters: die design characteristics or operational conditions such as shear rate and temperature), the temperature of stretching as well as the strain and strain rates.

CHAPTER 3: Scope Of The Work

3.1 Introduction

PTFE has become due to its outstanding properties an essential product in our daily lives. It is widely used nowadays from products such as tapes gaskets to body parts replacement. Although its processing techniques (involving pressing, paste extrusion and sintering) have been improved dramatically since their introduction, there are still issues that have to be studied to optimize them.

While several studies have been dedicated on the PTFE paste extrusion there is still a poor understanding on how the morphology of the produced extrudates affect the density and mechanical properties of the post-processed samples. Therefore, one of the main objectives of this work was to identify the effects of die design on the morphology of produced extrudates and their mechanical properties. Densitometry was also used to identify how the microstructure of the PTFE would affect its compressibility upon stretching. Models that describe these properties as a function of several important parameters discussed above are of paramount importance in this work. Finally, the effect of fibrillation on the PTFE will be elucidated on the Poisson's ratio of the material, after being tested under various conditions.

3.2 Thesis Objectives

This research project is fundamental in nature. It is hoped that a clearer insight into the nature of PTFE fibrillation and its relation to the Poisson's ratio will be elucidated by the end of this study. The particular research objectives of this proposal are summarized as follows:

1. To study the process of PTFE paste extrusion, namely: The effect of processing conditions (temperature and flow rate) on the mechanical properties of the produced extrudates for two different types of PTFE (homopolymer-copolymer). Although this has been studied to a large extent by others previously, it is a starting point for any project on PTFE paste extrusion and this is an objective unavoidably. For this part of the work a previously developed model has been used to model the extrusion pressure as a function of the geometrical parameters of the dies and the operating conditions. The process of paste extrusion will be examined under both a constant-speed and constant-pressure mode. It is believed that the first mode of operation leads to a constant diameter of extrudate while the second to a constant density. This is never examined before and it is important to see whether the diameter of the extrudate or its density can be changed in a controlled manner.

2. To identify the effects of die design characteristics on the morphology of produced extrudates by using SEM and further examine their mechanical properties by tensile testing (SER rheometer) as a function of extrusion temperature and geometrical parameters of dies as well as the testing temperature. Densitometry will also be used to identify the Poisson's ratio of these materials and its change during stretching.

3. To study the flow mechanism of the extruded samples from cylindrical dies (fibrils are oriented in 1-D) and specially designed flat dies (fibrils oriented in 2-D) to understand differences in the expansion of samples obtained by these two different die designs. Extrudates from a flat die possess fibrils oriented in two dimensions. In this case it would be of interest to understand how the Poisson's ratio is affected by 2-D fibril orientation. The orientation of the fibrils will be examined using depolarized Raman spectroscopy along with SEM imaging.

4. To understand the mechanism by which PTFE films produced by different extrusion processes, expand as a function of Hencky strain \mathcal{E} , Hencky strain rate $\dot{\epsilon}$ and temperature, T. The experimental data will be used to derive a suitable model (phenomenological with certain theoretical aspects). A steady-state mechanical property constitutive model for the ultimate strength will be derived for cylindrical (1-D) samples. Another model will be produced for flat samples (2-D) in which the Poisson's ratio which will be defined from the studies in objective 3, will be incorporated as well.

3.3 Thesis Organization

The first chapter of the thesis provides information on basic physical and chemical properties of PTFE. Moreover, some of its applications relevant to this thesis found for either its traditional or its expanded form are reviewed. The problem definition and the motivation of this work are also discussed. Following this introduction, important literature on paste extrusion and previously studied models on the pressure prediction during an extrusion process are also mentioned. A brief introduction on the Poisson's ratio and the categorization of materials according to the values of this ratio is also reviewed. Chapter 3 presents the objectives of the current study as well as the organization of this thesis. Chapter 4 follows with descriptions of the experimental apparatus and experimental protocols/procedures used in the current study. Chapter 5 is based on the study of the effect of the processing conditions on the mechanical properties for two types of PTFE. In this part of the work a previously developed model was used to model the extrusion pressure as a function of the geometrical parameters of

the dies and the operating conditions. The chapter is based on a journal paper that has already been published (M. Ansari, D. Vavlekas, J.L. McCoy, S.G. Hatzikiriakos, "Paste Extrusion and Mechanical Properties of PTFE", *International Polymer Processing*, XXX, 603-614 (2015)). Chapter 6 will be a study of two modes of operation examined for the first time. The first mode focuses on extrusions performed under constant speed, while the second on extrusion under constant load. It is believed that these two changes in mode can cause changes to the density or the diameter of the cylindrical extrudates. Chapter 7 focuses on identifying the effects of the die design characteristics on the mechanical properties of cylindrical extrudates, by tensile testing (SER rheometry). A steady-state mechanical property constitutive model for the ultimate strength has been derived for cylindrical (1-D) samples. Densitometry was used to identify the Poisson's ratio of these samples. The results are based again on a published paper (D. Vavlekas, M. Ansari, H. Hao, F. Fremmy, J.L. McCoy, S.G. Hatzikiriakos, "Zero Poisson's Ratio PTFE in Uniaxial Extension", *Polymer Testing*, 55, 143-151, (2016)). Chapter 8 discusses the results found for a specially designed flat die (fibrils oriented in 2-D) in which fibrils are oriented in two directions and how the Poisson's ratio is affected by 2-D fibril orientation. The orientation of fibrils was detected by both Raman spectroscopy and SEM images. This part of the work is also part of a manuscript published to *Polymer Testing* (D. Vavlekas, L.Melo, M. Ansari, E. Grant, F. Fremmy, J.L. McCoy, S.G. Hatzikiriakos, "Role of PTFE Paste fibrillation on Poisson's ratio", *Polymer Testing*, 61, 65-73, (2017)).

Finally the thesis is concluded in Chapter 9, where a general summary and contribution to knowledge are presented, as well as some recommendations for future work are listed.

CHAPTER 4: Materials And Experimental Equipment

4.1 Introduction

This chapter describes the materials and the experimental equipment used to study the fibrillation of the paste extrusion of PTFE and its relation to Poisson's ratio. The capillary rheometer is a valuable tool of this study since it can mimic the industrial ram extruder. Another indispensable tool of this work is the Sentmanat Extensional Rheometer (SER) which is used to measure the tensile strength of the extrudates at different temperatures and Hencky strain rates. Several other pieces of equipment and procedures were also used to characterize the properties of the produced extrudates.

4.2 Materials

4.2.1 PTFE Fine Powder Resins

PTFE powder resins have been supplied by Saint Gobain S.A. USA and DAIKIN Industries Ltd. The resin particles are in general, spherical in shape and they have a uniform size distribution. The samples are kept in the cold room (4°C) prior to use, to avoid any premature fibrillation, which will hinder the efficiency of paste preparation. As shown in the Tables 4.1 and 4.2 two resins have homopolymer structure, while the other two possess a modified structure (copolymer).

Table 4.1: Physical properties of PTFE resins provided by Saint Gobain

Resin	Type	Particle Size Diameter (µm)	Standard Specific Gravity
H-PTFE	Homopolymer	450	2.199
C-PTFE	Copolymer	543	2.153

Table 4.2: Physical properties of PTFE resins provided by DAIKIN.

Resin	Type	Particle Size Diameter (µm)	Standard Specific Gravity
F-104 HMW	Homopolymer	400-650	2.17-2.20
F-301	Copolymer	400-650	2.15-2.18

4.2.2 Lubricant (Isopar H)

The type of lubricant which is used in this work, is the isoparaffinic compound ISOPAR-H produced and supplied by ExxonMobil Chemicals. 18 % in weight of the lubricant will be used for all experiments, typically used in most PTFE paste extrusion operations. Table 3 (ExxonMobil : Isopar H, visited on 25/10/2014) summarizes its properties.

Table 4.3: Physical properties of Isopar H supplied by ExxonMobil

<i>Properties</i>	<i>Units</i>	<i>Typical values</i>	<i>Test Method</i>
Distillation range IBP-IDP	°C	179-187	ASTM D 86
Flash Point	°C	53	ASTM D 56
Density at 15°C	kg/dm ³	0.759	ASTM D 4052
Viscosity at 25°C	mm ² /s	1.80	ASTM D 445
Evaporation rate (n-BuaAc=100)	-	11	ASTM D 3539
KB value	-	26	ASTM D 1133
Aniline Point	°C	85	ASTM D 611
Aromatic content	%wt	<0.01	AMS 140.31
Color SAYBOLT	-	+30	ASTM D 156
Bromine Index	mg/100g	<5	ASTM D 2710
Surface Tension at 25°C	mN/m	23	ASTM D 1331
Refractive Index at 20°C	-	1.421	ASTM D 1218

Notes:

- Values indicated describe typical physical properties and do not constitute specification limits
- This product typically contains less than 10 ppm Benzene and less than 5 ppm Sulphur

4.3 Methods and Experimental Equipment

4.3.1 Paste Preparation

The PTFE powder was mixed with the lubricant (18 wt. %) at a temperature lower than 19°C in plastic cylindrical containers. The mixing container was placed on a horizontal roll mixer (15 rpm) for 30 minutes. The resulting paste was left overnight for ageing inside the fridge to allow more uniform wetting of particles. Paste of more than 10 days old was not used, since the lubricant concentration might have been decreased due to evaporation. Similar procedures have been used by Ariawan (PhD Thesis, 2001) and Ochoa (PhD Thesis, 2006).

4.3.2 Preforming Of Paste:

Pre-forming was performed by using a blind die in a capillary rheometer. The aged paste was placed into a piston driven capillary (Instron Testing model 1123 with a reservoir diameter of 9.5 mm) using a blank die. The paste within the capillary rheometer was compressed by a piston attached to the rheometer at an adjustable speed and a constant pressure (either 1.5 or 2 MPa) to produce a preform of uniform density and lubricant concentration. Previous studies have shown that the optimum pressure for preform is about 2 MPa for approximately 30 s. For preforming time more than 30 s, the lubricant migrates towards the end of the die, creating

undesirable lubricant concentration gradients (Ochoa, PhD Thesis, 2006). The preform was subsequently extruded by using different capillary dies having various geometrical characteristics. The various capillary dies used for studying the process of PTFE paste extrusion (Chapter 5), along with their geometrical characteristics are listed in Table 4.4.

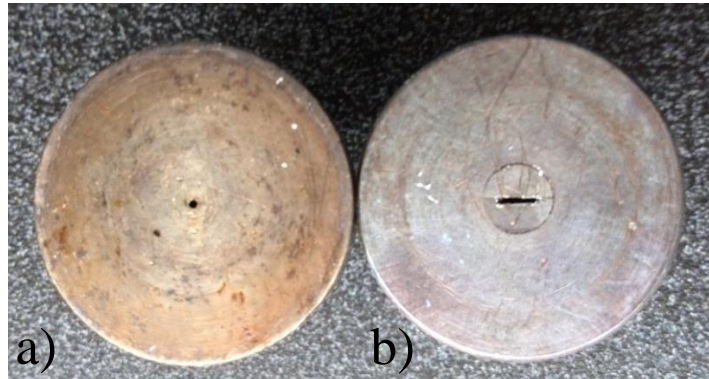


Figure 4.1: Two different dies which were used for the study of mechanical properties of the extrudates. Left die (a) is the cylindrical one, while on the right (b) the slit die can be seen. In both dies the fibrils were oriented in one dimension (1-D), due to the nature of the flow.

4.3.3 Capillary Extrusion

An Instron capillary rheometer was used to mimic the process of ram extrusion. A capillary rheometer consists of a barrel through which paste flows at a fixed speed, by means of either a piston moving in the reservoir or an imposed pressure force. It has four heating zones, which are connected to a temperature controller. The measured quantities are normally the flow rate Q and the driving pressure P_d , from which the rheological quantities of shear stress and apparent shear rate can be calculated.

A computer directly connected with the rheometer allows controlling of the extrusion process under various speeds. The paste was placed into a piston driven capillary (Instron Testing model 1123 with a reservoir diameter of 9.5 mm) and subjected to a mild compression pressure at 2 MPa for 30s to produce a preform of uniform density and lubricant concentration (see also section 4.3.2). The preform was subsequently extruded at various temperatures (25°C-150°C) through different capillary dies.

Extrusion experiments were performed using various dies of specified entrance angle (90°), L/D ratio and reduction ratio at a given temperature, which is denoted as T_p (extrusion temperature). The produced extrudates were tested in tensile mode for mechanical property characterization at various temperatures denoted as T_i (mechanical testing temperatures).

The capillary extrusions were performed under two different modes of operation (i) constant piston speed that results into a constant apparent shear rate defined by $\dot{\gamma}_A \equiv 32Q/\pi D^3$, where Q the flow rate (in³/min) and (ii) constant load that results into a constant extrusion pressure. In the first case the extrusion pressure is measured, while in the second mode the piston speed. This is used to calculate the apparent shear rate using $\dot{\gamma}_A = 8v_p D_b^2 / D^3$ where v_p is the piston speed (in/min). More details on these two modes of operation are given in Chapter 6. For all extrusion cases, upon completion of the extrusion, the extrudate was collected and analyzed only during the steady state period (steady extrusion pressure). The extrudate was cut into 100 mm specimen, in which the average diameter of the edges and the middle part were measured as well as its average specific gravity. The average diameter and density were measured before and after drying the extrudate in an oven overnight at 60°C.

Table 4.4: Characteristics of capillary dies used in the study of process of PTFE paste extrusion (Objective 1).

Type of Study	Diameter (mm)	Reduction Ratio $RR \equiv (D_b/D)^2$	Entrance Angle (°)	L/D Ratio
<i>Effect of Reduction ratio</i>	0.51	352	90	20
	0.76	156	90	20
	0.96	100	35	10
	1.27	56	90	20
<i>Effect of Die Entrance Angle</i>	0.51	352	15	20
	0.51	352	30	20
	0.51	352	60	20
	0.51	352	90	20

Another type of die used in this work had a planar cross section that promoted acceleration in both dimensions to form fibrils and orient them in two directions (2-D sample) (Fig. 4.2.a). The flat samples produced (Fig. 4.2.b) were cut in stripes in the transverse direction for mechanical testing (Fig. 4.2.c). Typical dimensions are 2.1-2.3 mm in width (parallel to the extrusion direction) and 1.3 mm in thickness. The mechanical properties in tensile were determined using the Sentmanat Extensional Rheometer (SER) whose operation is discussed next. Measurements were made at three Hencky strain rates (0.6, 1 and 3 s⁻¹) and three testing temperatures (25, 50, 100°C).

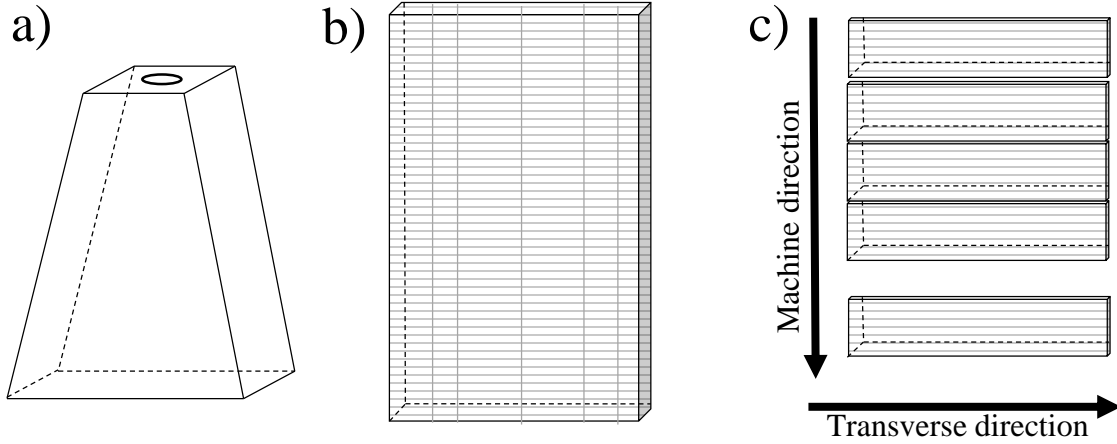


Figure 4.2: a) Schematic of flat die used, b) schematic of the flat extrudates produced and c) preparation of the sample pieces for uniaxial extension testing and Raman spectroscopy

4.3.4 Mechanical Property Characterization Of Samples

4.3.4.1 Sentmanat Extensional Rheometer (SER)

The Sentmanat Extensional Rheometer (SER) (Fig. 4.3) was used to test the samples in uniaxial extension. The SER was mounted on a MCR502 rheometer made by Anton Paar. It consists of two drums, where the main drum rotates by the host rheometer stem and the secondary drum rotates counterwise, due to the presence of intermeshing gears, which connect the two drums (Sentmanat, *et al.* 2005). Since the gap between the cylinders is fixed (sample's length), a constant rotation speed causes an exponential strain on the sample (Sentmanat, 2004; Delgadillo-Velazquez, *et al.* 2008; Aho, *et al.* 2010). The sample in the form of either strip (Ansari, *et al.* 2012) or cylindrical strand (Wang, *et al.* 2008) was mounted on these drums using smooth or rough clips. To avoid slippage of solid PTFE strands, samples were being twisted around the clips. Another benefit of this method is that there is no need to push the clips toward the drums, which may cause unwanted compressive deformation on sample's diameter. This ensures a uniform and pure uniaxial extensional deformation. The effect of temperature was also studied to assess the sensitivity of the material to changes in temperature.

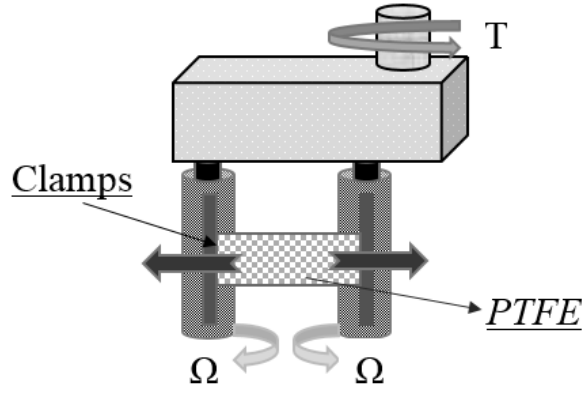


Figure 4.3: Schematic representation of SER fixture

In an extensional flow (Fig 4.3) the Hencky strain rate is given by: $\varepsilon_H = \ln\left(\frac{L}{L_o}\right)$ where L_o is the initial length of the sample and L the length of the sample at any time. By taking the derivative of the Hencky strain with respect to time, the Hencky strain rate is: $\dot{\varepsilon}_H = \frac{d\varepsilon_H}{dt} = \frac{1}{L} \frac{dL}{dt}$. For small deformations the length remains constant to L_o so the above equation becomes:

$$\dot{\varepsilon}_H = \frac{1}{L_o} \frac{dL}{dt} \quad (4.1)$$

The Hencky strain rate is related to the angular velocity of the drums and it is given by:

$$\dot{\varepsilon}_H = \frac{2\Omega R}{L_o} \quad (4.2)$$

where Ω is the drive shaft rotation rate (cycle/sec) and R is radius of the drums. The torque reading from the instrument can be converted into instantaneous force, which is: $T(t)=2R F(t)$. The cross sectional area $A(t)$ changes with respect to the initial sectional area A_o , exponentially as: $A(t) = A_o \exp(-\dot{\varepsilon}_H t)$. Finally the tensile stress can be calculated by:

$$\sigma_E = \frac{F(t)}{A(t)} = \frac{F(t)}{A_o \exp(-\dot{\varepsilon}_H t)} \quad (4.3)$$

The samples were collected and tested in tensile using the SER at 5 different Hencky strain rates, namely $\dot{\varepsilon} = 0.1-0.3-0.6-1-3$ (s^{-1}) and at four different temperatures ($T_f = 25-50-100-150$ °C) to study the effect of testing temperature on the tensile properties of PTFE extrudates, produced at different extrusion temperatures (Tables 4.5 & 4.6). To examine the

effect of extension on the density of the samples (Poisson's ratio), the samples were stretched at a fixed Hencky strain rate of $0.6 \text{ (s}^{-1}\text{)}$ up to a specific Hencky strain, before the failure point. Subsequently, the tensile stress was removed and the sample was allowed to relax for at least 24 hrs to determine the recovery and the changes of density upon relaxation.

Table 4.5: Extrusion & SER characteristics of the experimental study in Chapter 7

Extrusion Temperature (°C)			SER Temperature (°C)		
RR=56	RR=156	RR=352	RR=56	RR=156	RR=352
25	25	25	25	25	25
50	50	40	50	50	50
75	75	50	100	100	100
100	90	-	150	150	150
150	-	-	-	-	-

Table 4.6: Extrusion & SER characteristics of the experimental study in Chapter 7

Extrusion characteristics	
Paste	Homopolymer +18% Isopar H
Dies $2\alpha=90^\circ$, L/D=20	RR=352,156,56
Apparent Shear Rate (s^{-1})	517
Hencky Strain rate (s^{-1})	0.1-0.3-0.6-1-3

4.3.4.2 Compression and Tensile Testing (Com-Ten)

Another piece of equipment used for mechanical testing of samples in tensile mode was the Com-Ten fixture (Fig. 4.4). This uses linear tensile velocity. For these tests the amount of force that is required to stretch a material enough to cause permanent deformation (yield stress) is measured, as well as the maximum force measured before rupturing a material (ultimate strength) is calculated. The tensile mechanical properties were evaluated at room temperature. The instrument is equipped with a 10 kN-capacity load cell.

A schematic representation can be seen in the figure that follows. The sample which can be either cylindrical or rectangular extrudate is placed between the two clamps. The samples were elongated with the linear extensional rate of 25 mm/min, having the upper clamp only moving, while the lower was kept steady. The average values along with their standard error are reported in this work.

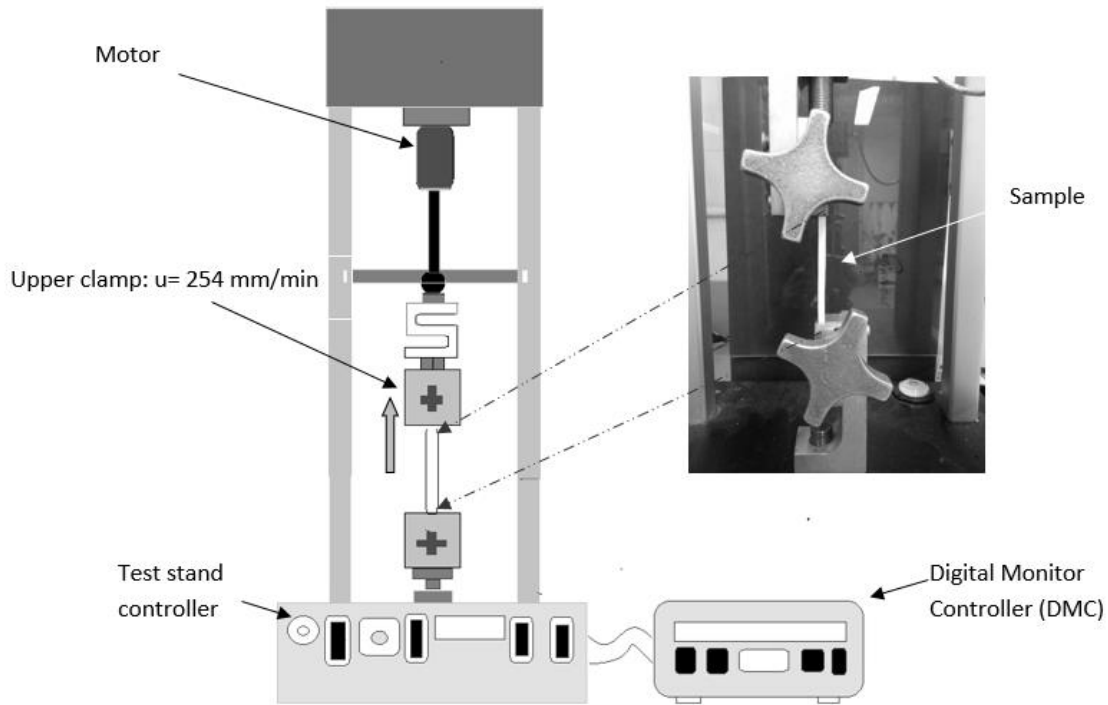


Figure 4.4: Test system overview of the Com-Ten fixture.

4.3.5 Determination of Poisson's Ratio

The determination of the Poisson's ratio was made for the various samples extruded either cylindrical or flat. As discussed above, these were tested in the SER fixture. Changes in the width and thickness of the extrudates were monitored using a digital Nikon D90 camera. These changes were converted into Poisson's ratio values, defined as the negative ratio of the transverse strain/extension to the axial strain/extension. The dimensions of the sample in both directions were determined as a function of time and/or different levels of strains using Eq. 4.4.

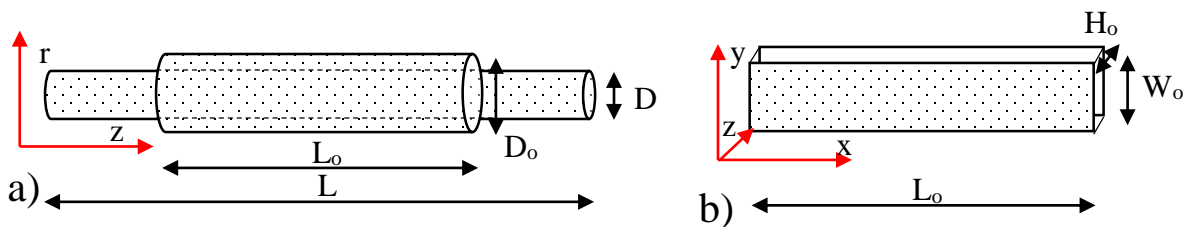


Figure 4.5: a) Schematic of a cylindrical (1-D) sample extended in the longitudinal direction and the change in the width of the sample presented and b) schematic of a flat extrudate (2-D), where all the dimensions of interest are shown, for evaluating the Poisson's ratio

For the case of the cylindrical sample (a), the Poisson's ratio is given by the following equation:

$$\nu_{zr} = -\frac{d\varepsilon_r}{d\varepsilon_z} \quad \text{or} \quad d\varepsilon_r = -\nu \cdot d\varepsilon_z \quad (\text{by setting } \nu_{zr} = \nu \text{ for sake of simplicity}) \text{ from}$$

where we obtain:

$$d\varepsilon_r = \frac{dD}{D_o} = -\nu \cdot d\varepsilon_z \quad \Rightarrow \quad \int_0^{\varepsilon_z} -\nu \cdot d\varepsilon_z = \int_{D_o}^D \frac{dD}{D_o} \quad \Rightarrow \quad -\nu \cdot \varepsilon_z = \ln\left(\frac{D}{D_o}\right) \quad \text{or}$$

$$\ln\left(\frac{D}{D_o}\right) = -\nu \cdot \dot{\varepsilon}_z^H \cdot t \quad (4.4)$$

Where D is the diameter of the sample at time t , D_o is the initial diameter of the sample and $\dot{\varepsilon}_z^H$ the Hencky strain rate used for this case. It is noted that Eq. 4.4 can be used to determine the Poisson's ratio as a function of time/ strain /strain rate, provided that tensile tests are done at different strain rates. For the case of the flat extrudate (Fig. 4.5b) the Poisson's ratio was determined by monitoring again with the use of the same camera, the changes on both the directions W : width or H : thickness, denoted as ν_{xy} and ν_{xz} correspondingly. For this case the following equations apply:

$$\ln\left(\frac{W}{W_o}\right) = -\nu_{xy} \cdot \dot{\varepsilon}_x^H \cdot t \quad \text{and} \quad \ln\left(\frac{H}{H_o}\right) = -\nu_{xz} \cdot \dot{\varepsilon}_x^H \cdot t, \quad \text{where } W, W_o \text{ the width of the sample}$$

at time t and the initial correspondingly and H, H_o the thickness of the sample at time t and the initial correspondingly.

4.3.6 Densitometer

The specific gravity (relative density) of the samples was measured by using the MD-300S Electronic Densitometer made by Qualitest International Inc (ASTM D 792). The mechanism of measurements is based on the buoyancy force i.e. by measuring the sample's weight loss upon inserting it into the water bath (with known density), one can calculate the specific gravity and the sample's volume.

4.3.7 *Field Emission-Scanning Electron Microscopy*

To study the quality and extent of fibrils formed under various conditions, SEM was used. The samples were cut in small rectangular shapes and were mounted on SEM stubs. The upper layer of the 1-D (fibrillation in 1-direction) samples was removed by using a very sharp tweezers, in order for the central layers of the samples to be viewed. The samples were painted before viewing with a colloidal silver paint, making sure not to cover the region of interest, since it has been found in the past that it was extremely important to have a well formed conducting path from the specimen surface to the SEM stub. The colloidal silver was allowed to dry overnight in an oven at either 38 or 60 °C (or for 1 hr under infra-red light), before proceeding to sputter coating. For the sputter coater the Leica EM MED 020 device was used available in the dentistry department of the University of British Columbia, Centre for High-Throughput Phenogenomics. This High-Vacuum Sputtering device with electron deflection, produces very fine-grained metal films and the PTFE samples were coated with Iridium at a film thickness of 8 nm. For imaging, the FEI Helios NanoLab 650 dual beam scanning electron microscope (SEM) was used with low acceleration voltage of 1 KV and beam diameter of 30 μm .

4.3.8 *Raman spectroscopy*

Polarized confocal Raman spectroscopy (Christy, *et al.* 2015) was used to determine the orientation of fibrils in both 1-D and 2-D extrudates (Chemistry department of the University of British Columbia). Spectra were collected from a Wide-Field Confocal Interferometric Backscattering (iSCAT)-Raman Microscopy. To have consistent results regardless of sample orientation, the laser excitation beam was depolarized. A 632.8nm Helium-Neon (HeNe) laser serves as the Raman probe. The laser is linearly polarized in a plane parallel to the surface of the table. Incident light is expanded and collimated, then directed towards an Olympus PLAPON 60x 1.42 NA oil-immersion objective by a 633nm long-pass filter (LPF) at 633nm. Backscattered Stokes-shifted light bypasses the LPF as it propagates towards the spectrometer. Confocal light is focused through a 100 μm pinhole. A Glan Thompson polarizer allows the user to select a polarization either parallel or perpendicular to that of the incident radiation. Raman light is dispersed by a Princeton Instruments IsoPlane SCT320 spectrograph and recorded using a PIXIS 100B back-illuminated CCD detector. A three-axis piezo-electric drive translates the sample with respect to the objective lens.

Twenty-five spectra were coadded from a $20 \times 20 \mu\text{m}$ area producing a representative spectrum for each region of interest (ROI). This process is repeated three times across separate ROI's for each sample. Background subtraction is applied using an iterative discrete wavelet transform (DWT) algorithm (Galloway, *et al.* 2009) with a symlet-5 basis wavelet and decomposition scale of six over ten iterations.

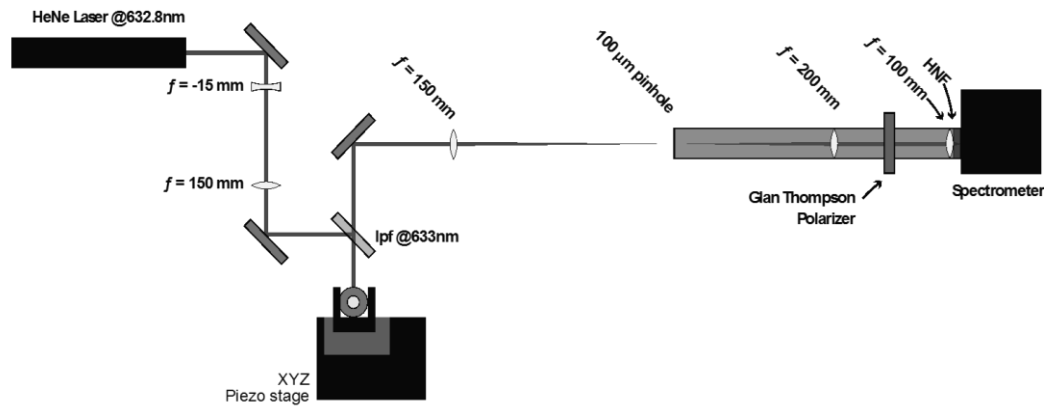


Figure 4.6: Schematic of the experimental setup of Raman spectroscopy (Christy, *et al.* 2015)

CHAPTER 5: Paste Extrusion and Mechanical Properties of PTFE

5.1 Introduction

Polytetrafluoroethylene (PTFE) is a highly crystalline polymer, which can be synthesized in the form of either homopolymer or copolymer using emulsion polymerization and it is commercially available in the form of fine powder (0.2-0.3 μm particle size) (O'Leary & Geil, 1967). As also discussed in the introduction, it is impractical to melt-extrude PTFE due to its very high melting temperature of approximately 342°C and melt viscosity of about 10 GPa.s (Sperati, 1989). Instead, it is possible to process PTFE at room temperature by mixing the PTFE powder with a suitable lubricant at concentrations typically ranging from 16 wt. % to 25 wt. % to produce a paste (Mazur, 1995; Ariawan *et al.* 2001; 2002a; 2002b; Ochoa & Hatzikiriakos, 2004; 2005; Ochoa, *et al.* 2006). After aging the prepared paste for about 24 hr, the paste is compressed under typical mild pressures of 1-2 MPa to form a billet (preform) nearly free of air (Ariawan, *et al.* 2001; Ochoa & Hatzikiriakos, 2004). The preform can be extruded using a ram driven extruder through dies, which typically possess contraction entry zones where fibrillation occurs that gives the good dimensional stability of the final product (more details have been discussed in section 2.2).

Since the physical and mechanical properties of the final product are a direct function of the quality and quantity of these fibrils, it is important to control the fibrillation process using proper processing conditions and die design. Previous studies (Ariawan, *et al.* 2001; Ochoa & Hatzikiriakos, 2005; Ardakani, *et al.* 2013a, 2013b) have shown that parameters such as the type of PTFE (molecular weight, percent and type of comonomer), the amount and type of lubricant, the extrusion temperature and die geometry characteristics including the reduction ratio, the contraction angle and to some extent the length-to-diameter ratio affect the fibrillation process and the amount and quality of the formed fibrils (also see sections 2.2 in chapter 2). While extensive studies exist on the paste extrusion of PTFE, very few have addressed carefully the mechanical properties of extrudates. Namely: (i) the dynamic response of extrudates in tensile deformation and how these are affected by the characteristics of the deformation and (ii) the density changes of extrudates in tensile deformation. These properties are important in deciding the final quality of products in operations such as tape extrusion and wire coating.

Moreover, it has been shown that the mechanical and physical properties of PTFE extrudates can also be modified by post-extrusion processing such as calendaring, stretching and thermal treatment (US PATENT 3.953.566-GORE R.W. 1976; Kurumada, *et al.* 1998; Huang, *et al.* 2008; Choi & Spruiell 2010; Ranjbarzadeh-Dibazar, *et al.* 2014). Therefore, it is possible to tailor the microstructure of the final product by applying proper extrusion and post-extrusion conditions. To this end a thorough understanding of the structure of PTFE extrudates and how this changes with post-processing i.e. stretching, is crucial.

The chapter is organized as follows: Firstly, the experimental results of the paste extrusion of two types of PTFE resins (a homopolymer and a copolymer) are discussed. The extrusion pressure is modelled as a function of flow rate and geometrical characteristics of dies by using a simple analytical model based on the *radial flow hypothesis* (Snelling & Lontz, 1960; Ariawan, *et al.* 2002b). The mechanical properties of the extrudates are evaluated in tensile mode and the effects of extrusion parameters (flow rate and die geometrical characteristics) are next discussed. Finally, the density changes of extrudates in tensile mode are also discussed and a simple model that takes into account the Poisson's ratio is developed to describe them. It has been shown that due to its fibrillated structure, fast drawing and heating of PTFE sheets would lead to creation of a porous microstructure (US PATENT 3.953.566-GORE R.W. 1976). This implies that the material is compressible and its density would change during extensional deformation. Caddock and Evans (1989) have shown that the Poisson's ratio for certain PTFE extrudates varies between 0 to -14 depending on the strain applied to the material.

5.2 Extrusion Process

Figures 5.1 and 5.2 depict the effect of reduction ratio, RR and apparent shear rate, $\dot{\gamma}_A \equiv 32Q/\pi D^3$, on the transient and steady-state extrusion pressure of C-PTFE paste (Table 4.1), respectively. First, Fig. 5.1 shows typical response obtained in transient paste extrusion, where there is a gradual increase of pressure until a maximum is reached. Until this maximum pressure, there is minimal flow due to jamming of the particles at the entrance (Snelling & Lontz, 1960; Ebnesajjad, 2000; Ariawan, *et al.* 2002a; Haw, 2004). At the maximum, the jammed network breaks and flow starts, while the extrusion pressure drops gradually to its steady-state value. It can be seen from Fig. 5.1 that the maximum increases with the reduction

ratio. Similar behavior can be observed for the variation of the steady-state extrusion pressure with the reduction ratio (Fig. 5.2).

These observations are consistent with the model developed by Ariawan *et al.* (2002a) which is later modified by Ardakani *et al.* (2013a). Fits of the Ardakani model (Ardakani *et al.* 2013a) are shown in Fig. 5.2 as continuous lines with the model parameters listed in Table 5.1 (discussed and presented below). The details of this model have been discussed before (Equation 2.6 in Chapter 2). As mentioned earlier, this model is based on the radial flow hypothesis, which assumes that paste particles have the same velocity at the same spherical radial distance from the virtual apex of the die conical zone (Snelling & Lontz, 1960). According to the radial flow hypothesis, the maximum rate of deformation in the die conical zone is proportional to the reduction ratio. Therefore, the extrusion pressure is a strong function of flow rate (apparent shear rate) for dies with higher reduction ratio as it can be seen in Fig. 5.2. Table 5.1 lists the definition and the values of the parameters that best fit the experimental results. Results for three different extrusion cases are listed, for paste extrusion of C-PTFE at 25°C and 50°C and for H-PTFE at 25°C.

Table 5.1: Radial flow model parameters (Equation 2.6).

Parameter	Definition	H-PTFE+18wt% Isopar-H(T=25°C)	C-PTFE+18wt% Isopar-H (T=25°C)	C-PTFE+18wt% Isopar-H (T=50°C)
f	Friction coefficient	0.012	0.015	0.003
n	Elastic power-law index	3.3	3.3	3.3
m	Viscous power-law index	0.95	0.97	0.95
$C' [kPa]$	Elastic proportionality constant	16.56	16.56	16.56
$K [kPa.s^m]$	Viscous proportionality constant	8.98	8.98	8.98

Another interesting result is that both the maximum and the steady-state pressures for the die having $RR=100$ are lower than the other dies. The entrance angle for all dies are the same ($2\alpha=90^\circ$) except for die with $RR=100$ which is $2\alpha=35^\circ$. Considering the smaller entrance angle of this die, one can conclude that the contribution of entrance angle in PTFE paste extrusion is a more dominant factor compared to that of the reduction ratio.

Figures 5.1 & 5.2 show the effect of entrance angle on the extrusion pressure drop for several dies having the same $L/D=20$ and $RR=351$. The steady-state pressure decreases with increase of the entrance angle from $2\alpha=10^\circ$ to $2\alpha=30^\circ$. The decrease in the extrusion pressure

at small entrance angles is similar to the trend predicted for polymer melts and other fluids using the lubrication approximation (Dealy & Wissbrun, 1990).

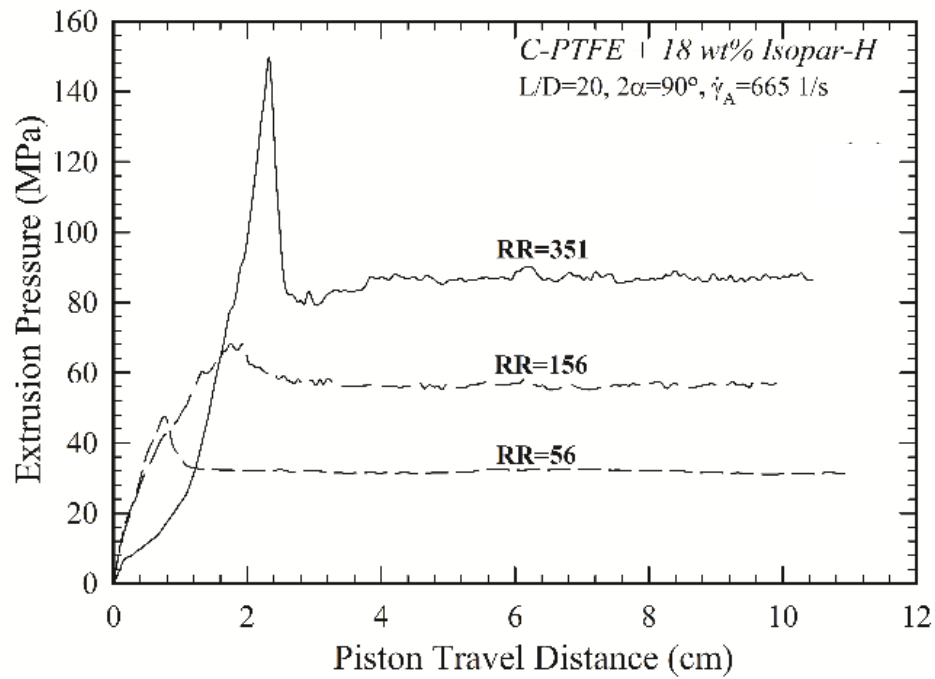


Figure 5.1: Effect of reservoir/die reduction ratio on transient extrusion pressure drop for the paste of C-PTFE+18 wt. % Isopar-H at room temperature

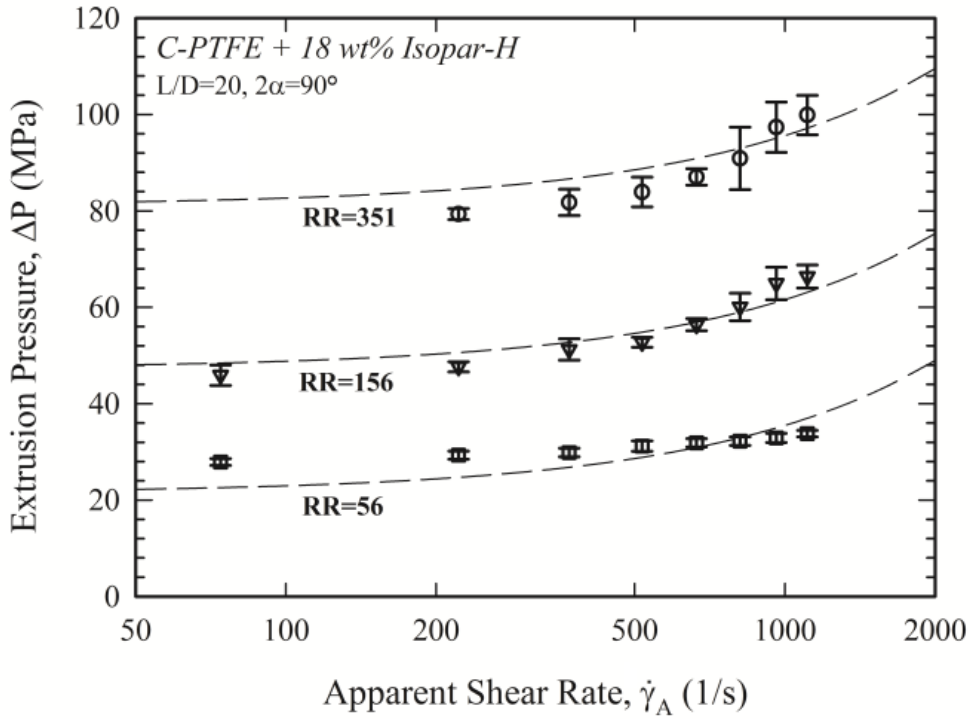


Figure 5.2: Effect of reservoir/die reduction ratio on steady state extrusion pressure drop for the paste of C-PTFE+18 wt. % Isopar-H at room temperature

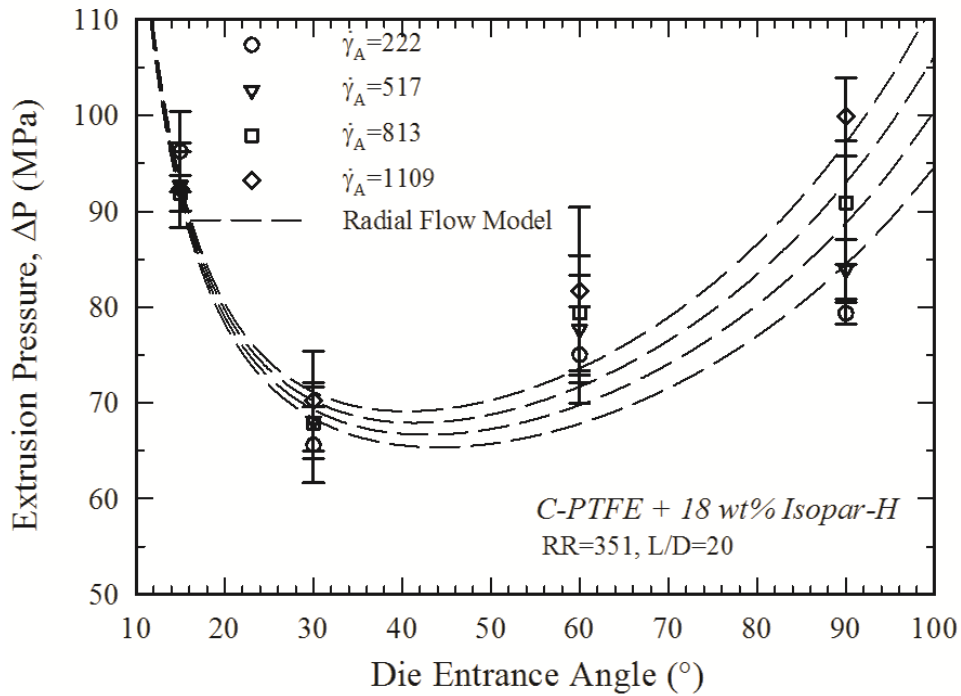


Figure 5.3: The effect of die contraction angle on the steady state extrusion pressure for the paste of C-PTFE+18 wt. % Isopar-H at room temperature

However, the lubrication approximation predicts a monotonic decrease in the extrusion pressure with increasing die entrance angle, which is not consistent with the experimental results plotted in Fig. 5.3. Beyond a certain entrance angle, the extrusion pressure increases with increasing α , as is commonly observed with the extrusion of elastic solids (Horrobin & Nedderman, 1998).

Fig. 5.4 shows the effect of the type of PTFE resin on the extrusion pressure for two dies with $RR=56$ and $RR=351$. For both dies, the extrusion pressure is slightly higher for C-PTFE.

Regarding the effect of temperature, as it is depicted in Fig. 5.5, the extrusion pressure decreases by increasing the temperature. This can be explained by the lower viscosity and higher wettability of the lubricant at higher temperatures, which results in a better lubrication and therefore possibly in a higher degree of fibrillation (Ochoa *et al.* 2006). Moreover, increasing the temperature has almost no effect on the shape of steady-state extrusion pressure vs. apparent shear rate (Fig. 5.5).

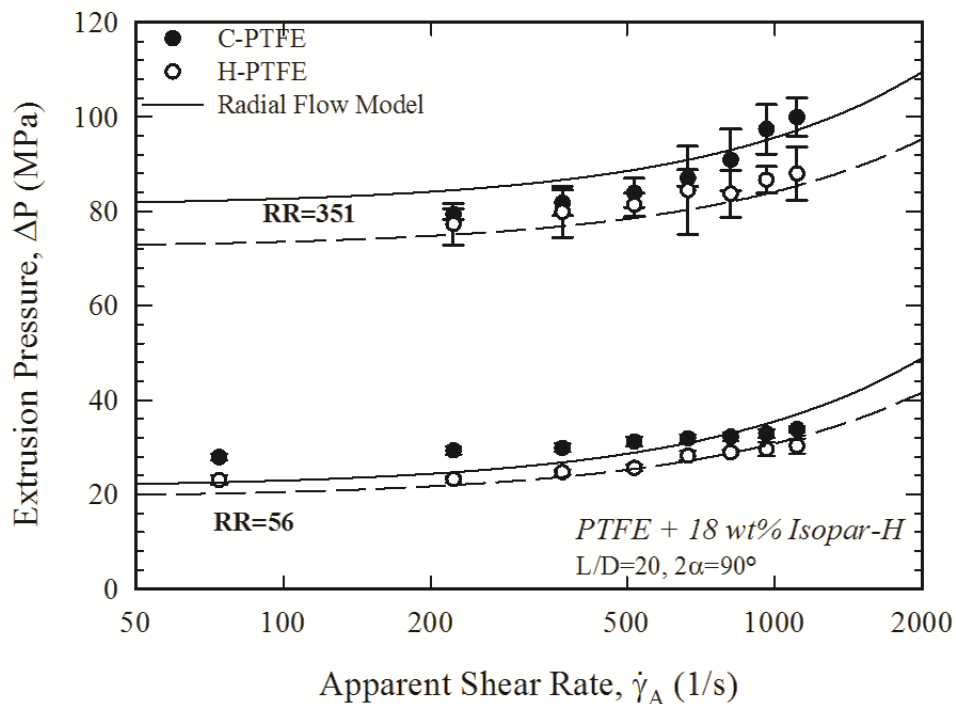


Figure 5.4: The effect of type of PTFE resin on the steady state extrusion pressure for the paste of PTFE+18 wt. % Isopar-H at room temperature

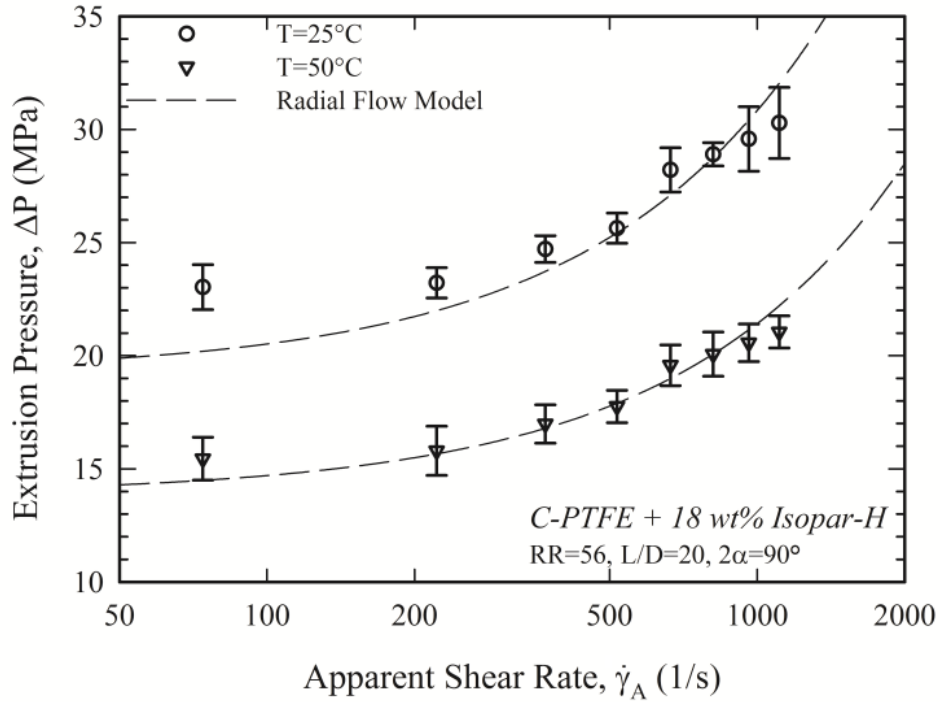


Figure 5.5: The effect of processing temperature on the steady state extrusion pressure drop for the paste of H-PTFE+18 wt. % Isopar-H

5.3 Tensile Mechanical Properties

Fig. 5.6 shows a typical transient paste extrusion experiment. The transient curve is subdivided into five different zones. In zone 1, significant compression is obtained due to jamming with minimal flow. In zone 2, flow is initiated until a steady-state extrusion pressure is obtained. In zones 3, to 5 the extrusion pressure assumes its steady-state value. Simply three equal zones in this steady state region were defined to study the variation (if any) of the mechanical properties under steady state. The purpose of this is to study the mechanical properties of extrudates collected in each zone separately.

Fig. 5.7 depicts a typical tensile test result (engineering tensile stress versus engineering strain, $\epsilon_E \equiv \Delta l/l_0$ where Δl is the change in the sample length and l_0 the initial length of the sample) defining the four mechanical properties considered in this study. The *Young's modulus*, E , is defined as the slope of the curve during the initial linear deformation. The intersection of a line with slope equal to E from 1% offset strain with the curve, results in the value defined as the *yield stress* σ_y . For stiffer materials like metals this offset is chosen as low as 0.2%. However, for softer materials like PTFE, 1% is typically chosen (same in the present

study). The *ultimate tensile strength* σ_u , is defined as the maximum tensile stress and finally the *ultimate elongation*, ϵ_u which is the sample's failure point.

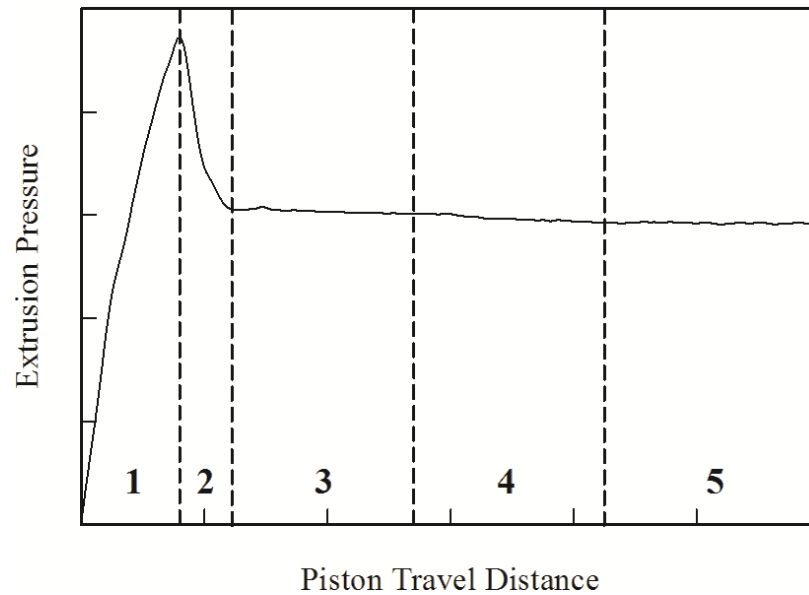


Figure 5.6: The definition of 5 extrusion zones for a typical transient pressure extrusion curve

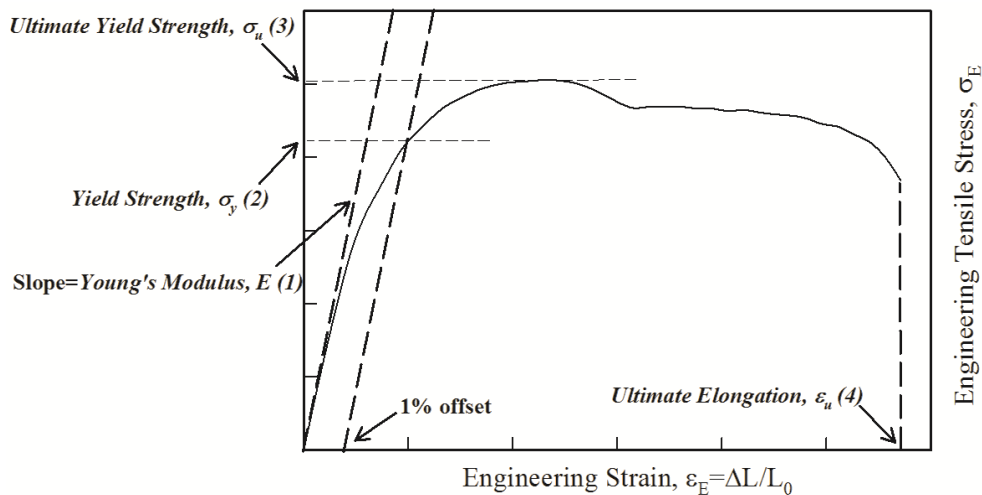


Figure 5.7: Typical tensile experiment (stress-strain curve) to illustrate the definition of four mechanical properties considered in this study

The effect of die reduction ratio RR , on the mechanical properties of extrudates collected in the five different pressure zones (Fig. 5.6) in terms of the four properties is illustrated in Fig. 5.8.a-d. From these results, one can conclude that the extrusion zone has an insignificant

effect on the mechanical properties. However, it appears that the reduction ratio (RR) plays a significant role. The elastic modulus in Fig. 5.8.a increases significantly with reduction ratio from $RR=56$ to 351 at the fixed entrance angle of $2\alpha=90^\circ$. The same trend can also be seen in Fig. 5.8.b and c for the yield stress at 1% and the ultimate tensile strength, respectively. It has been shown in previous studies that mechanical properties like tensile strength increase with reduction ratio (Ardakani, *et al.* 2013b). This is largely due to the higher degree of fibrillation that can be formed in dies having a higher reduction ratio (larger extensional strain at the die entry). Unlike the mechanical properties mentioned above, the ultimate elongational strain decreases with increase of RR . The fibrils have been extended significantly within the die having a higher RR and therefore exhibit less extensibility.

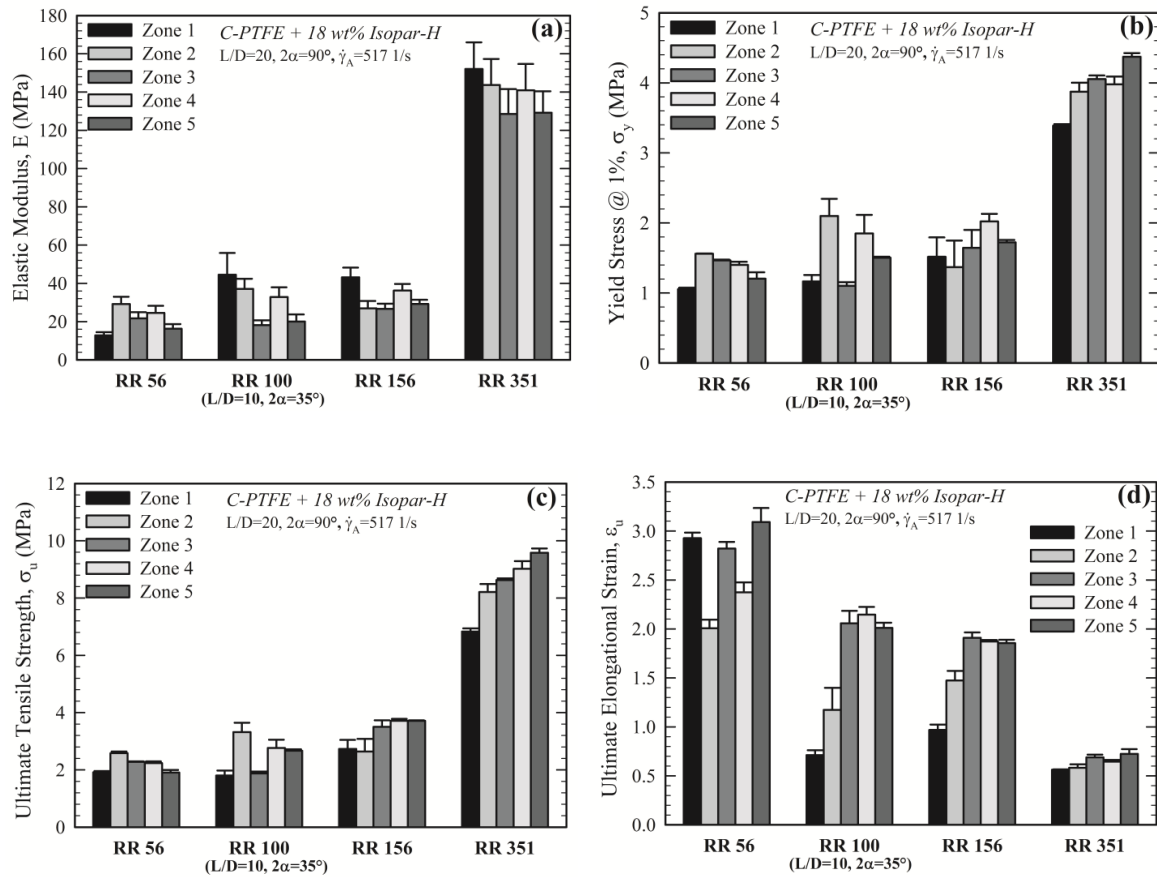


Figure 5.8: The effect of the reduction ratio and extrusion zone on (a) elastic modulus, (b) yield stress @ 1% offset, (c) ultimate tensile strength and (d) ultimate elongational strain for $C\text{-PTFE}+18\text{ wt. \% Isopar-H}$ extrudates

Fig. 5.9.a-d also show the same mechanical properties as a function of the apparent shear rate for two dies with reduction ratios of 56 and 351. These results show that the apparent shear rate does not have much of an effect on the mechanical properties of the extrudates. Previous studies (Ochoa & Hatzikiriakos, 2005; Ardakani, *et al.* 2013b) have shown that the mechanical properties decrease slightly with increase of the apparent shear rate. Breakage of the fibrils due to high strain rate at the die entry has been assumed to be responsible for that. However, based on these results, it can be concluded that the level of fibrils breakage is very low or of the same order at different flow rates.

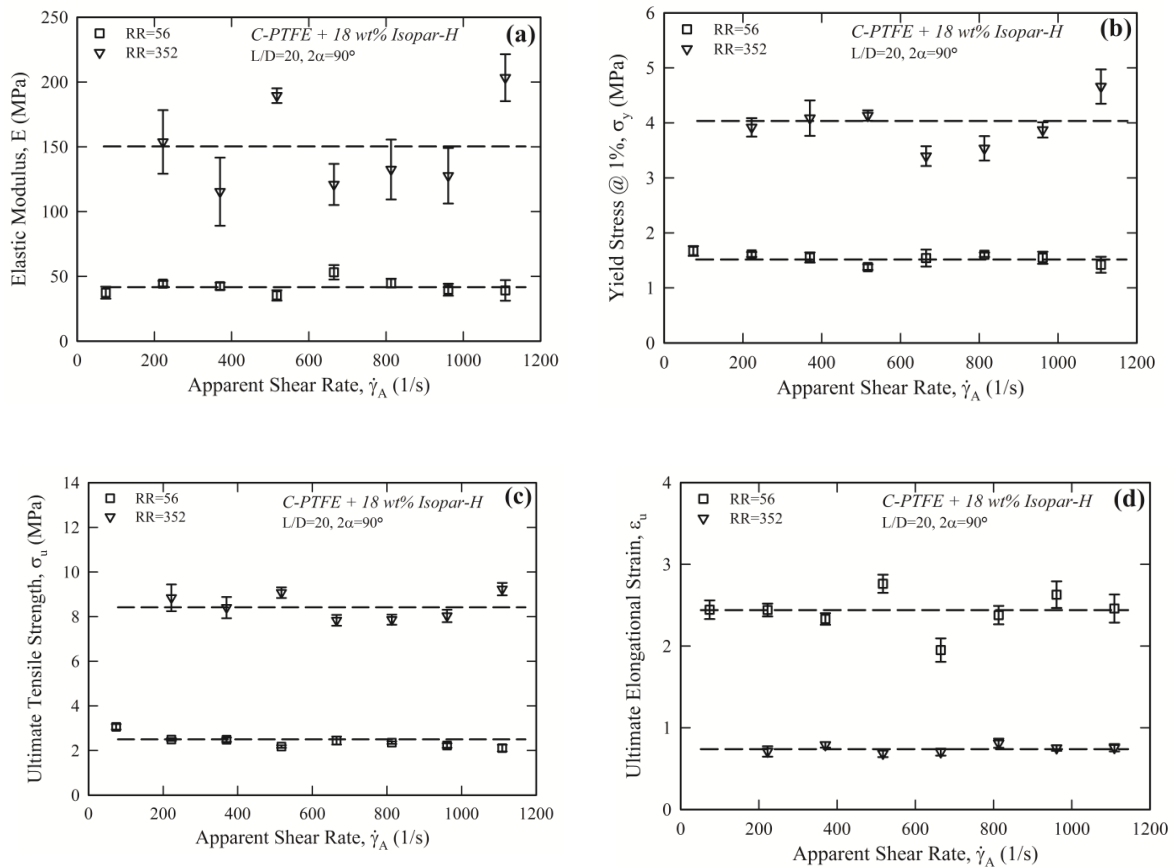


Figure 5.9: The effect of apparent shear rate on (a) elastic modulus, (b) yield stress @ 1% offset, (c) ultimate tensile strength and (d) ultimate elongational strain for C-PTFE+18 wt.% Isopar-H extrudates for dies with reduction ratios of 56 and 351

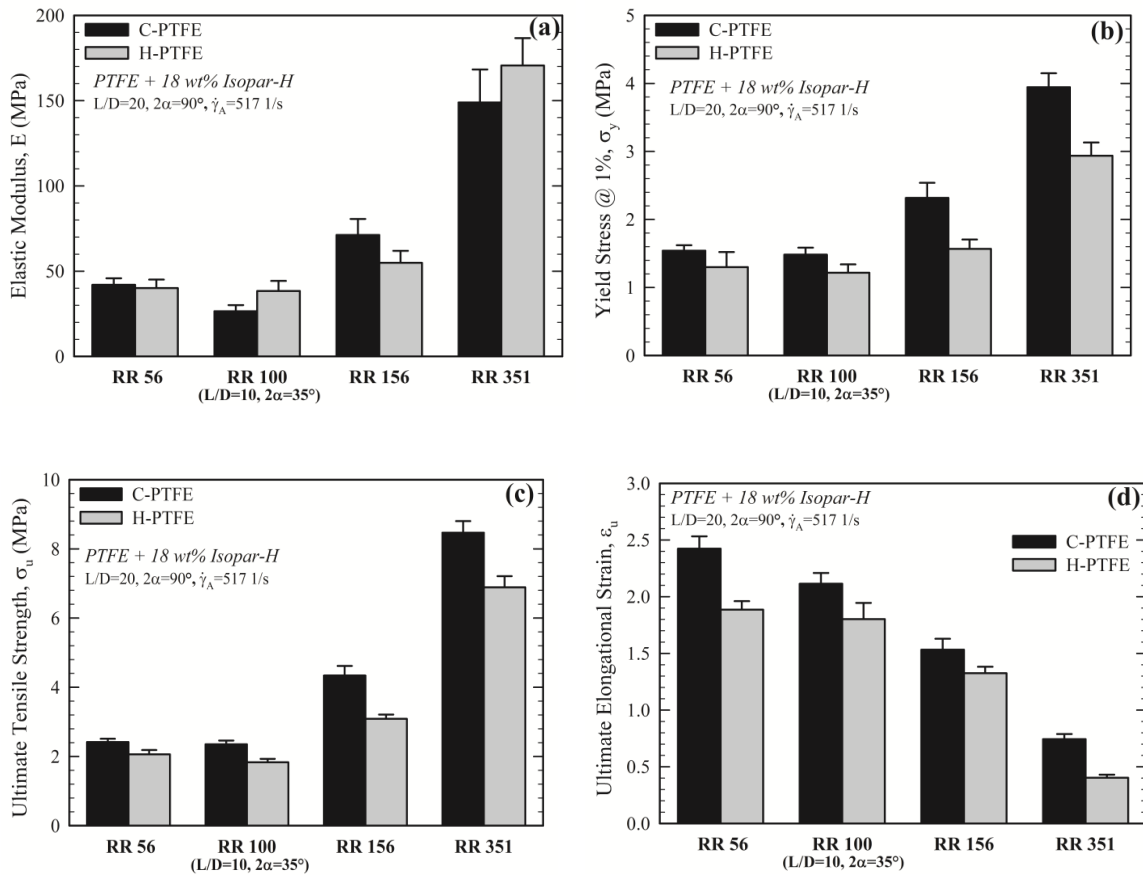


Figure 5.10: The effect of PTFE resin type on (a) elastic modulus, (b) yield stress @ 1% offset, (c) ultimate tensile strength and (d) ultimate elongational strain for dies different reduction ratio

Fig. 5.10a-d compare the mechanical parameters of the two PTFE resins for dies with different reduction ratios. The results show that the mechanical properties (σ_y , σ_u and ϵ_u) of C-PTFE are higher than those of H-PTFE. Although these differences are not large, however they are statistically meaningful. This is possibly due to small molecular differences that control the agglomeration states of these two PTFE samples. The effect of reduction ratio is also about the same for both resins.

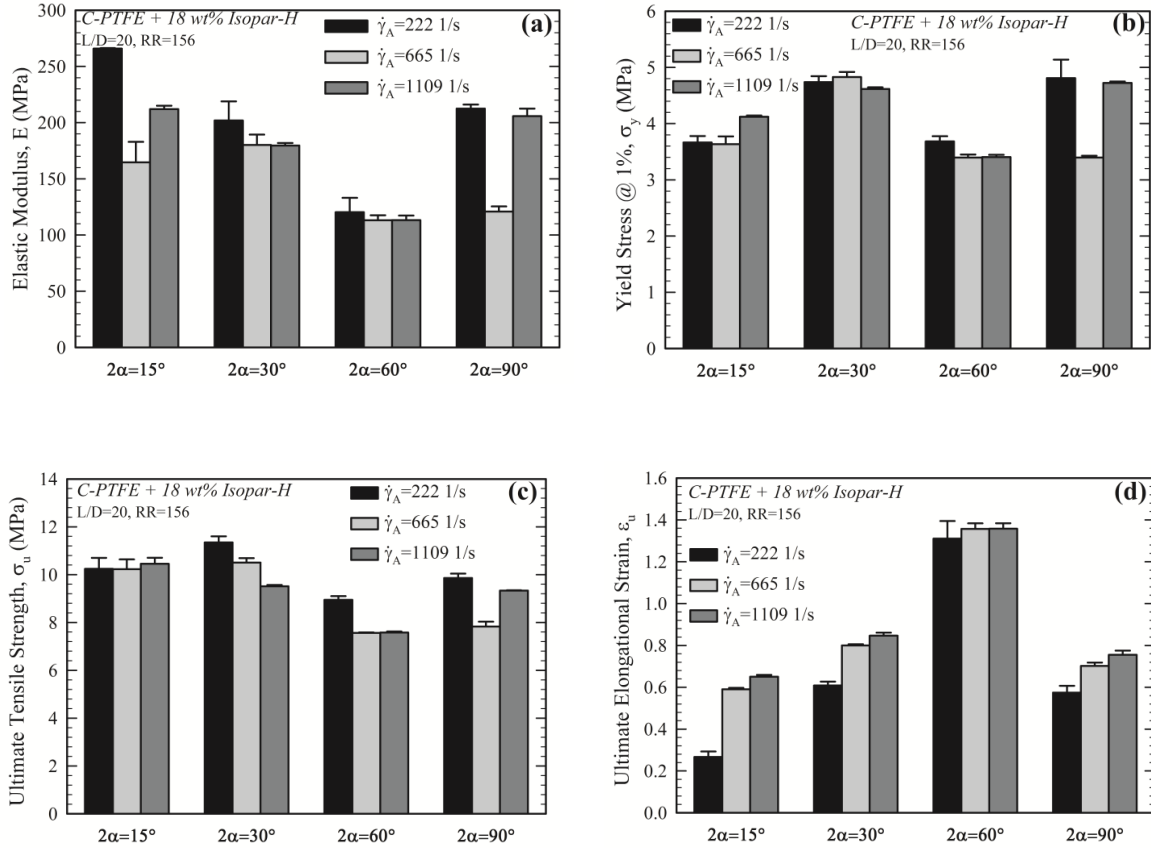


Figure 5.11: Effect of contraction angle on (a) elastic modulus, (b) yield stress @ 1% offset, (c) ultimate tensile strength and (d) ultimate elongational strain for C-PTFE+18 wt. % Isopar-H extrudates

Fig. 5.11a-d illustrate the effect of contraction angle on the mechanical properties of C-PTFE extrudates at three different values of the apparent shear rate. It can be seen in Fig. 5.11a that there is a minimum in the elastic modulus at $2\alpha=60^\circ$. The same trend can be seen for the ultimate tensile strength in Fig. 5.11c. On the other hand, the ultimate elongational strain as can be seen in Fig. 5.11d shows a maximum at $2\alpha=60^\circ$. The same trend has been observed in previous studies (Ochoa & Hatzikiriakos 2005, Ardakani, *et al.* 2013b). Ardakani, *et al.* (2013b) stated that since the Hencky strain at the die entry is a weak function of die entrance angle, the residence time is longer at smaller contraction angles. This leads to formation of more and stronger fibrils, which are responsible for the observed higher mechanical properties.

5.4 Densitometry

As it was discussed before, the microstructure of the PTFE extrudates can also be modified by post-extrusion processes such as calendaring, uniaxial and biaxial stretching including thermal treatment. This enables one to produce PTFE products with specific properties. Due to their unique fibrillated structure, PTFE extrudates possess non-isotropic and compressible structure (Guo, *et al.* 2010). Fig. 5.12a-e show the specific gravity of PTFE extrudates collected from dies having different reduction ratios as a function of the engineering strain in tensile stretching tests. The results show that the specific gravity is initially constant at low levels of strain (roughly less than 0.1) after which there is a significant reduction (volume expansion). The reduction in density as a result of stretching can be inferred from the increase in the porosity of PTFE films in previous studies (Kurumada, *et al.* 1998; Kitamura, *et al.* 1999; Huang, *et al.* 2008; Lalia, *et al.* 2013; Wang, *et al.* 2014). This clearly indicates that the samples expand at longer elongation levels with PTFE behaving as an auxetic material.

Considering the Poisson's ratio (ν) and the extensional engineering strain $\varepsilon_E = \Delta l/l_0$, one may derive the following equation for the specific gravity (or relative density RD) as a function of these two parameters:

$$RD = \frac{RD_0}{(1 + \kappa\varepsilon_E)^{1-2\nu}} \quad (5.3)$$

where RD_0 is the specific gravity at $t=0$ and κ is the portion of the imposed strain recovered. The inclusion of the effect of *recoverable strain* is due to the elastic behavior of the PTFE extrudates, which results in a retraction in the length after removing the applied tensile stress. The continuous lines are fits of Eq. 5.3 to the experimental data with the value of recoverable strain listed on the graphs (its variation and dependence is discussed below). Note that a value of $\nu=0$ results in the fitting shown in Fig. 5.12a-e, from where it is calculated the best strain recovery coefficient for each case. Thus, PTFE extruded under these conditions is a zero Poisson's ratio material.

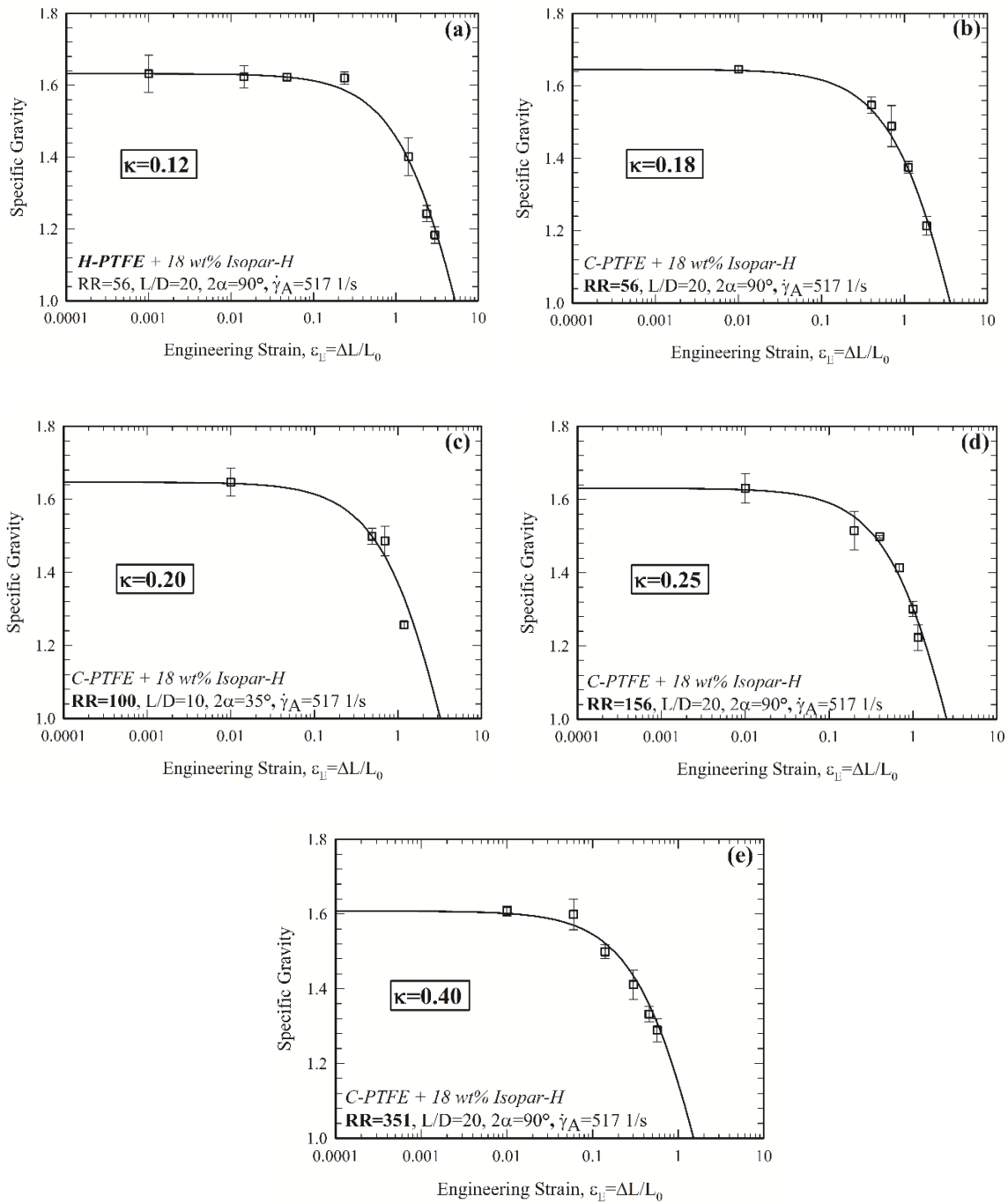


Figure 5.12: The effect of extensional strain on the specific gravity of the PTFE extrudates

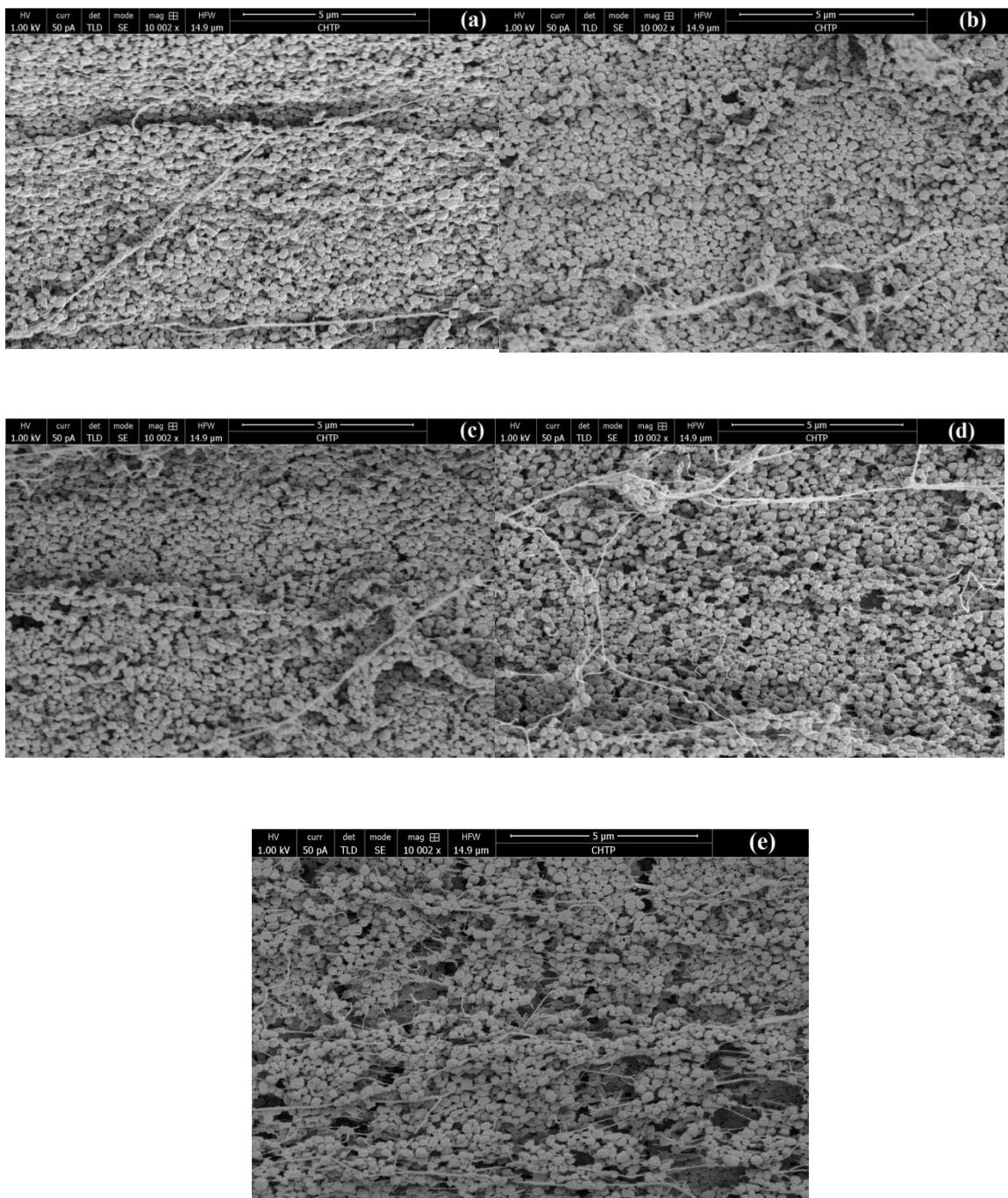


Figure 5.13: SEM micrographs of H-PTFE extrudates processed from die with $RR=56$ at extensional strain levels of (a) 0, (b) 23.8%, (c) 142%, (d) 237% & (e) 300%. The samples were extruded and extended in the horizontal direction

Figures 5.13a-e present the SEM micrographs of H-PTFE samples extruded from a die with $RR=56$, stretched at different levels of strains. As it is clear from these images, the structure consists of packed particles connected with submicron sized fibrils elongated in the direction of flow (horizontal direction). Since most of the fibrils are in the direction of

extensional deformation, the particles which consist of PTFE crystallites will not deform and in fact move in the lateral direction. This is responsible for having the width of sample remained unchanged during the tensile experiment. This implies that the Poisson's ratio is close to 0 for this material.

Fig. 5.14 depicts the recovered strain, ε_r as a function of time which is defined as:

$$\varepsilon_r(t) = \frac{[l_r(t) - l_0]}{l_0} \quad (5.4)$$

where l_r and l_0 are the extrudate lengths after removing tensile stress and at $t=0$, respectively. In this figure, the lines represent fits to the experimental data showing power-law behavior. The slope of the lines represents the time scale of the recovery. The steeper the slope is, the faster the recovery. From these results, one may conclude that the recovery process is faster when the extrudate is stretched more. Moreover, according to Eq. 5.4, $\varepsilon_r(0)$ and $\varepsilon_r(\infty)$ are the imposed and ultimate recovered strains, respectively. Therefore the parameter κ in Eq. 5.3 can be calculated as $\kappa = \varepsilon_r(\infty)/\varepsilon_r(0)$ which is found to take values with an average of 0.18 (Fig. 5.13b) for the experimental data depicted in Fig. 5.14.

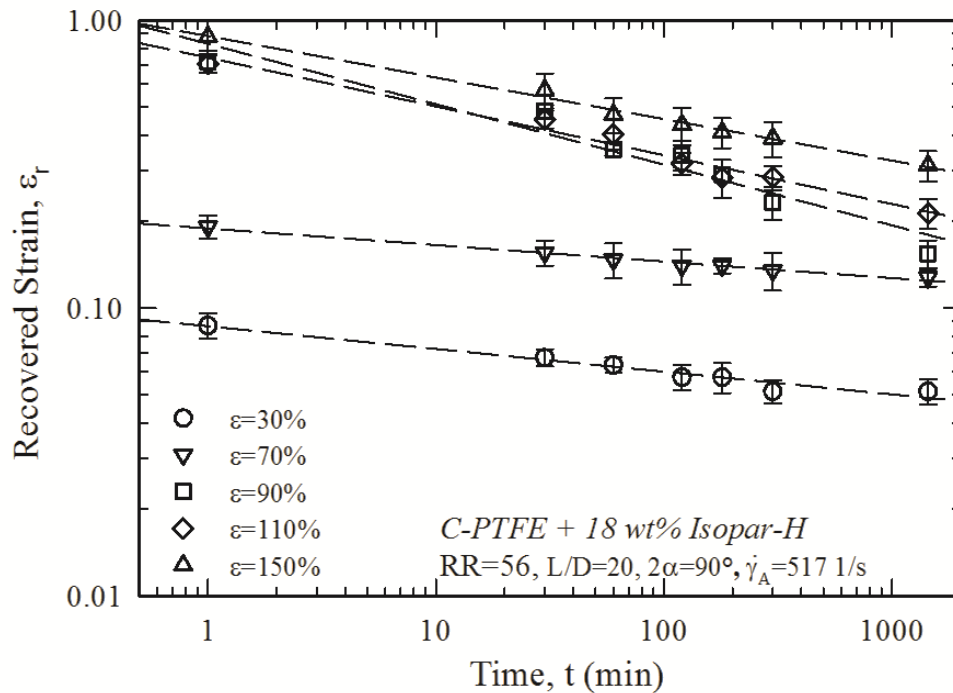


Figure 5.14: The recovered strain versus time for different extensional strains for C-PTFE+ 18 wt. % Isopar-H extruded from die with reduction ratio of 56

Another method to calculate the value of κ is to use SEM micrographs. As it can be seen from Fig. 5.13a-e, imposing extensional deformation would lead to breakage of some fibrils and creation of voids. The area of the voids and particles were calculated using *ImageJ* (image analyzing software). The value of \mathcal{K} found to be in the range of 0.09-0.14 for different levels of strain. This agrees with the value of 0.12 determined from fitting the data in Fig. 5.12a.

Fig. 5.15 illustrates that a linear relationship exists between the strain recovery coefficient \mathcal{K} and the reduction ratio of the die. In other words, the extrudates obtained from dies having a different *RR*, have a certain morphology characterized roughly by this single parameter \mathcal{K} . The higher the value of \mathcal{K} for high reduction ratio implies a higher elasticity of the extrudates due to its higher level of fibrillation.

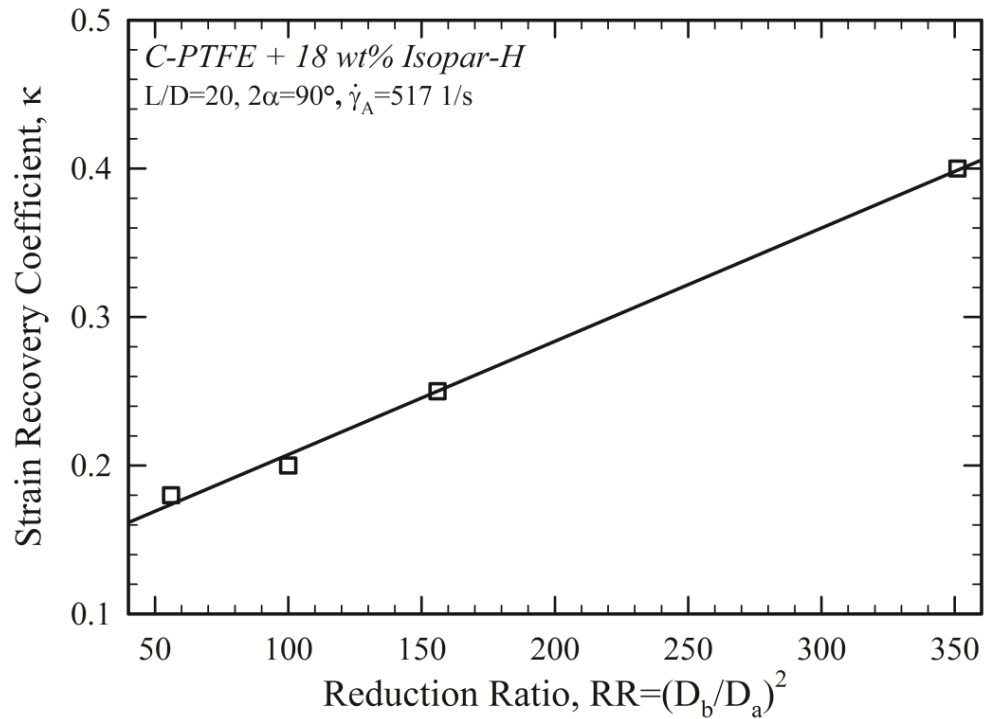


Figure 5.15: The strain recovery coefficient κ as a function of reduction ratio for C-PTFE+ 18 wt. % Isopar-H extrudates

5.5 Summary

In this chapter we have studied the extrusion of two types of PTFE pastes, a homopolymer and a copolymer using dies with different reduction ratios (RR) and entrance angles. In all cases the transient pressure drop has shown a maximum followed by a plateau (steady-state). The extrusion pressure shows a weak increase with shear rate over a wide range

of flow rates and a more significant increase with reduction ratio. Moreover, the extrusion pressure exhibited a minimum for entrance angle around 30° . A simple analytical model based on the radial flow hypothesis has been found to represent the extrusion pressure adequate well as a function of flow rate (shear rate) and geometrical characteristics of the capillary dies.

The extrudates collected at different processing conditions were dried and tested in uniaxial extension to assess their effect on mechanical properties. The tensile mechanical properties of PTFE paste extrudates were also studied. Four different properties were defined and studied, namely the tensile Young modulus, the yield stress, the ultimate tensile strength and the ultimate elongational strain. The tensile modulus, yield stress and ultimate tensile strength of the obtained extrudates were found to be increasing functions of reduction ratio, although the opposite effect was found for the ultimate elongational strain. It has been concluded that the extrudates become stiffer and less extensible by increasing the die reduction ratio. On the other hand, it was shown that the entrance angle has a small effect on the extrudate stiffness although a maximum has been obtained at the contraction angle of 60° for the ultimate elongational strain.

Finally, it was found that the specific gravity of the PTFE extrudates decreases in uniaxial extension due to its compressibility. The PTFE paste extrudates show a Poisson's ratio equal to zero in tensile experiments, thus exhibiting expansion (significant density reduction with stretching). It was also shown that the effect of tensile strain on the specific gravity can be modeled simply by taking into the account the Poisson's ratio, which was found to be zero for this material and the strain recovery that is the portion of the imposed strain that is recovered upon removal of the imposed tensile stress.

CHAPTER 6: Effect Of Extrusion Mode On PTFE Extrudates: Flow Rate Control Vs. Load Control

6.1 Introduction

In this chapter the process of paste extrusion will be examined under two modes of operation, namely i) flow rate control and ii) load control. It is hypothesized that the former mode of operation leads to a constant diameter of extrudate, while the second to a constant density. For some industrial operations or products it is desirable to have a control of density (wire/cable industry for constant dielectric properties) (Nelson, 1983) and in others to have control of diameter or width (stretch tapes) (Ebnesajjad, 2017).

This hypothesis has not been examined or tested before and it is important to study whether or not the diameter of the extrudate or its density could be changed in a controlled way. For the rate control mode, the capillary extrusions were performed under a constant apparent shear rate defined by:

$$\dot{\gamma}_A \equiv 32Q / \pi D^3 \quad (6.1)$$

where Q is the flow rate and D is the die diameter.

For the load control mode, the experiments were performed under a constant extrusion pressure. In this mode the apparent shear rate was calculated based on the following equation

$$\dot{\gamma}_A \equiv 8v_p D_b^2 / D^3 \quad (6.2)$$

where v_p is the piston speed. The resin that was used specifically for these experiments was HMW H-PTFE F104 provided by DAIKIN. The physical properties of this resin are listed in Table 4.2. The PTFE pastes used were prepared as described in Chapter 4 using Isopar H (15.25 or 18 wt. %).

6.2 Extrusion Under Flow Rate Control Mode

Fig. 6.1 shows a typical extrusion test in terms of the transient pressure (right axis – continuous line) and average diameter of the extrudate (left axis) as functions of time. The H-PTFE paste was extruded with a die having a reduction ratio, $RR=56$ at a constant shear rate of $\dot{\gamma}_A = 74 s^{-1}$. As seen from the results depicted in Fig. 6.1 there was practically no difference in the diameter between the dried and wet samples. The average diameter of the wet samples was $1.272 \pm 0.012 mm$ while that of the dry samples was $1.273 \pm 0.010 mm$. The increase of

pressure towards the end of the extrusion run has also been reported in the past by previous researchers (Ariawan, PhD Thesis, 2001; Ochoa, PhD Thesis, 2006) and it has to do with the liquid migration of the lubricant, which leads to an increase in the extrusion pressure (the paste becomes drier towards the end). However, the increase of the diameter towards the end of the extrusion was noticed also in these experiments and might also be attributed to the increase of the pressure due to lube migration.

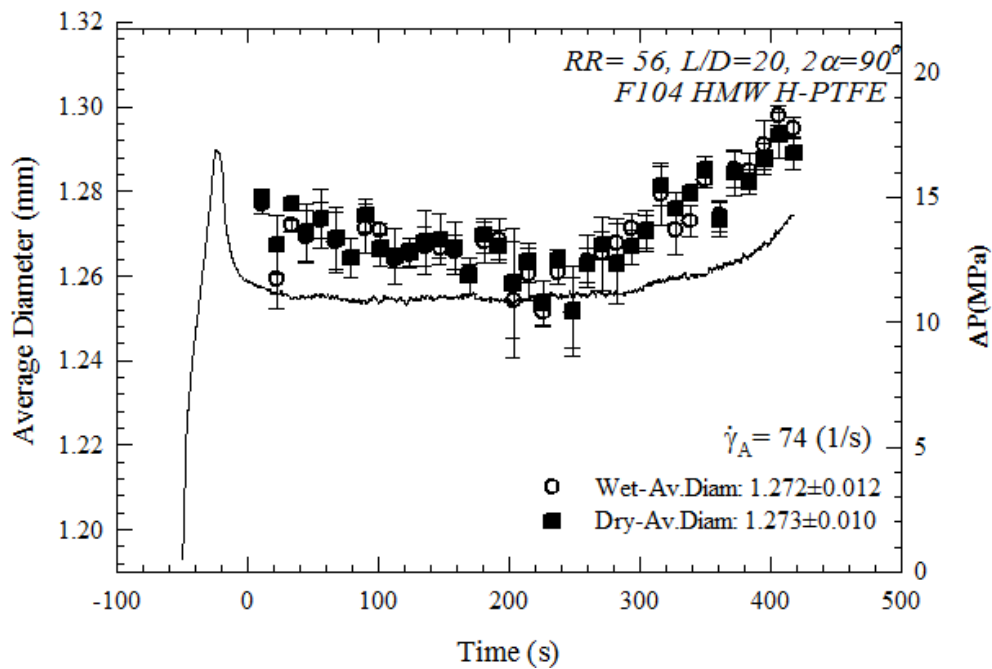


Figure 6.1: Average diameter of wet and dry extrudates produced at a capillary extrusion of PTFE paste (F104 HMW H-PTFE) at the shear rate of 74 s^{-1}

Fig.6.2 depicts the specific gravity of the extrudates for the same experiment at $\dot{\gamma}_A = 74 \text{ s}^{-1}$. The specific gravity of the wet sample fluctuates due to variability of the lubricant concentration in each segment (nonuniformity due to mixing in the preparation of the preform). However, for the case of dry samples the specific gravity has more steady values (less fluctuations). As was also listed in the graph, the average specific gravity of the wet samples was 1.651 ± 0.07 , whereas that of the dry samples was 1.598 ± 0.034 . A small reduction in the density after drying is also seen (3.2%) due to lube evaporation.

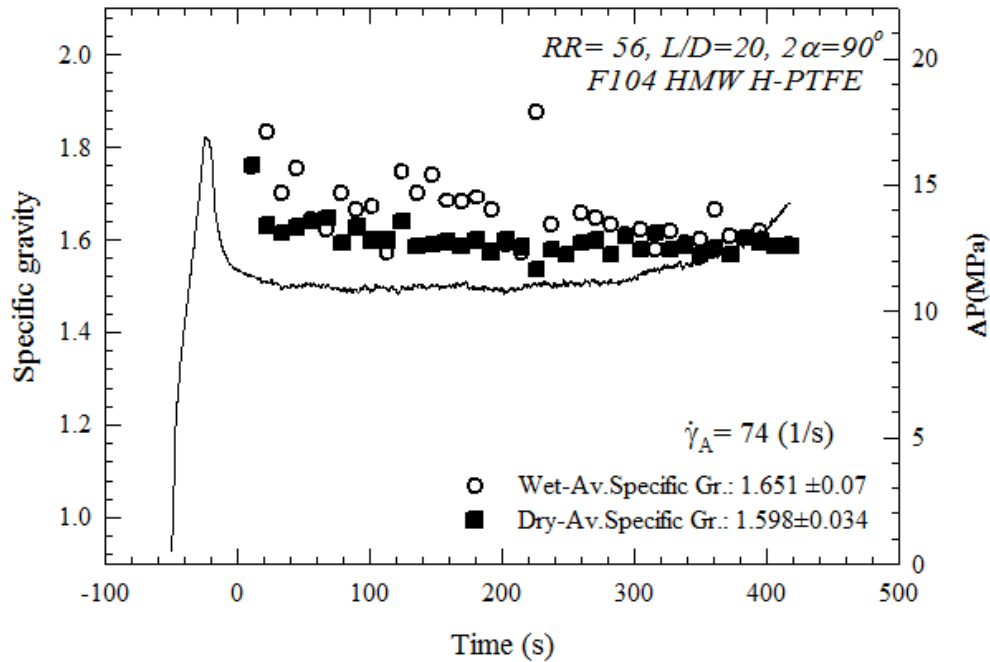


Figure 6.2: Average specific gravity of wet and dry extrudates produced at a capillary extrusion of PTFE paste (F104 HMW H-PTFE) at the shear rate of 74 s^{-1}

Fig. 6.3 shows the comparison of the average diameter and the average specific gravity of dry extrudates for the same experimental run (Fig. 6.1 and 6.2). It is noted that although the average diameter remains constant during the steady state extrusion, this is not the case for the average specific gravity, which seems to exhibit more fluctuating values (also seen from the standard deviation reported above).

When similar experiments were performed at higher shear rates namely $\dot{\gamma}_A = 517 \text{ s}^{-1}$ and $\dot{\gamma}_A = 1109 \text{ s}^{-1}$ respectively, increase in the extrusion pressure due to lubricant migration was not observed. These experiments are faster and liquid migrations is indeed a function of time observed only at low extrusion rates (Ariawan, *et al.* 2001). A higher extrusion rate implied significantly less time and this minimizes liquid migration. However, the same trends are observed for the extrudate diameter and specific gravity from the results plotted in Fig. 6.4 and 6.5, that is the extrudates appear to have constant diameter and specific gravity with higher fluctuating values in specific gravity. The results are summarized in Table 6.1 and 6.2 for the diameter and specific gravity at three apparent shear rate values.

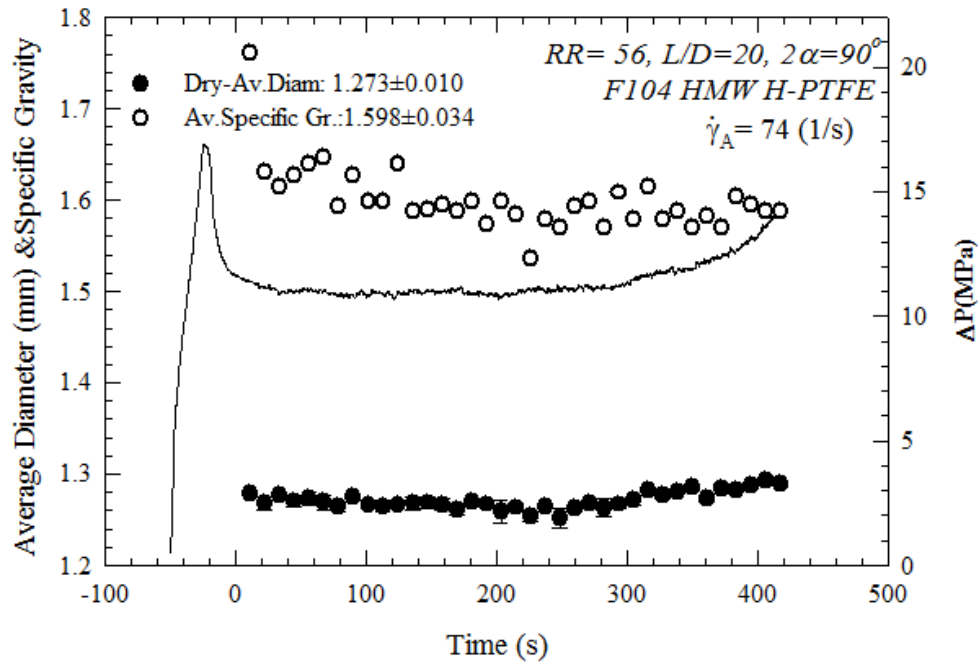


Figure 6.3: Average diameter and specific gravity of dry extrudates produced at a capillary extrusion of PTFE paste (F104 HMW H-PTFE) at the shear rate of 74 s^{-1} .

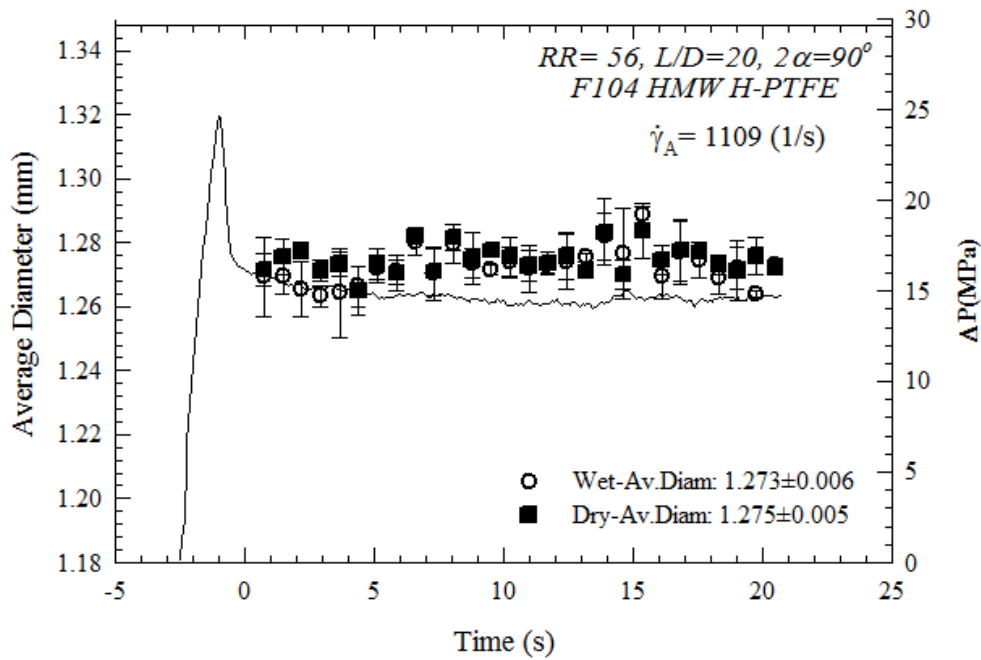


Figure 6.4: Average diameter of wet and dry extrudates produced at a capillary extrusion of PTFE paste (F104 HMW H-PTFE) at the shear rate of 1109 s^{-1} .

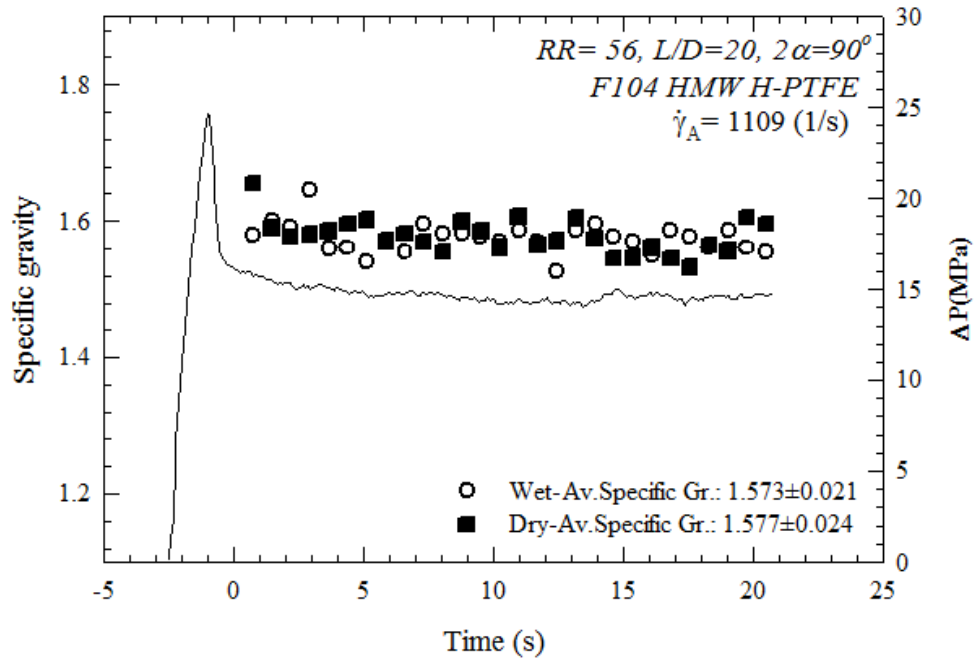


Figure 6.5: Average specific gravity of wet and dry extrudates produced at a capillary extrusion of PTFE paste (F104 HMW H-PTFE) at the shear rate of 1109 s^{-1}

Table 6.1: Average diameter and specific gravity of wet extrudates produced from die with RR=56 under flow rate control (shear rate) mode

$\dot{\gamma}_A$ (s^{-1})	\bar{D} (mm)	SD (mm)	$\bar{\rho}$	SD
74	1.272	0.012	1.651	0.070
517	1.264	0.008	1.672	0.088
1109	1.273	0.006	1.573	0.021

Table 6.2: Average diameter and specific gravity of dry extrudates produced from die with RR=56 under flow rate control (shear rate) mode

$\dot{\gamma}_A$ (s^{-1})	\bar{D} (mm)	SD (mm)	$\bar{\rho}$	SD
74	1.273	0.010	1.598	0.034
517	1.266	0.005	1.602	0.022
1109	1.275	0.005	1.577	0.024

6.3 Extrusion Under Load Control (Pressure Drop) Mode

Fig. 6.6 shows the apparent shear rate results (right axis) of H-PTFE extruded with a die having RR=56 under a constant fixed pressure (11.1 MPa) along with the average change in diameter of wet and dry extrudates (left axis) as functions of time. The experiment started initially under constant flow rate to initiate flow and once it reached steady state, it was switched to constant load (pressure) mode. Eq.6.2 was used to calculate the average apparent

shear rate from the piston speed which was found to be 92 s^{-1} . Another method for calculating the apparent shear rate was from weighing the mass of the extrudate collected during steady state over a specified period of time. For example for one case the extruded mass was found to be 7.78 g and the extrusion time was 256 s. The volumetric flow rate is $Q = \frac{\dot{m}}{\rho} = \frac{m}{\rho t}$ and from Eq. 6.1. $\dot{\gamma}_A = \frac{32Q}{\pi D^3} = 89 \text{ s}^{-1}$, a value very close to the value of 92 s^{-1} calculated from Eq.6.2.

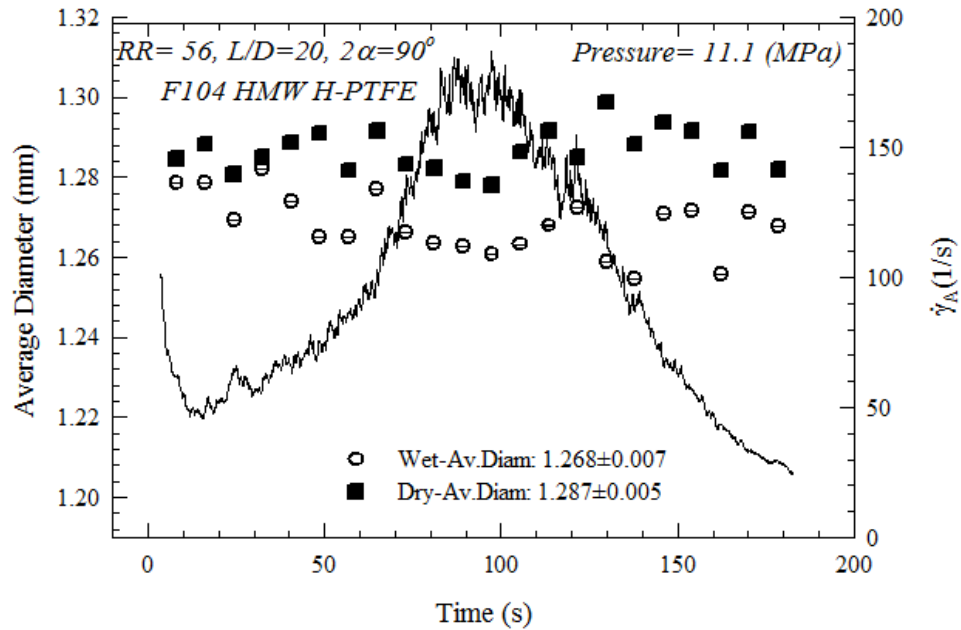


Figure 6.6: Average diameter of wet and dry extrudates produced under load control mode (11.1 MPa)

Fig.6.6 shows that under this mode of operation the average diameter changes between wet and dry sample due to elastic recovery upon removing the lubricant by drying it in a vacuum oven overnight.

Fig.6.7 shows for the same constant pressure of $P = 11.1(\text{MPa})$, that the specific gravity of the wet sample fluctuates due to nonuniform lubricant concentration in each segment. However, for the case of dry samples, the specific gravity has steadier (less fluctuating) values. Fig.6.8 again compares the results for the dry samples in average diameter and specific gravity. The trends observed are the same as in constant speed (shear rate) mode that is the average diameter exhibits less fluctuations compared to that of the specific gravity. That becomes more

obvious by noting the standard deviation values for both the diameter and specific gravity values of the dried samples: 0.005 and 0.033 correspondingly.

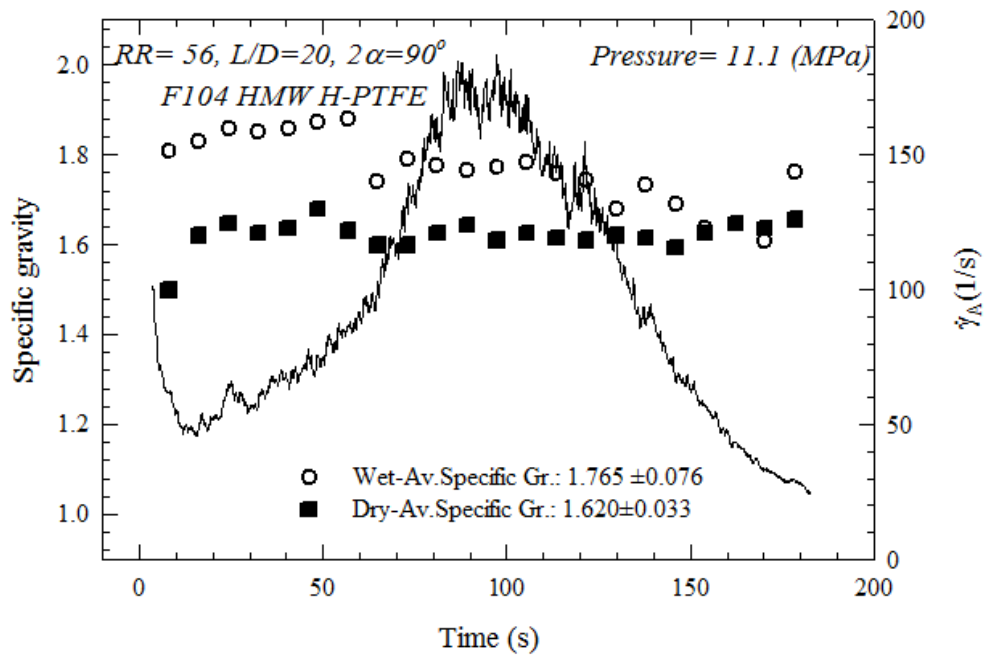


Figure 6.7: Average specific gravity of wet and dry extrudates produced under load control mode (11.1 MPa)

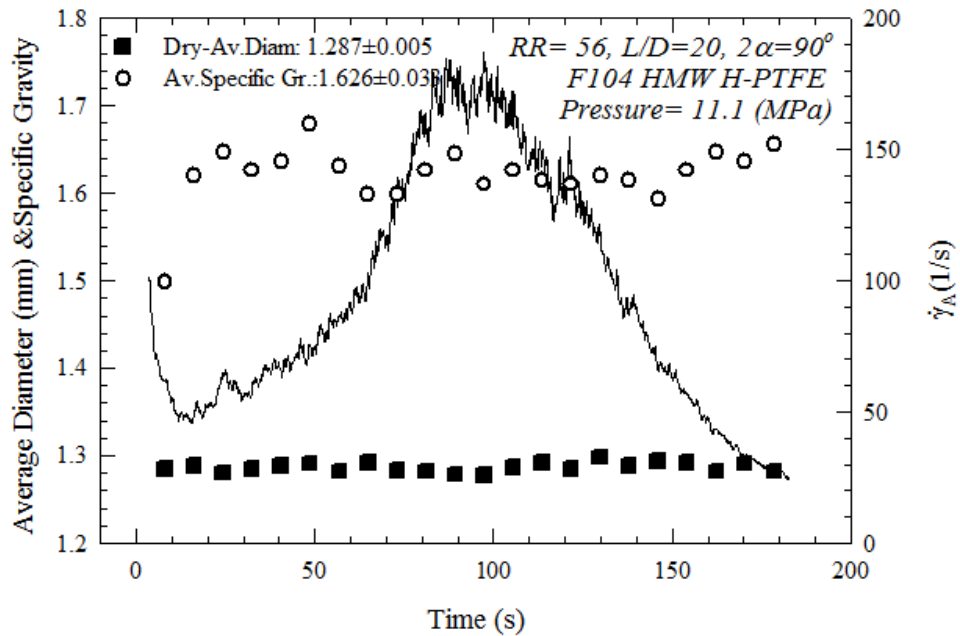


Figure 6.8: Average diameter and specific gravity of dry extrudates produced under load control mode (11.1 MPa)

Similar experiments were performed at higher loads namely at 16.66 (MPa) and 18.63 (MPa) and identical trends were observed with those discussed for the load control mode of 11.1 MPa i.e. density has steadier values for dried extrudates. Fig. 6.9, 6.10 and 6.11 present the results for the highest load of 18.63 MPa used. It can be concluded for all cases that the average diameter for the dried samples increases compared to the diameter of wet samples. The specific gravity shows the same trend for all cases tested as for shear rate mode control (drier sample gives steadier values to density). The data for the second mode (load control) are summarized in Tables 6.3 and 6.4.

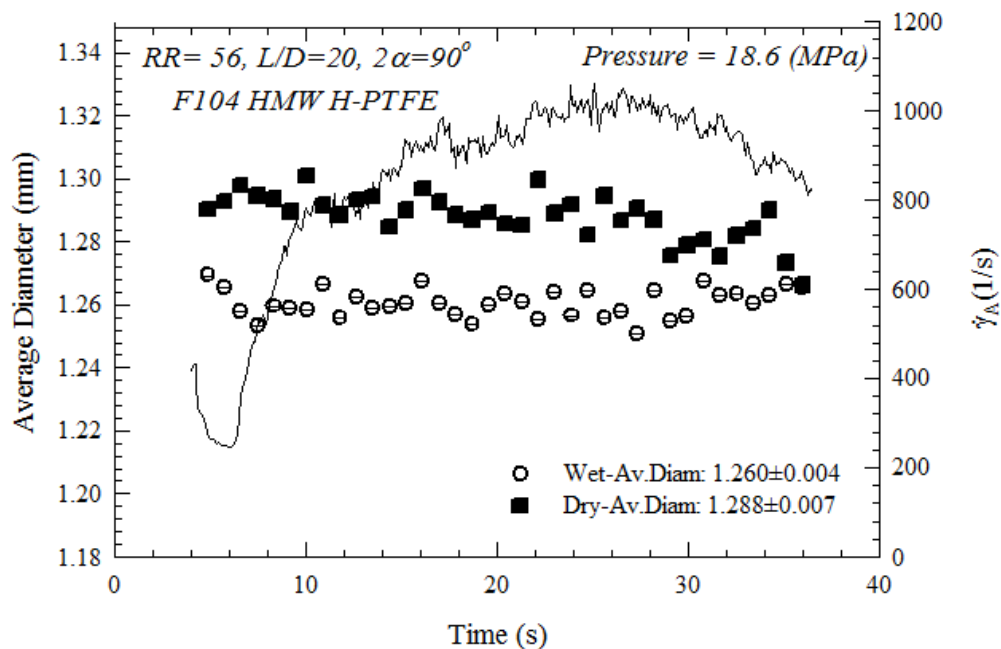


Figure 6.9: Average diameter of wet and dry extrudates produced under load control mode (18.6MPa)

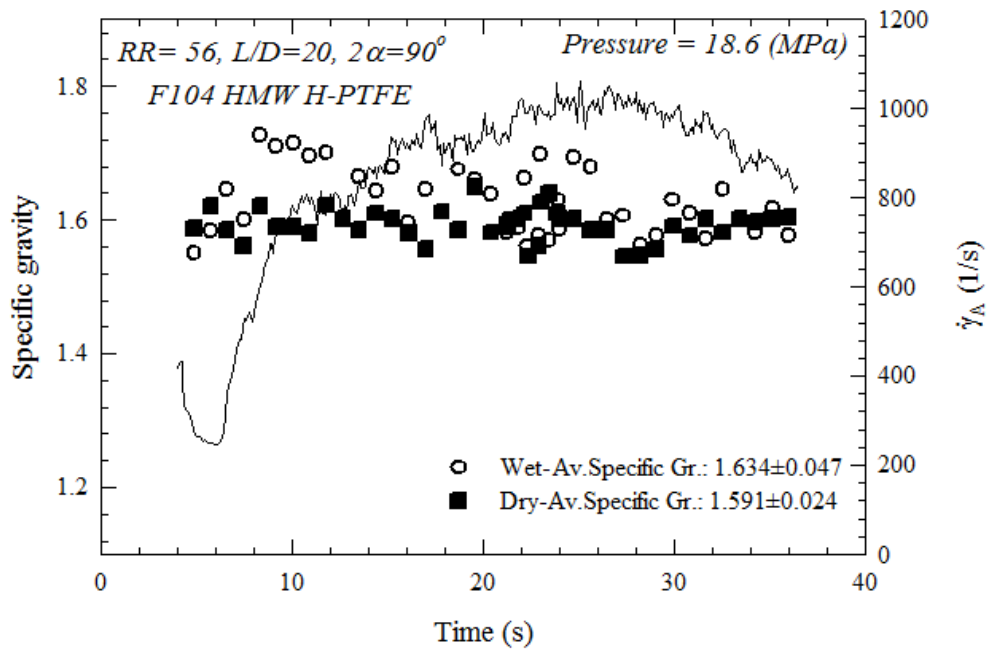


Figure 6.10: Average specific gravity of wet and dry extrudates produced under load control mode (18.6 MPa)

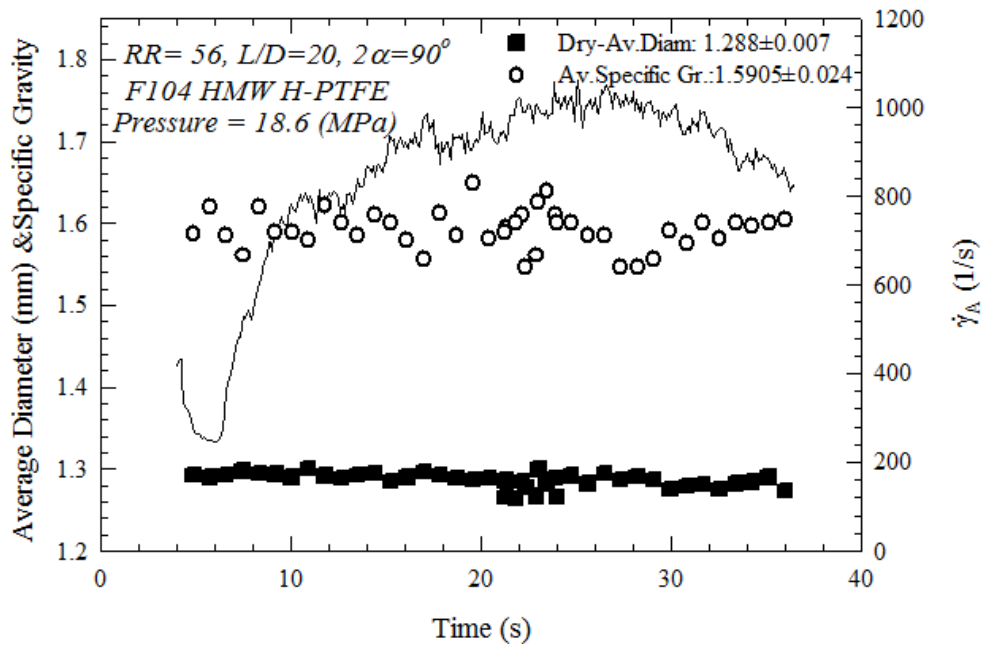


Figure 6.11: Average diameter and specific gravity of dry extrudates produced under load control mode (18.6 MPa)

Table 6.3: Average diameter and specific gravity of wet extrudates produced from die with RR=56 under load control (Pressure)

$\dot{\gamma}_A$ (1/s)	\bar{D}	SD	$\bar{\rho}$	SD
74	1.268	0.007	1.765	0.076
517	1.263	0.006	1.702	0.063
1109	1.261	0.008	1.634	0.047

Table 6.4: Average diameter and specific gravity of dry extrudates produced from die with RR=56 under load control (Pressure)

$\dot{\gamma}_A$ (1/s)	\bar{D}	SD	$\bar{\rho}$	SD
74	1.287	0.005	1.620	0.033
517	1.286	0.005	1.610	0.025
1109	1.288	0.007	1.591	0.024

Comparing the data listed in Tables 6.3 and 6.4, it can be concluded that under load control mode, the diameter of the sample slightly increases upon removal of the lubricant from the oven. However, the density remains almost the same for both modes of operation. So far it can be concluded that both modes of operation show similar results with some minor differences which seem to be more due to experimental error.

Table 6.5 summarizes the results obtained when the process is operating under both control modes and calculating the apparent shear rate values for the load control mode from Eq.6.2. The results are depicted on Fig 6.12 in terms of the flow curves. The open symbols show the average pressure drop that corresponds to the extrusion of the whole PTFE paste in the reservoir. There is an error of less than 10% between the two modes of operation (acceptable and attributable to experimental error). To explain the differences in the pressure drop between the two modes of operation we have repeated the experiments by performing both modes on the same experimental run i.e. the experiment started at shear rate control mode and when the steady state pressure drop was reached, it was switched to load control mode. The results for three different shear rates can be seen on the same flow curve with filled symbols. As discussed above this type of experimental agreement (within 10%) is considered acceptable.

Table 6.5: Values of the flow curve for both modes of operation under different runs

Shear Rate Control Mode		Load Control Mode	
$\dot{\gamma}_A$ (1/s)	P(MPa)	$\dot{\gamma}_{A,CALC.}$ (1/s)	P(MPa)
150	11.94	169.6	12.49
221	12.19	225.3	14.37
517	14.44	526.4	16.23
813	16.21	810.9	17.49
1109	17.28	1023.8	18.92

Table 6.6: Values of the flow curve for both modes of operation under same runs

Shear Rate Control Mode		Load Control Mode	
$\dot{\gamma}_A$ (1/s)	P(MPa)	$\dot{\gamma}_{A,CALC.}$ (1/s)	P(MPa)
221	12.50	261	12.50
517	14.00	515	14.00
1109	15.95	933	15.95

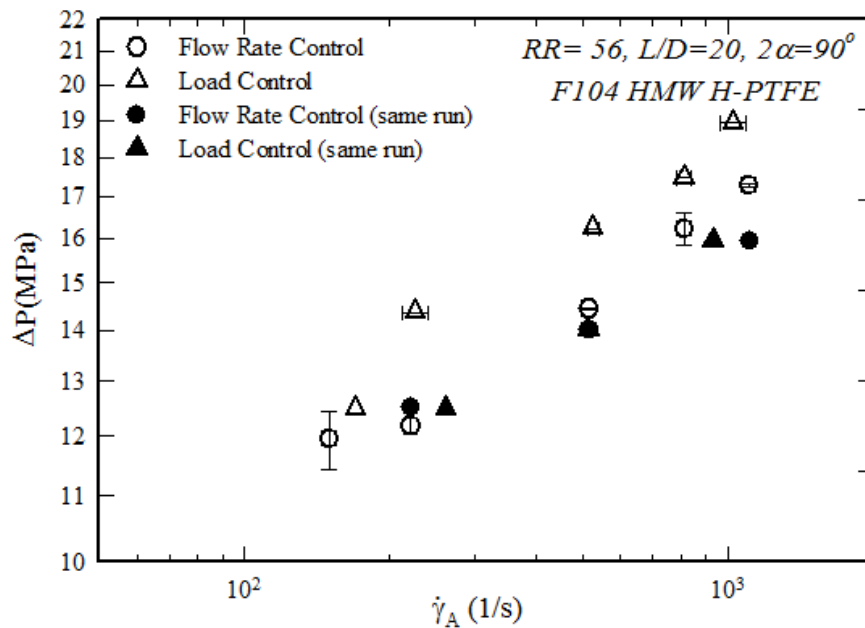


Figure 6.12: Flow curve of PTFE (F104 HMW H-PTFE) paste obtained for both modes of operation using a die having $RR=56$.

Fig. 6.13 and 6.14 are sample transient results under both modes of operation under the same experimental run. The same trend was observed with a maximum shear rate peak at low shear rates (see Fig. 6.6). At higher shear rates, the shear rate values are steadier due to minimal lubricant variation.

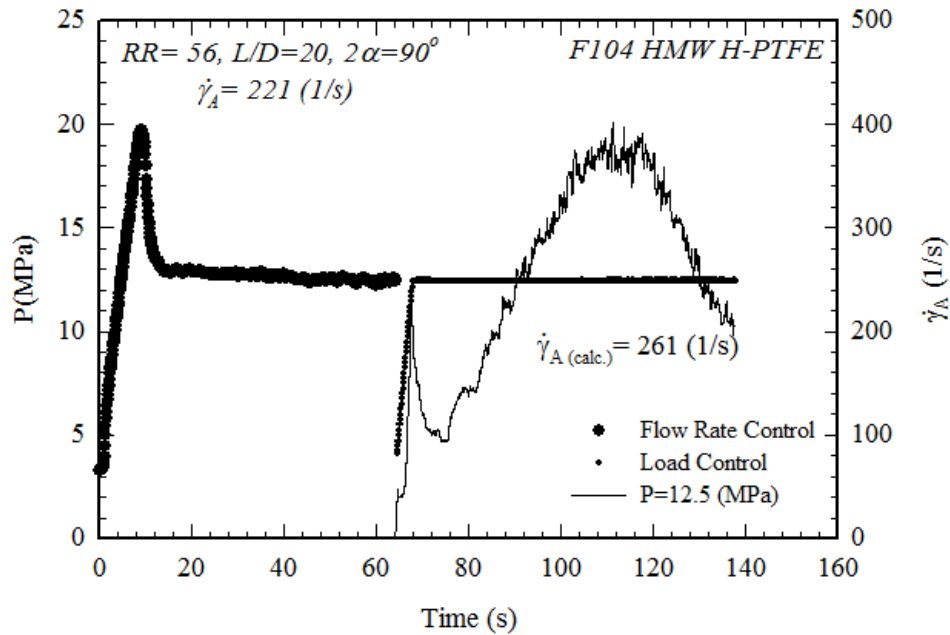


Figure 6.13: Both modes of operation during the same experimental run. The run started with constant flow rate control ($221s^{-1}$) and switched to constant load control (pressure drop of 12.5 MPa) once steady state was reached.

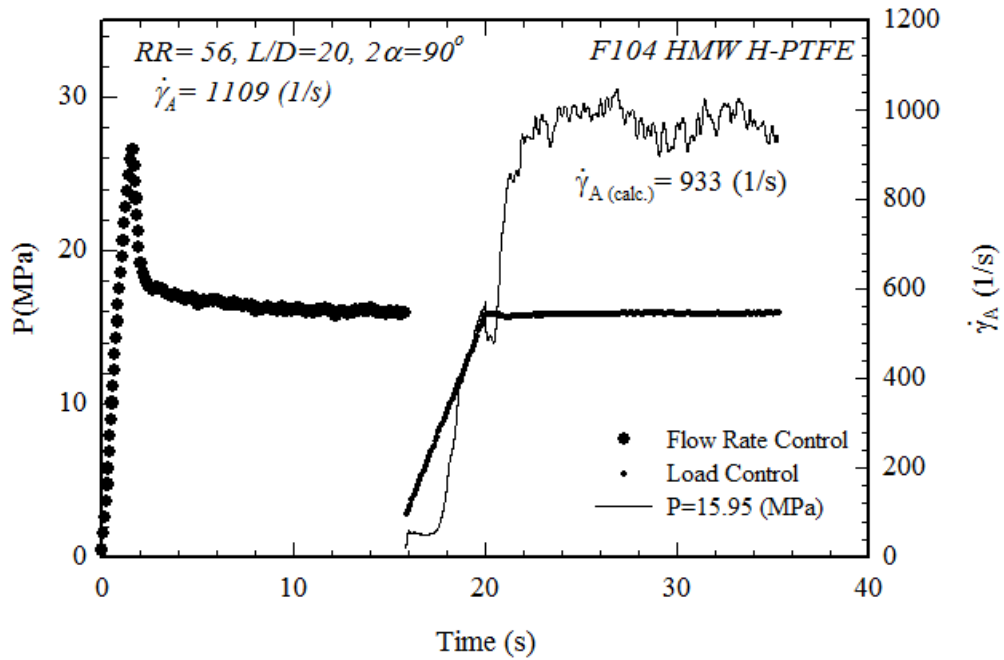


Figure 6.14: Both modes of operation during the same experimental run. The run started with constant flow rate control ($1109s^{-1}$) and switched to constant load control (pressure drop of 15.95 MPa) once steady state was reached.

For consistency reasons the previous experiment was done using a high density polyethylene melt (HDPE), tested at three different values of shear rate. The results are gathered on Table 6.7. From the results listed in Table 6.7 and the flow curve plotted at Fig.6.15, both modes of operation for this material, result similar and reproducible results.

Table 6.7: Values of the flow curve for both modes of operation under same runs for HDPE

Shear Rate Control Mode		Load Control Mode	
$\dot{\gamma}_A$ (1/s)	P(MPa)	$\dot{\gamma}_{A,CALC.}$ (1/s)	P(MPa)
100	7.2	136	7.2
400	11.9	482	11.9
1000	15.9	830	15.9

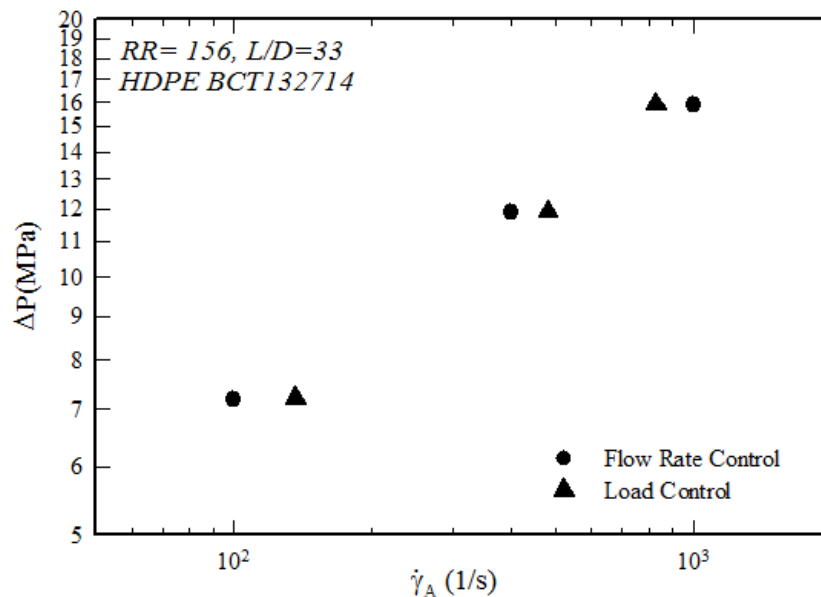


Figure 6.15: Flow curve of HDPE (BCT132714) obtained for both modes of operation using a die having RR=156

Experiments were also performed to study the effects of RR of the die on the extrudate diameter and density under both modes of operation. The optimal RR range for resin F-104 according to the manufacturer is up to 1000 (with best results shown at RR=500). Thus by increasing the RR 400 (available die) was within the specifications (Daikin, visited on 01/05/2017 and 30/04/2017). The paste was tested for a medium shear rate (517 s^{-1}) again under both modes of operation. The same results were obtained and these are summarized in Tables 6.8 and 6.9.

The last experiment was to examine the effect of lubricant concentration on the extrudate diameter and density under both modes of operation. The lubricant was decreased from 22pph

(18.03 wt. %) to 18pph (15.25 wt. %). Again the trends observed were similar for all other cases examined above. The flow curves for these cases are plotted in Fig. 6.16 and 6.17. The error for Fig.6.16 between the results obtained for the two modes of operation was less than 5%, while for the second case at the lower lubricant concentration, was even less.

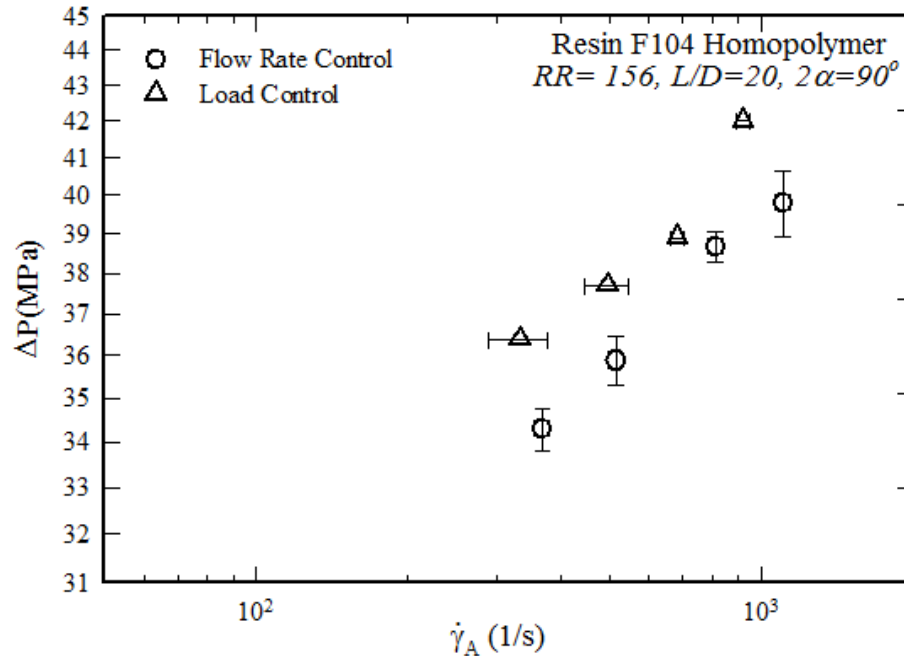


Figure 6.16: Flow curve of PTFE (F104 HMW H-PTFE) paste obtained for both modes of operation using a die having RR=156.

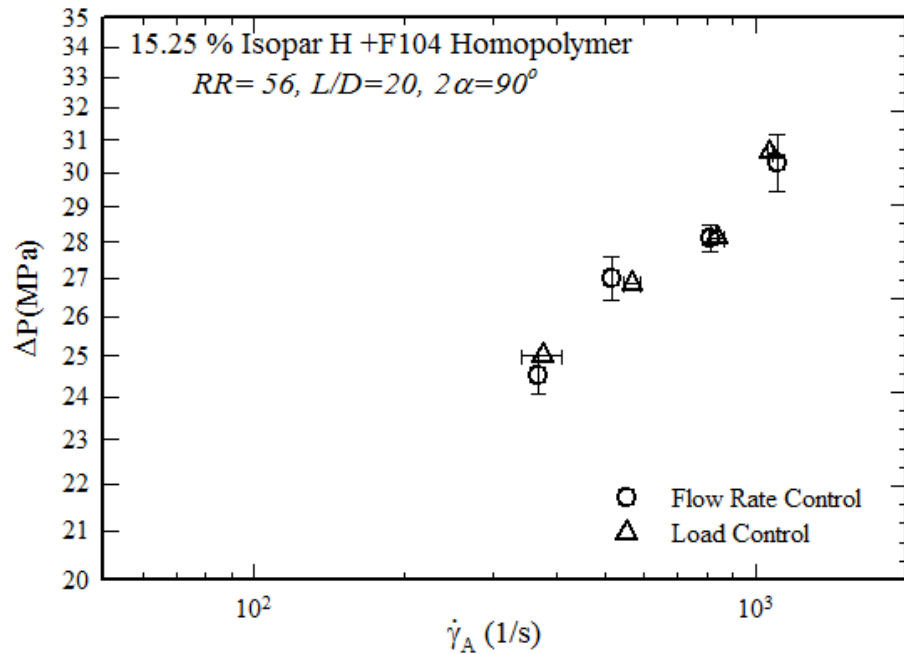


Figure 6.17: Flow curve of PTFE (F104 HMW H-PTFE) paste obtained for both modes of operation using a die having RR=56 and decreased lube concentration (15.25 wt. %).

Table 6.8: Average diameter and specific gravity of wet extrudates for PTFE (F104 HMW H-PTFE) tested under different lube concentrations, dies with different RR values for both modes of operation

Shear Rate Control Mode					Load Control Mode	
Lube C	RR	$\dot{\gamma}_A$ (1/s)	\bar{D} (mm)	$\bar{\rho}$	\bar{D} (mm)	$\bar{\rho}$
18%	56	74	1.272±0.012	1.65±0.07	1.268±0.007	1.77±0.08
18%	56	517	1.264±0.008	1.67±0.09	1.263±0.006	1.70±0.06
18%	56	1109	1.273±0.006	1.57±0.02	1.261±0.008	1.63±0.05
18%	156	517	0.760±0.005	1.57±0.05	0.763±0.006	1.57±0.07
18%	400	517	1.399±0.002	1.60±0.04	1.403±0.008	1.62±0.04
15%	56	517	1.289±0.002	1.65±0.04	1.283±0.004	1.72±0.07

Table 6.9: Average diameter and specific gravity of dry extrudates PTFE (F104 HMW H-PTFE) tested under different lube concentrations, dies with different RR values for both modes of operation

Shear Rate Control Mode					Load Control Mode	
Lube C	RR	$\dot{\gamma}_A$ (1/s)	\bar{D} (mm)	$\bar{\rho}$	\bar{D} (mm)	$\bar{\rho}$
18%	56	74	1.273±0.010	1.60±0.03	1.287±0.005	1.62±0.03
18%	56	517	1.266±0.005	1.60±0.02	1.286±0.005	1.61±0.02
18%	56	1109	1.275±0.005	1.58±0.02	1.288±0.007	1.59±0.02
18%	156	517	0.762±0.005	1.60±0.06	0.764±0.008	1.61±0.05
18%	400	517	1.403±0.002	1.59±0.02	1.416±0.008	1.59±0.02
15%	56	517	1.288±0.001	1.60±0.03	1.284±0.002	1.63±0.02

6.4 Summary

Extrudates produced at different conditions (different shear rates, reduction ratios and lube concentrations), were tested under two modes of operation (flow rate control vs load control). It was hypothesized that at least in an industrial environment, the first mode could lead to possibly variation in density, while the second mode to possible variation of diameter. Experiments in the laboratory scale showed that both modes of operation lead to similar results for the operating parameter values tested. Possible explanations in this difference between the industrial and laboratory scale might be the type of resins used or different procedures during extrusion performance or preform production. It would have been of interest to find the conditions under which these differences could be noticeable in a laboratory scale, so that products of high consistency in terms of mechanical properties could be produced.

CHAPTER 7: Zero Poisson's Ratio PTFE In Uniaxial Extension

7.1 Introduction

In this chapter the mechanical properties of PTFE extrudates are studied in detail with respect to Poisson ratio and density changes during testing. It has been shown that the mechanical properties (e.g. tensile strength and elastic modulus) of the PTFE paste extrudates, regardless of whether they are sintered, are directly related to the degree and quality of fibrillation (Ariawan, *et al.* 2002a; Ochoa & Hatzikiriakos, 2005; Ardakani, *et al.* 2013a). Although PTFE is of great industrial interest, there are few detailed studies on the mechanical properties of paste extruded PTFE. The tensile strength of PTFE paste extrudates, as a representative parameter of its mechanical properties, has been shown to slightly decrease with increasing of processing flow rate (Coleman, 1978; Ardakani, PhD Thesis, 2014; Patil, *et al.* 2006). This is due to breakage of some fibrils because of the higher elongational strain rate in the die inlet. However, the opposite trend has been reported for melt extruded PTFE fibres (Mc Gee & Colier, 1986). The reduction ratio also increases the ultimate strength at a given extrusion rate (apparent shear rate) (Ochoa, PhD Thesis, 2006; Ardakani, PhD Thesis, 2014; Ariawan, PhD Thesis, 2001; Ansari, *et al.* 2015). This is attributed to both the higher elongational strain and longer residence time which results in more fibril formation. To the best of our knowledge, the tensile properties of PTFE paste extrudates in uniaxial extension has not been studied systematically as a function of Hencky strain rate and temperature. Such systematic data can also be used to develop models for optimizing these properties.

The mechanical and physical properties of the final PTFE product can be modified by tailoring its microstructure using proper extrusion and post-extrusion conditions such as calendaring (Huang, *et al.* 2007) stretching and thermal treatment (US PATENT 3.953.566-Gore R.W. 1976; Kurumada, *et al.* 1992; Huang, *et al.* 2008; Choi & Spruiell 2008; Ranjbarzadeh-Dibazar 2014; Endo, *et al.* 1998). For example controlled porosity of PTFE sheets can be formed via fast drawing and heating process (Huang, *et al.* 2007; US PATENT 3.953.566-Gore R.W. 1976; Liu, *et al.* 2015). This phenomenon which is due to the fibrillated structure indicates that the material is compressible and its density changes upon extensional deformation. Caddock and Evans (1989) have shown that the Poisson's ratio for certain PTFE extrudates varies between -14 to 0 depending on the applied strain.

In chapter 5 the tensile properties of PTFE extrudates obtained by extruding pastes at room temperature through cylindrical dies having different reduction ratios, were studied. In this chapter these properties have been studied for extrudates processed at various extrusion temperatures using the Sentmanat Extensional Rheometer (SER) (Sentmanat, US Patent, 6.578.413) at different Hencky strain rates and temperatures. In addition the Poisson ratio is central in this study. The microstructure of the extrudates is analyzed using SEM to correlate the degree of fibrillation to the observed mechanical properties. The goal here is to develop a model to describe the ultimate strength of these PTFE extrudates as a function of testing temperature, Hencky strain rate and the processing conditions including the die reduction ratio and extrusion temperature.

7.2 *Transient Tensile Stress*

The Matsuoka model (Eq.2.8) was used to fit tensile experimental data obtained for PTFE extrudate samples produced at different extrusion temperatures and tested at different temperatures and Hencky strain rates. It should be noted that the Hencky strain, $\dot{\epsilon}_H$, was constant through these experiments, but not $\dot{\epsilon}_E$ which is the linear strain in this model. The relation between linear and Hencky strain rates is $\dot{\epsilon}_E = (1 + \epsilon_E) \dot{\epsilon}_H$. The first exponential factor involving the parameter "C" from Eq.2.8 describes yielding and shows the position of the maximum (ultimate strength). The second exponential factor has a strain rate dependence, where λ is an empirical average value of relaxation times and n is a width parameter. As the width of the distribution vanishes, n approaches zero (Matsuoka, 1986).

Figure 7.1 illustrates with open symbols the tensile results at Hencky strain rate of 0.6 s^{-1} and four different testing temperatures for PTFE samples extruded at $T_p=25^\circ\text{C}$ through a die with reduction ratio of 156 and the fitting of Matsuoka Model (Eq. 2.8) are presented as dash-lines. The fitting parameters at various testing temperatures are listed in Table 7.1.

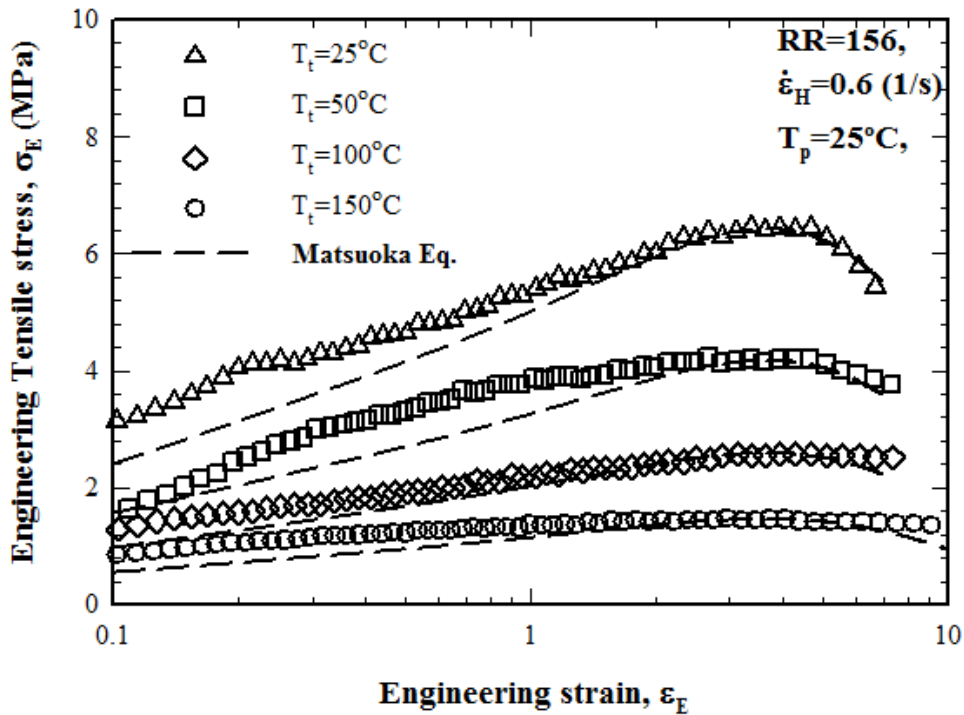


Figure 7.1: Tensile results at $\dot{\epsilon}_H = 0.6 \text{ s}^{-1}$ at four different temperatures for PTFE samples extruded at $T_p = 25^\circ\text{C}$ through a capillary die with reduction ratio of 156. The dash-lines are best fitting of Eq. 2.8 (Matsuoka Eq.).

Table 7.1: List of fitting parameters of Eq. 2.8 at various temperatures.

Parameter	Unit	$T_t=25^\circ\text{C}$	$T_t=50^\circ\text{C}$	$T_t=100^\circ\text{C}$	$T_t=150^\circ\text{C}$
E_0	MPa	150	100	62	35
C	-	0.2	0.2	0.2	0.2
λ	s	0.024	0.024	0.024	0.024
n	-	0.33	0.33	0.33	0.33
ν	-	0	0	0	0

Although the fittings are not perfect, particularly at low engineering strains, the model can successfully predict the location and level of ultimate strength. It is interesting to note that all the fitting parameters listed in Table 7.1 are constant except E_0 . This parameter is related to the crystalline region of the sample (Matsuoka, *et al.* 1986) and therefore is expected to depend on temperature. The higher the testing temperature, T_t , the lower the value of E_0 , since samples become softer upon heating. These results are in agreement with previous studies (Speerschneider, *et al.* 1963; Wang, *et al.* 2011). The values of E_0 follow an Arrhenius function (Eq. 7.1) in terms of the testing temperature T_t , as it is depicted in Fig.7.2.

$$E_0 = A \exp \left[\frac{-E_t}{R} \left(\frac{1}{T_t} - \frac{1}{T_{t,ref}} \right) \right], \quad (7.1)$$

Where R is the universal gas constant, $T_{t,ref} = 25^\circ C$ and $E_t = 11.7$ kJ/mol.

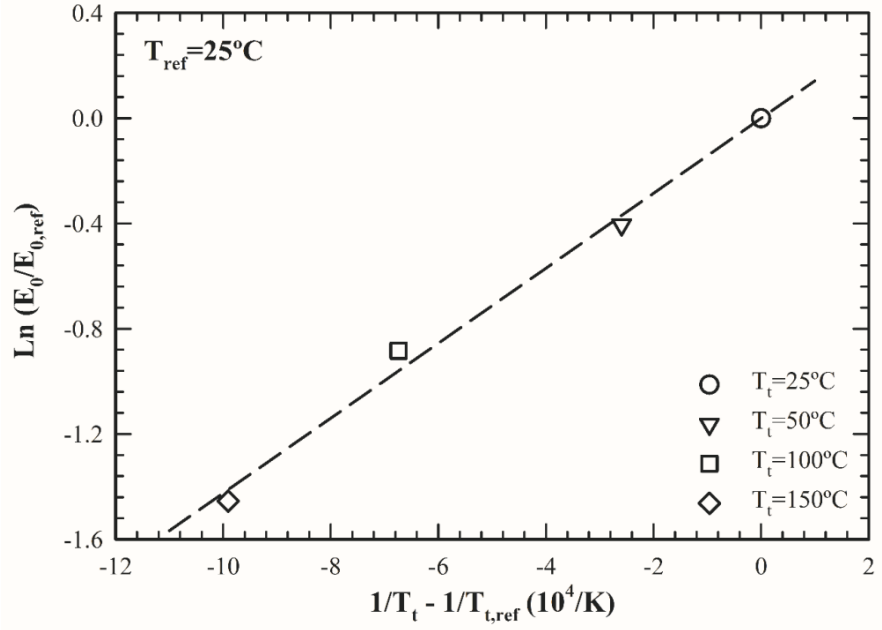


Figure 7.2: Elastic Modulus E_0 versus testing temperature, T_t , for PTFE samples extruded at $T_p=25^\circ C$ through a capillary die with reduction ratio of 156. The slope results in an activation energy of 11.7 kJ/mol.

Figure 7.3 illustrates the tensile results at four different Hencky strain rates at testing temperature, $T_t=50^\circ C$. The dash-lines show again the fitting of the experimental data using the Matsuoka model, Eq. 2.8. The same feature as Figure 7.1 can be seen here, i.e. excellent prediction of the ultimate strength and its location regardless of its early stage under predictions. Moreover, it is interesting that the position of the maximum (ultimate strain, ϵ_u) appears to remain constant, but the ultimate strength increases with strain rate.

Table 7.2 shows the fitting parameters of Matsuoka model (Eq. 2.8) at various strain rates. Comparing to fitting parameters listed in Table 7.2, the relaxation time λ is no longer constant and decreases with strain rate showing a dependence on the rate of stretching as expected. However, it appears that the product of $\lambda \times \dot{\epsilon}_u$ is almost constant (~ 0.014) showing

that the relaxation time scales inversely proportional to the rate of stretching, an expected finding. The modulus is constant as these experiments refer to the same testing temperature.

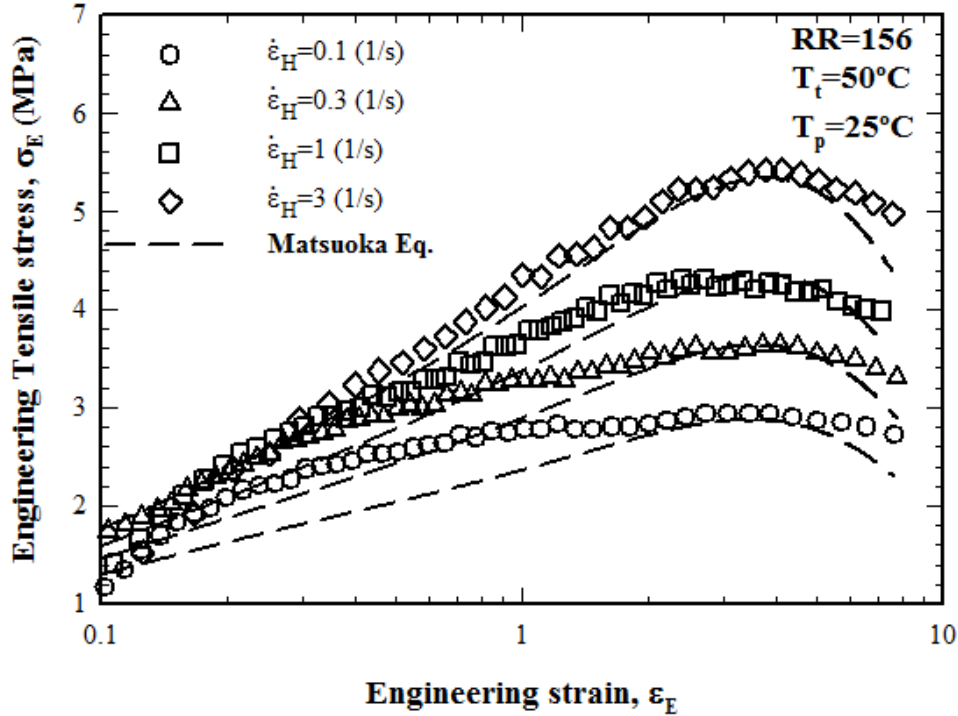


Figure 7.3: Tensile results at four different Hencky strain rates tested at $T_t=50^\circ\text{C}$ for PTFE samples extruded at $T_p=25^\circ\text{C}$ through a capillary die with reduction ratio of 156. The dash-lines are best fitting of Eq. 2.8.

Table 7.2: List of fitting parameters of Eq.2.8 at different Hencky strain rates.

Parameter	Unit	$\dot{\epsilon}_H=0.1$ (1/s)	$\dot{\epsilon}_H=0.3$ (1/s)	$\dot{\epsilon}_H=0.6$ (1/s)	$\dot{\epsilon}_H=1$ (1/s)	$\dot{\epsilon}_H=3$ (1/s)
E_0	MPa	100	100	100	100	100
C	-	0.2	0.2	0.2	0.2	0.2
λ	s	0.108	0.043	0.024	0.0147	0.0059
n	-	0.33	0.33	0.33	0.33	0.33
ν	-	0	0	0	0	0

To summarize, it appears from the fitting of the experimental data that E_0 is a function of the testing temperature (T_t) following Equation 7.1, λ scales with the inverse of the Hencky strain rate, n is constant and the Poisson's ratio is zero. Finally C is a function of reduction ratio (RR) that influences the degree of fibrillation and thus the overall strength of the extruded paste.

7.3 Ultimate Strength

Fig. 7.4. depicts the ultimate strength as a function of Hencky strain rate at four different tensile test temperatures (T_t) for PTFE samples extruded at $T_p=50^\circ\text{C}$ through a die with a reduction ratio of 156. The results show a power-law trend with a constant exponent of $b = 0.16$ (Eq. 7.2).

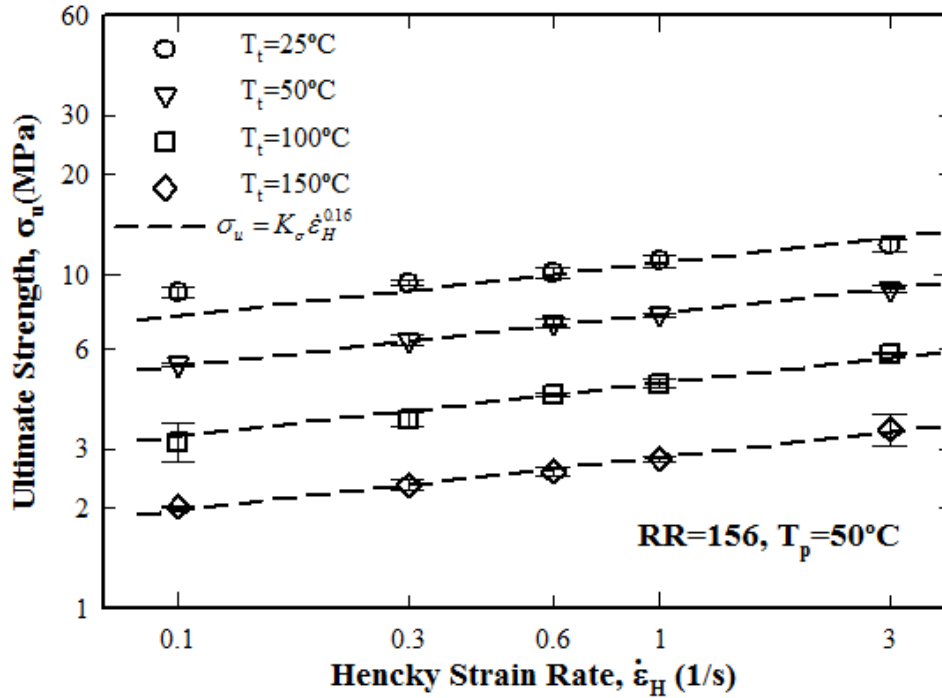


Figure 7.4: Ultimate strength as a function of Hencky strain rate at four different tensile temperatures for PTFE samples extruded at $T_p=50^\circ\text{C}$ through a die with reduction ratio of 156.

This trend is nearly the same for all the experimental results obtained by using the capillary dies having different reduction ratios and processing (extrusion) temperatures.

$$\sigma_u = K_\sigma \dot{\epsilon}_H^b \quad (7.2)$$

Considering Eq. 2.8, Matsuoka (1986) has shown a power-law trend for the ultimate strength as a function of engineering strain rate. Wang, *et al.* (2011) also found a power-law relationship for the elastic modulus and tensile strength with strain rate for short fibre reinforcement Polyamide-6. Moreover, a careful analysis of Ochoa's (Ochoa, PhD Thesis, 2006) data interestingly exhibit the same power-law exponent of 0.16 for similar PTFE extrudates.

While the power-law exponent, b , is constant, the prefactor, K_σ in Eq.7.2. is a function of tensile testing and processing (extrusion) temperatures, as well as the die reduction ratio of the capillary die used. The dependency of this parameter to the tensile testing temperature for various die reduction ratios and processing (extrusion) temperatures are depicted in Fig. 7.5.

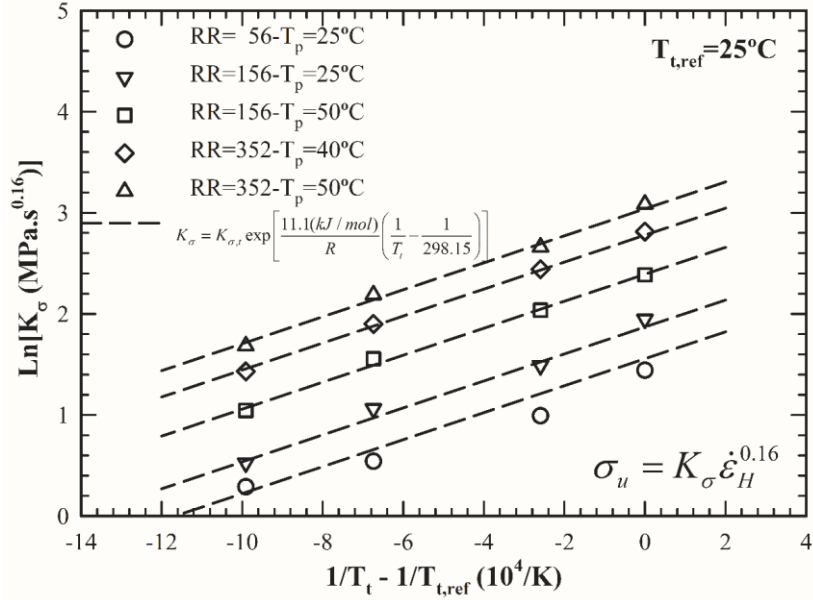


Figure 7.5: $\sigma_u - \dot{\epsilon}_H$ power-law prefactor (K_σ) as a function of tensile temperature for PTFE samples extruded at different extrusion temperatures through dies with various reduction ratios. The dash-lines are the fitting of Arrhenius equation with a constant slope.

It is clear that the results can be described using an Arrhenius equation by considering a reference tensile temperature of $T_{t,ref} = 25^\circ C$, with a constant activation energy of $E_t=11.1$ kJ/mol (Eq. 7.3).

$$K_\sigma = K_{\sigma,t} \exp \left[\frac{-E_t}{R} \left(\frac{1}{T_t} - \frac{1}{T_{t,ref}} \right) \right] \quad (7.3)$$

Interestingly this value is very close to the activation energy of the Eq. 7.1 fitting parameter ($E_0=11.7$ kJ/mol). This indicates that both E_0 and ultimate strength are dealing with the morphology of the sample and its fibril structure. Koo & Andrews (1969) have reported the activation energies of 86 and 79 kJ/mol for some compression molded PTFE samples in creep experiments which had different levels of crystallinity. Wang, *et al.* 2011 have also reported the tensile modulus of a 3-layer PTFE sample (a porous layer sandwiched by two

compact ones) at different temperatures with an activation energy of 15.4 kJ/mol can be obtained from their data. The much lower values obtained in our study can be attributed to the presence of voids in our samples.

The analysis so far has considered the effects of Hencky strain rate and tensile testing temperature, T_t , while the effects of processing (extrusion) temperature and die reduction ratio are incorporated into the prefactor of the Eq. 7.3, $K_{\sigma,t}$. These will be considered next.

Fig. 7.6 illustrates the dependence of this parameter, $K_{\sigma,t}$, on the processing (extrusion) temperature for capillary dies of various reduction ratios, RR . All results can be described again by an Arrhenius equation (Eq.7.4), with the activation energies (E_p) and prefactor ($K_{\sigma,p}$) as function of die reduction ratio, RR .

$$K_{\sigma,t} = K_{\sigma,p} \exp \left[\frac{-E_p}{R} \left(\frac{1}{T_p} - \frac{1}{T_{p,ref}} \right) \right] \quad (7.4)$$

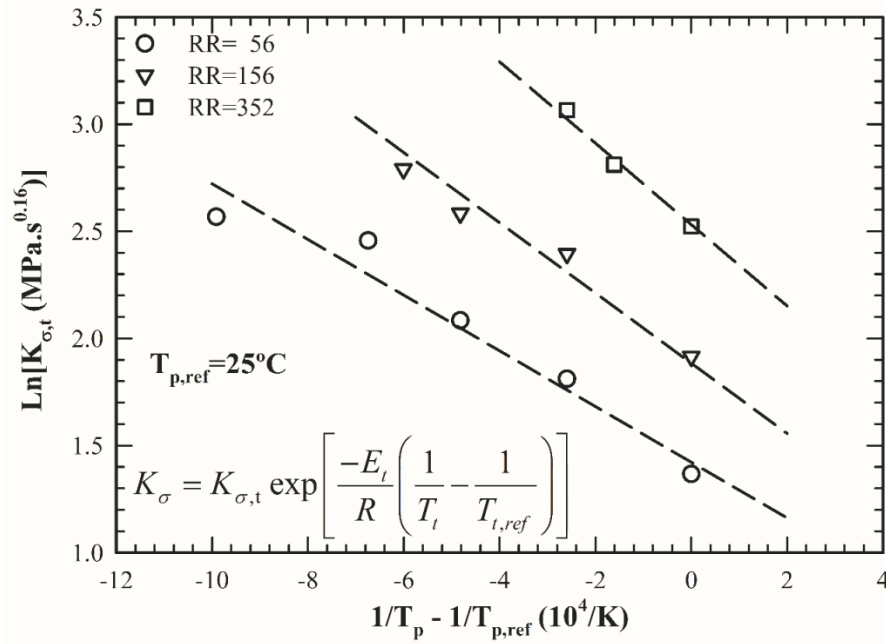


Figure 7.6: $K_{\sigma} - T_t$ Arrhenius prefactor ($K_{\sigma,t}$) as a function of processing temperature for PTFE samples extruded through dies with various reduction ratios. The dash-lines are the fitting of Arrhenius equations.

The dependence of activation energy on the processing (extrusion) temperature and die reduction ratio indicates that the processing temperature has a direct impact on the rheology

of the paste, which in turn affects the morphology of the fibril network. It was shown previously (Mc Gee & Collier 1986; Ochoa, PhD Thesis, 2006) that increasing the extrusion temperature would lead typically to a higher degree of fibrillation. Moreover, as the die reduction ratio increases (stronger elongational die entry), the sensitivity of the fibrillation process to the processing temperature is higher. Fig. 7.7.a & Fig. 7.7.b show the dependence of the activation energy and the prefactor $K_{\sigma,p}$ of Eq.7.4 on the die reduction ratio, respectively. Eq. 7.5 & Eq.7.6 describe these dependencies as follows:

$$E_p = E_{p,0} \ln RR \quad (7.5)$$

$$K_{\sigma,p} = K_0 RR^a \quad (7.6)$$

Combining all the above analysis, one can describe the ultimate strength for PTFE paste extrudates as a function of tensile testing and processing (extrusion) temperature, tensile Hencky strain rate, as well as the die reduction ratio using Eq. 7.7. The values of the proposed model parameters are listed in Table 7.3.

$$\sigma_u = K_0 RR^a \exp\left[\frac{-E_{p,0} \ln RR}{R} \left(\frac{1}{T_p} - \frac{1}{T_{p,ref}}\right)\right] \exp\left[\frac{-E_t}{R} \left(\frac{1}{T_t} - \frac{1}{T_{t,ref}}\right)\right] \dot{\epsilon}_H \quad (7.7)$$

Table 7.3: List of the values of parameters of Eq.7. 7

Model Parameter	Unit	Value
K_0	MPa.s ^{0.16}	0.36
a	-	0.6
$E_{p,0}$	kJ/mol	2.68
$T_{p,ref}$	K	298.15
E_t	kJ/mol	-11.1
$T_{t,ref}$	K	298.15
b	-	0.16

Figs. 7.8.a – 7.8.d summarize the results for ultimate strength as a function of Hencky strain rates for different cases along with the predictions of proposed model (Eq. 7.7). These results show that the proposed model can describe the effects well within $\pm 35\%$. It should be noted that the results plotted in Fig 7.8.d, (capillary die having RR=100) were not used in the fitting process of the parameters of Eq. 7.7. This die has a different entrance angle (35° rather

than 90°). In spite of this, the model predicts these data adequately well (Fig7.8.d). It is also noted that the entrance angle does not have a monotonic effect on the tensile properties, i.e. there is a minimum around 60° as was also reported previously and described well by the present model (Ardakani, PhD Thesis, 2014; Ariawan, PhD Thesis, 2001; Ochoa, PhD Thesis, 2006).

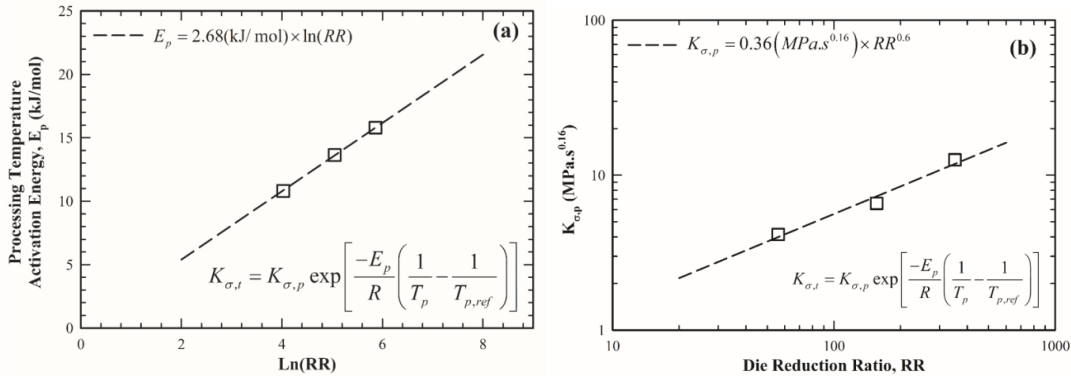


Figure 7.7: $K_{\sigma,t} - T_p$ Arrhenius (a) activation energy (E_p) and (b) prefactor ($K_{\sigma,p}$) as a function of die reduction ratio. The dash-lines are the fittings of the specified equations in each figure.

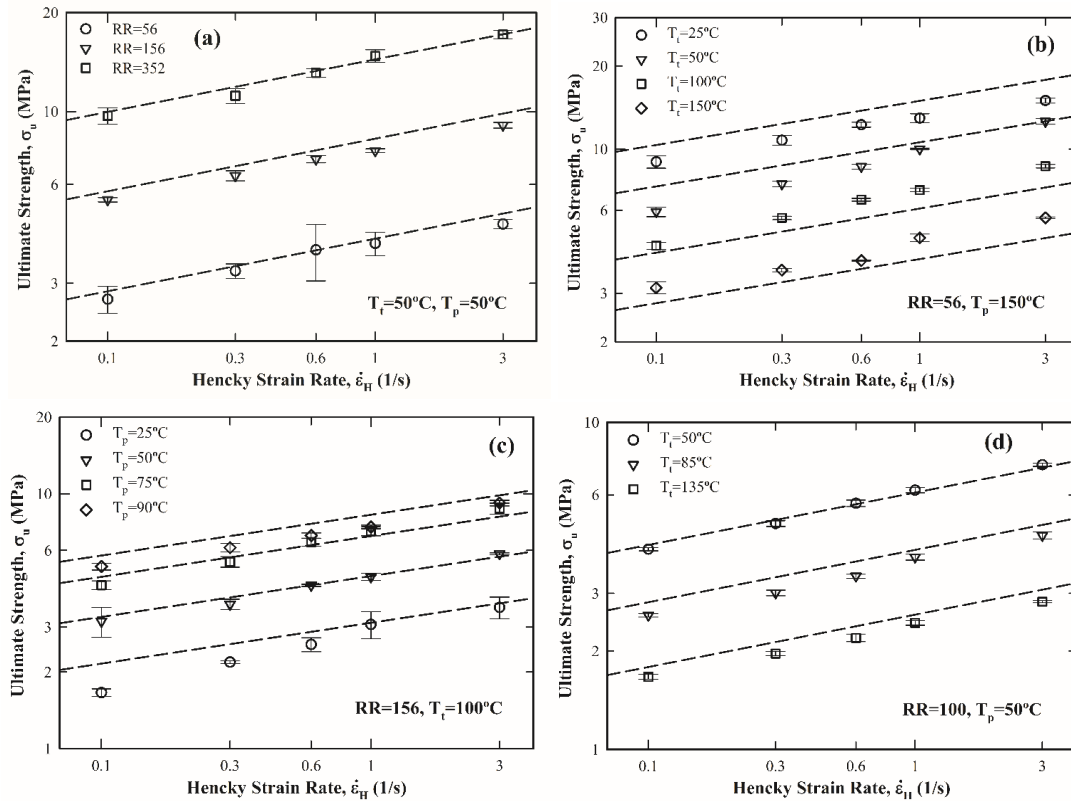


Figure 7.8: The predictions of Eq. 7.7 for ultimate strength as a function of Hencky strain rate as dash-lines for (a) different die reduction ratio at T_i and $T_p=50^\circ\text{C}$, (b) different tensile temperatures for $RR=56$ and $T_p=150^\circ\text{C}$, (c) different processing temperatures for $RR=156$ and $T_i=100^\circ\text{C}$ and (d) different tensile temperatures for $RR=100$ and $T_p=50^\circ\text{C}$

7.4 Densitometry

Previous studies have shown that due to the unique fibrillated structure of PTFE extrudates, stretching leads to formation of the voids within the material (US PATENT 3.953.566-Gore R.W. 1976; Kurumada, *et al.* 1998; Huang, *et al.* 2008; Choi & Spruiell, 2010; Ranjbarzadeh-Dibazar, *et al.* 2014; Endo, *et al.* 1998). This indicates the material is compressible (expanding upon stretching) and its Poisson's ratio is less than 0.5 (Caddock & Evans, 1989). In fact as was discussed previously, the Poisson's ratio is zero for these cylindrical samples possessing fibrils most oriented in the axial direction. Therefore, one can expect that the density of PTFE extrudates changes during tensile deformation (Ansari, *et al.* 2015).

In our previous paper (Ansari, *et al.* 2015) we have shown that the relative density (RD) also reported as Specific Gravity, is a function of elongational strain described by Eq. 5.3. In the present study the SER fixture was used to perform uniaxial extensional deformation and the stretching is in form of exponential (Hencky strain). However, since the length of the sample is confined within the drums space in the SER extensional rheometric fixture, the engineering strain ε_E can be replaced by ε_H in Eq. 5.3, which is a more proper parameter to be used in rheology.

Figures 7.9.a – 7.9.c depict the relative density as a function of Hencky strain for PTFE extrudates processed at two extrusion temperatures of $T_i=25$ and 50°C through dies having reduction ratios of $RR=56$, 100 and 156 , respectively. As it was mentioned in the experimental section, the samples were stretched at a fixed Hencky strain rate of $0.6 \text{ (s}^{-1}\text{)}$ up to a specific Hencky strain. Subsequently, the tensile stress was removed and sample was allowed to relax for at least 24 hrs. As it was discussed elsewhere (Ansari, *et al.* 2015), due to their viscoelastic nature, the elongated samples recoil during relaxation and this needs to be determined to calculate the ultimate relative density of the fully relaxed material. This recovery coefficient, in Eq. 5.3 was treated as a fitting parameter by noting that the Poisson's ratio is nearly zero in all of our experiments. The dash-lines are the best fitting of the Eq. 5.3 using the values of κ shown in the legends of Fig 7.9.a-c. The physical significance of κ is a measure of elasticity, which is related directly to the morphology of fibrils. This can be seen in Fig.7.10 which shows a linear relationship between κ and die reduction ratio.

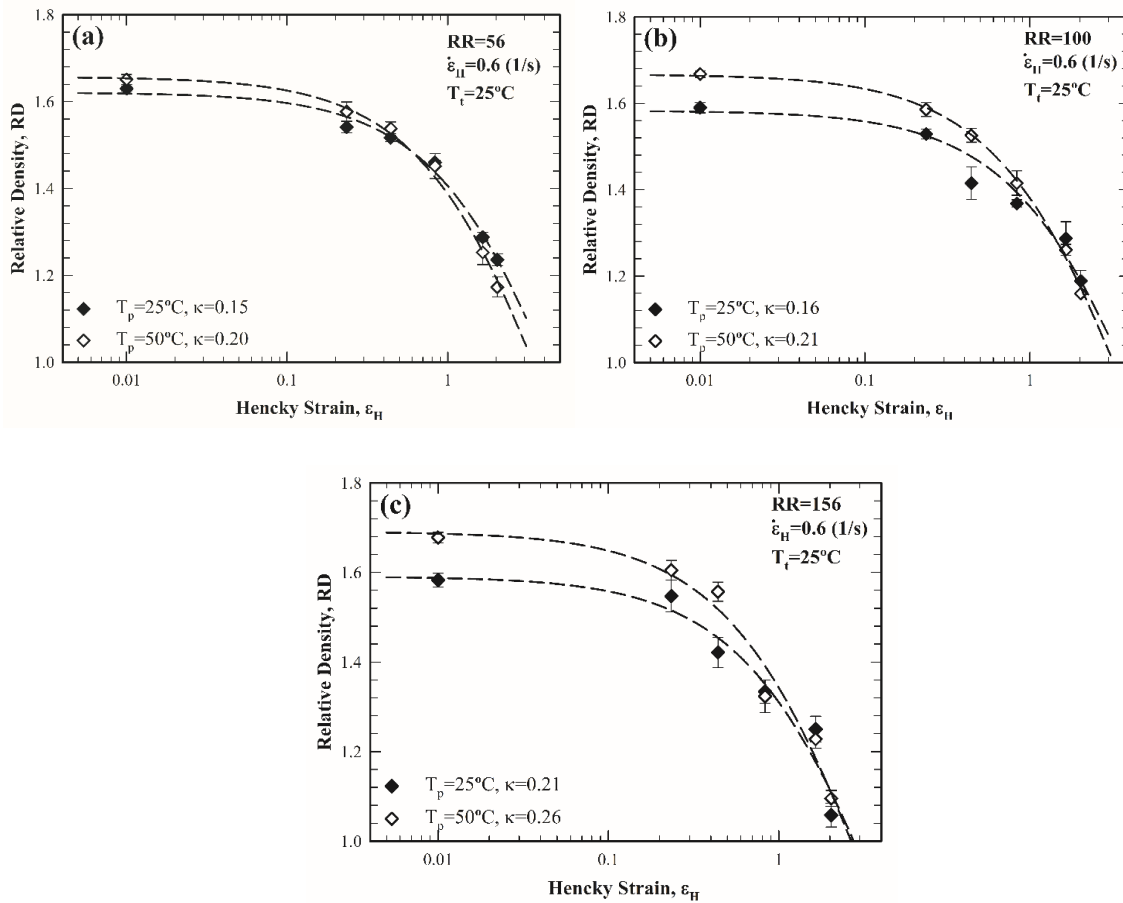


Figure 7.9: The relative density as a function of Hencky strain for extrudates collected at processing temperatures of 25°C (closed symbols) and 50°C (open symbols) extruded through dies with a) RR=56, b) RR=100 and c) R=156. The dash lines are the fitting of Eq.7.8.

One feature in this graph (7.10) is the higher values of κ for extrudates processed at higher temperatures, which implies a higher degree of fibrillation and therefore more elasticity. The data from our previous study (Ansari, *et al.* 2015) which were produced using Com-Ten tensile testing (linear extensional rate of (1/s)) rather than a constant Hencky strain rate used in the present work (SER extensional rheometer) are also plotted in Fig.7.10. It is interesting to see that κ is higher for this case compared to the data of the present study. This can be due to breakage of some fibrils in higher and stronger extensional deformation which reduces its elasticity.

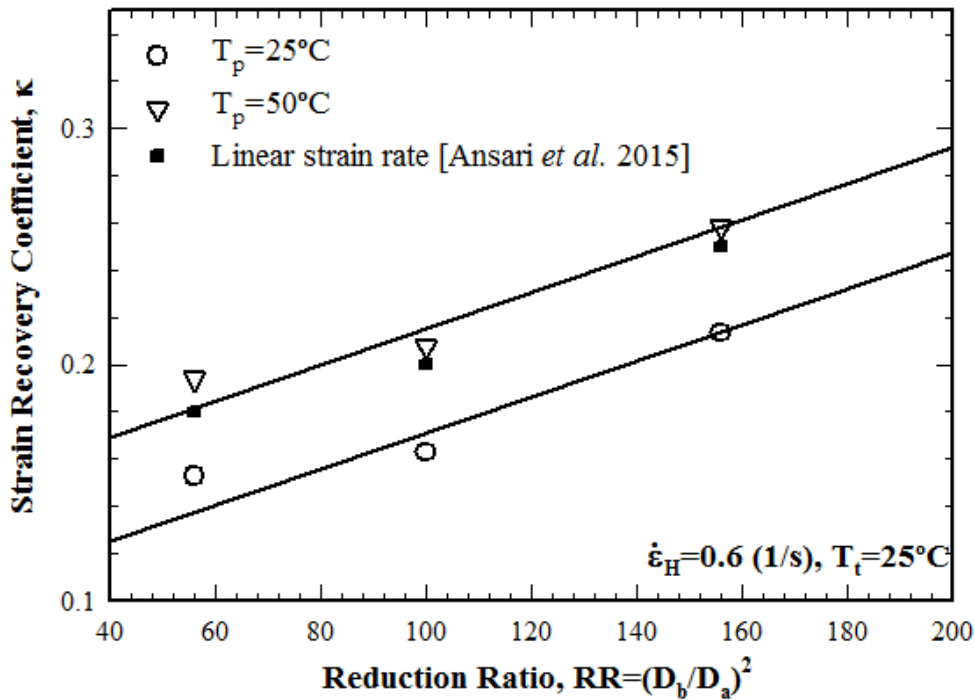


Figure 7.10: The strain recovery coefficient as a function of reduction ratio. The closed symbols are collected from our previous study (Ansari, et al.2015)

7.5 SEM Micrographs

Fig. 7.11 a & b depict the SEM micrographs of extrudates processed at $T_p=25^\circ\text{C}$ through dies with $RR=100$ & 156 , respectively. The dotted arrow between images a,b & c,d shows the direction of the flow. From these images one can see that the structure consists of packed particles connected with submicron sized fibrils elongated in the direction of flow. This microstructure can be controlled and modified by applying different modes of deformation by means of post-processing, such as those in calendaring, stretching or thermal treatment (US PATENT 3.953.566-Gore R.W. 1976, 1976; Kurumada, et al. 1998; Huang, et al. 2008; Choi & Spruiell, 2010; Ranjbarzadeh-Dibazar, et al. 2014). It is clear from these images that the degree of fibrillation increases with reduction ratio (Ochoa & Hatzikiriakos, 2005; Ariawan, et al. 2002b; Patil, et al. 2006; Ardakani, et al. 2013a). This also supports the results in previous section regarding the increase of the strain recovery coefficient, with RR. Moreover, Fig. 7.11c & d illustrate the effect of processing temperature on fibrillation for samples extruded through a die with $RR=56$ and $T_p=75$ and 150°C , respectively. Increasing the processing temperature leads to formation of more fibrils, which was discussed in "Ultimate strength" section as well.

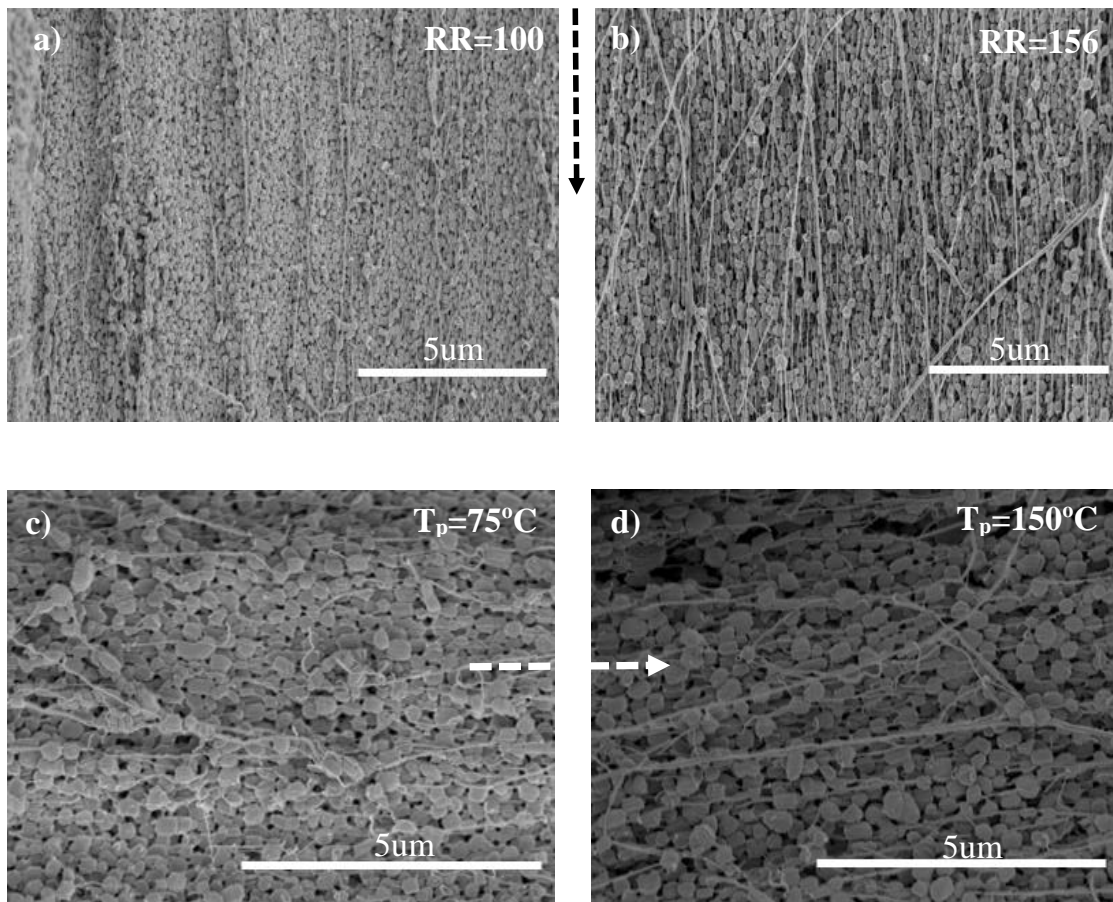


Figure 7.11: SEM micrographs for PTFE extrudates illustrating their differences in fibrillated structure. Images (a) & (b) show the differences in fibrils when using dies with different RR (the larger the RR the more the fibrils), and (c) & (d) show the difference in fibrils when extruding at different extrusion temperature. The higher the extrusion temperature the higher the fibrillation. The arrows represent the extrusion direction.

7.6 Summary

The tensile mechanical properties of PTFE paste extrudates collected from different processing conditions (extrusion temperature and reduction ratio) were studied using the SER fixture at various Hencky strain rates and temperatures.

First the transient tensile results were shown to be described by a theoretical model developed by Matsuoka (1986). The fitted parameter were found to have a physical meaning related to the temperature of the extrusion at which the tested samples were produced, the testing temperature as well as the rate of stretching. A steady-state phenomenological tensile stress model was developed to predict the ultimate strength as a function of these parameters and was tested successfully for another die with completely different geometrical

characteristics. It was found that the ultimate strength increases with Hencky strain rate following a power-law behavior, while decreases with the tensile testing temperature. The extrusion temperature has also shown an increasing effect on the ultimate strength. Both these temperature effects can be described with Arrhenius equations. The tensile temperature activation energy was found to be constant and independent of the processing conditions, although the activation energy of processing temperature was an increasing function of the reduction ratio. The fibrillation microstructure appeared in SEM micrographs were used to support the results.

Finally, due to their compressibility, the relative density of the PTFE extrudates was showed to be a decreasing function of Hencky strain. The data could be modeled by considering the Poisson's ratio, which was seen to be close to zero for this material and the strain recovery that is the portion of the imposed strain that is recovered upon removal of the imposed tensile stress.

CHAPTER 8: Role Of PTFE Paste Fibrillation On Poisson's Ratio

8.1 Introduction

We have seen so far that post-extrusion conditions such as sintering (Ochoa, PhD thesis, 2006) or stretching can also alter the mechanical properties of the final PTFE product. In our previous work (Vavlekas, *et al.* 2016) we have shown that PTFE is compressible with Poisson's ratio nearly zero. Moreover, a simple model taking Poisson's ratio into account was developed to describe density changes. The extrudates in that case were produced by a cylindrical die with the orientation of the fibrils being aligned parallel to extrusion direction (1-D fibrillated samples). Furthermore, the ultimate strength in the tensile experiments using the Sentmanat Extensional Rheometer (SER) was modeled as a function of testing temperature, processing temperature, Hencky strain rate and reduction ratio (RR) of the die (Vavlekas, *et al.* 2016). This model was compared with the viscoelastic Matsuoka model (1986)(Eq. 2.8), where Poisson's ratio appears as a material parameter. It was shown that this model successfully predicts the ultimate strength of our experimental results by considering a Poisson's ratio equal to zero.

In this work, the effect of fibrillation on Poisson's ratio for extrudates produced from flat dies, are investigated. Raman spectroscopy is used to quantitatively describe the degree of fibril orientation in the extrudates, by measuring the polarized Stokes-shifted light in the directions parallel and perpendicular to the extrusion directions. Raman intensity ratios at specific peaks were calculated in the two directions to quantitate the preferred fibril orientation at five different locations on the extrudates. The quality of fibrils can be described in terms of their degree of orientation and continuousness within the extrudate. Previous studies have shown that there is a variation in the scattering intensity at major Raman shifts of 722 cm^{-1} and 1407 cm^{-1} between the two polarization geometries. There is a general agreement that the band at 722 cm^{-1} is due to C-F and C-C stretching while that at 1407 cm^{-1} corresponds to C-C (backbone) stretching. The ratio of the Raman scattering intensities between the two polarization geometries, may provide a quantitative measure of the preferred fibril orientation (Ariawan, *et al.* 2002b).

The tensile strength of an extrudate could be used as a macroproperty indicator of the microstructure. The effect of relative orientation on Poisson's ratio in these samples will be

studied in detail. For example, it is desirable to correlate the relative orientation to Poisson's ratio such that samples of preferred expansivity can be produced in various applications (i.e. fabrication of hybrid stents where zero-effective Poisson's ratio is preferred (Douglas, MSc Thesis, 2012) or fabrics of controlled porosity where the Poisson's ratio in the negative range is more ideal (Carta, *et al.* 2016).

8.2 Effect Of Hencky Strain Rate And Testing Temperature (T_i) On Poisson's Ratio

Fig.8.1 depicts the instantaneous Poisson's ratio as a function of the Hencky strain for a tensile test. The Poisson's ratio gradually increases from nearly zero to 0.1 indicating sample expansion. The sample was extruded and tested at room temperature and stretched uniaxially at the Hencky strain rate of 1 s^{-1} . The change in the width of the sample was monitored with the use of the camera as explained earlier (Chapter 4, §4.3.5). The same procedure was repeated for the thickness. Based on the dimension changes in both the width and thickness, the average Poisson's ratio was calculated by using Eq. 4.4. Fig.8.2.a) depicts the average Poisson's ratio for the width of the sample for different testing temperatures. The Poisson's ratio is nearly independent of the Hencky strain rate and decreases with rising temperature. Fig.8.2.b) shows that similar trends apply for the thickness of the samples. The overall conclusion for both cases is that Poisson's ratio is practically zero for both the dimensions of the 2-D sample.

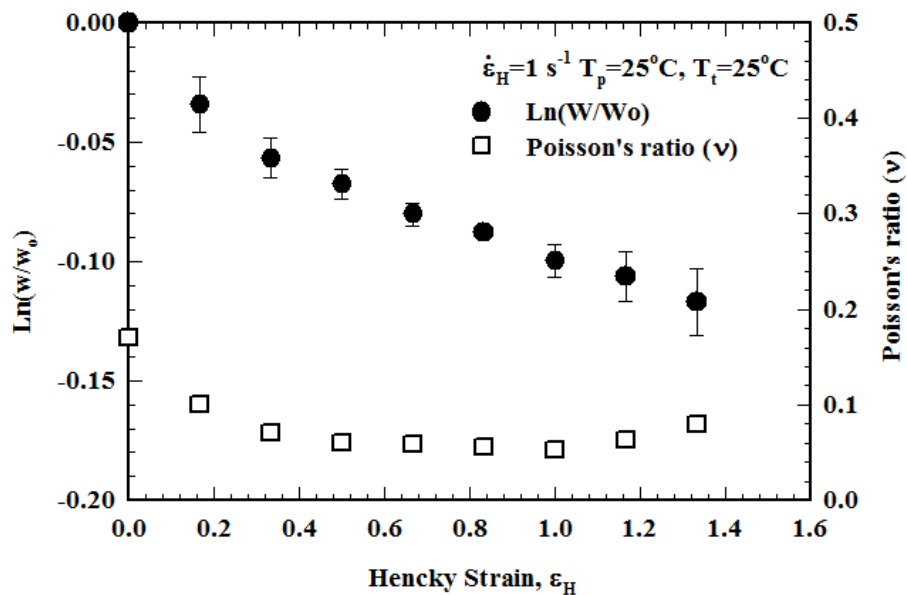


Figure 8.1: Typical graph that shows the change of the width of the sample during uniaxial extension as a function of Hencky strain and the corresponding Poisson's ratio values

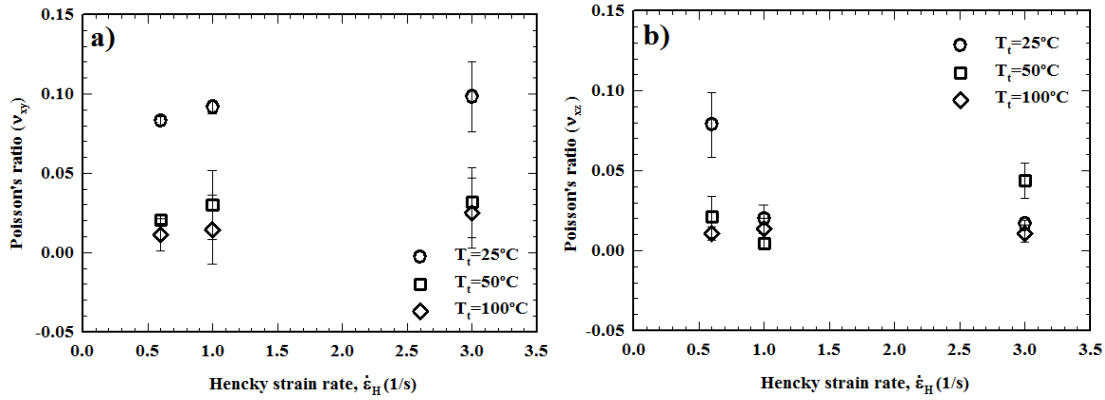


Figure 8.2: Poisson's ratio values in a) width and b) thickness directions of PTFE 2-D extrudates at three different Hencky strain rates and three different testing temperatures

8.3 Transient Tensile Stress

Fig.8.3 plots the tensile results (open symbols) at Hencky strain rate of 0.6 s^{-1} for PTFE samples extruded at $T_p=25^\circ\text{C}$ (extrusion temperature) and tested at four different temperatures. The dashed lines present the Matsuoka Model fitting (Eq. 2.8). Fitting parameter values are listed in Table 8.1. These results show that the model successfully predicts the location and level of the maximum (ultimate strength). This was found to be the case for 1-D samples (Vavlekas, *et al.* 2016). All fitting parameters remain constant, except from the modulus E_0 . This parameter is related to the crystalline region of the sample (Matsuoka 1986) and is therefore expected to depend on temperature. Upon heating, the samples become softer and therefore E_0 is expected to decrease (Vavlekas, *et al.* 2016; Speerschneider, 1963; Wang, *et al.* 2011). This parameter follows an Arrhenius function (Eq. 7.1) in terms of the testing temperature T_t , with $E_t = 11.4 \text{ kJ/mol}$. The value for E_t for the 1-D samples was nearly the same as this for the 2-D ones ($E_t = 11.7 \text{ kJ/mol}$).

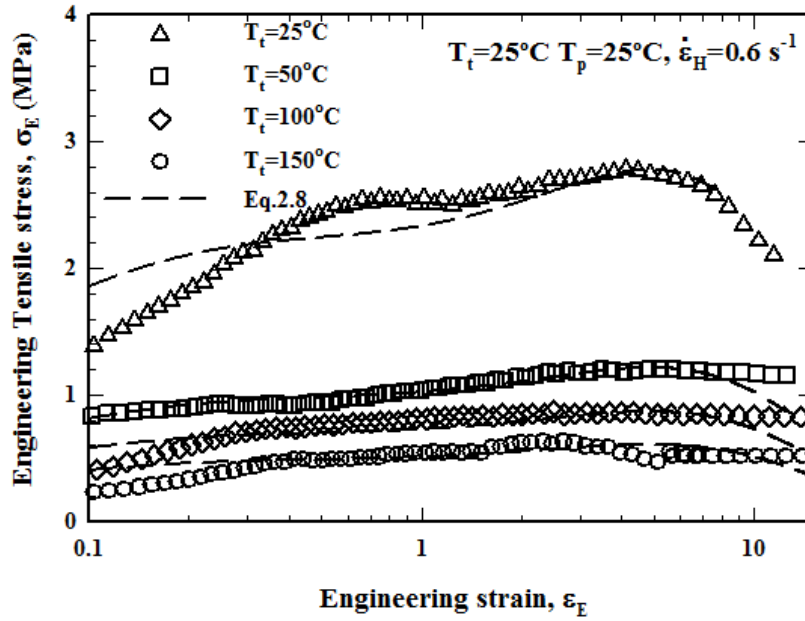


Figure 8.3: Tensile results at $\dot{\epsilon}_H = 0.6 \text{ s}^{-1}$ at four different temperatures for PTFE samples extruded at $T_p = 25^\circ\text{C}$ through a specially designed die. The dash lines are best fitting of Eq. 2.8

Table 8.1: List of fitting parameters of Matsuoka Eq. (2.8) at various temperatures

Parameter	Unit	$T_i=25^\circ\text{C}$	$T_i=50^\circ\text{C}$	$T_i=100^\circ\text{C}$	$T_i=150^\circ\text{C}$
E_0	MPa	160	70	50	35
C	-	0.14	0.14	0.14	0.14
λ	s	0.0205	0.0205	0.0205	0.0205
n	-	0.38	0.38	0.38	0.38
ν	-	0	0	0	0

Fig. 8.4 shows the tensile results at three different Hencky strain rates at the testing temperature, $T_i=25^\circ\text{C}$, along with fits of the Matsuoka model (dash-lines). Overall, the fitting of the Matsuoka model is acceptable. Once again, the position and the level of the maximum for each curve (ultimate strength) are predicted successfully. The same trend has been observed and reported for the 1-D samples (Vavlekas, *et al.* 2016). The higher the strain rate, the higher the ultimate strength, while the position of the maximum remains practically the same. The corresponding fitting parameters are listed in Table 8.2. The relaxation time λ is the only parameter that changes for the 2-D samples, decreasing with increasing strain rate. This shows a dependence on the rate of stretching. The product of $\lambda \times \dot{\epsilon}_H$ is almost constant (~ 0.015), which is similar to the 1-D fibrillated sample findings. This shows the relaxation time scales inversely with the rate of stretching.

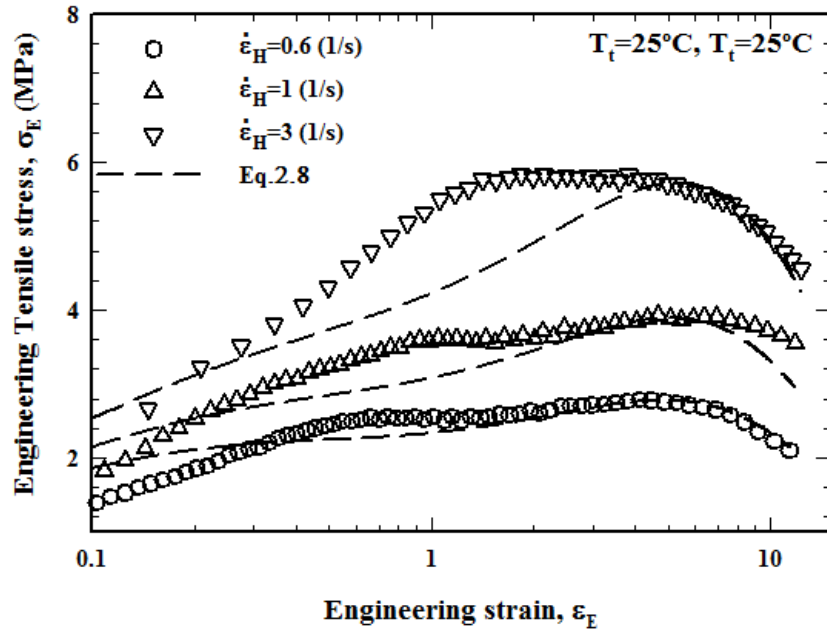


Figure 8.4: Tensile results at three different Hencky strain rates tested at $T_i = 25^\circ\text{C}$ for PTFE samples extruded at $T_p = 25^\circ\text{C}$ through the 2-D die. The dash-lines are best fitting of Eq. 2.8

Table 8.2: List of fitting parameters of Eq. 2.8 at different Hencky strain rates

Parameter	Unit	$\dot{\epsilon}_H = 0.6$ (1/s)	$\dot{\epsilon}_H = 1$ (1/s)	$\dot{\epsilon}_H = 3$ (1/s)
E_0	MPa	160	160	160
C	-	0.14	0.14	0.14
λ	s	0.0205	0.0148	0.0062
n	-	0.38	0.38	0.38
ν	-	0	0	0

In summary, for both 1-D and 2-D structures, E_0 is a function of the testing temperature (T_i), λ scales with the inverse of the Hencky strain rate, n is constant for all samples and the Poisson's ratio is nearly zero.

Table 8.3: List of fitting parameters of Eq. 2.8 for samples with different fibrillation

Parameter	Unit	1-D (RR=156)	2-D (RR=28)
		$T_i=25^\circ\text{C}$	$T_i=25^\circ\text{C}$
E_0	MPa	150	160
C	-	0.20	0.14
λ	s	0.024	0.021
n	-	0.33	0.38
ν	-	0	0

Table 8.3 illustrates the comparison between the Matsuoka model parameters for 1-D and 2-D structure samples, calculated by using the experimental results at room temperature. The parameter E_0 , which is related to the crystalline structure of the material slightly increases, since 2-D structure samples is more crystalline (different alignment of molecules during extrusion, which leads to different material properties (Bagher & Reza, 2015)). C is a function of the reduction ratio (RR) that influences the degree of fibrillation and thus the overall strength of the extruded paste. The drop of the value from 0.20 to 0.14, is attributed to the decrease of the reduction ratio (RR defined as the ratio of the initial cross section to final cross section) for the specific comparison between the two samples (from 156 to 28). The width parameter n , increases and this might be attributed to the 2-D structure formation of the fibrils.

8.4 Raman spectroscopy Analysis

Polarized confocal Raman spectroscopy is used to characterize PTFE fibril orientation. The depolarization ratio ' ρ ', defined as the intensity ratio between the perpendicular and parallel components of Raman light, provides information on fibril orientation with respect to the polarization of incident radiation:

$$\rho_{\perp/\parallel} = \frac{I_{perpendicular}}{I_{parallel}} \quad (8.1)$$

For ratios close to one, there is no preferred orientation of fibrils. For ratios less than one, the preferred orientation of fibrils is dominantly aligned parallel to the incident polarization and vice versa. Porto notation describes the optical geometry for a polarized experiment. The notation consists of four letters with syntax A(BC)D, where 'A' is the propagation direction of the incident light, 'B' is the polarization axis of the incident light, 'C' is the polarization axis of the scattered light and 'D' is the propagation direction of the scattered light.

Fig. 8.5 is a diagram of an unpolarized PTFE spectrum. The vibrational modes of interest, predicted by density functional theory (DFT) calculations (Quarti, *et al.* 2013), includes a C-F symmetrical stretch and C-C bend at 722 cm^{-1} , C-C rock at 1269 cm^{-1} , C-C wag at 1398 cm^{-1} and C-C symmetrical stretch at 1407 cm^{-1} . The C-C symmetric stretching band at 1407 cm^{-1} is of particular interest because its intensity varies with the orientation of the fibrils relative to the incident polarization direction. The total response of the system was checked using CCl_4 as a reference (Ariawan, PhD Thesis, 2001).

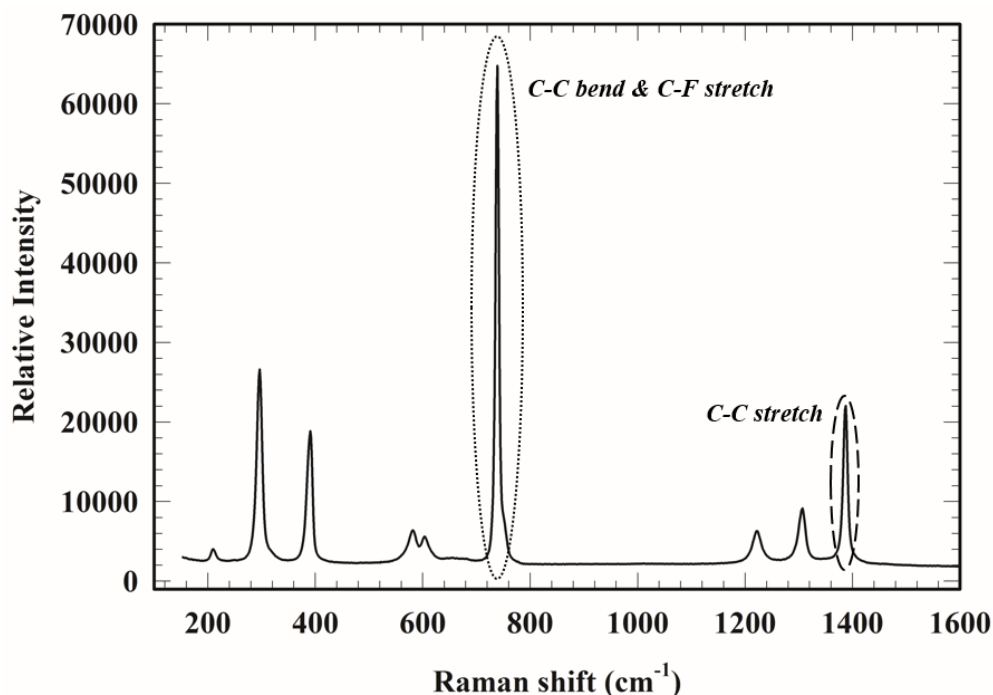


Figure 8.5: Typical PTFE Raman Spectrum. Prominent vibrational modes of interest range from 700 – 1500 cm^{-1} , with the C-C symmetrical stretch at 1407 cm^{-1} being of primary interest

For 1-D PTFE samples, fibrils are aligned along the extrusion direction. When the polarization plane of the incident light is parallel with the extrusion direction, the overwhelming majority of backscattered light is returned along the same polarization axis. This is evident for both the 1-D cylindrical die extrudate in Fig. 8.6a) and the 1-D slit die extrudate in Fig. 8.6b).

When the same experiment is performed on a 2-D sample, where the polarization axis is again aligned with the main fibrillation direction, the perpendicular component becomes significant. This is because the fibrils are no longer oriented along just one axis; rather they are crosshatched to some degree in the XY plane.

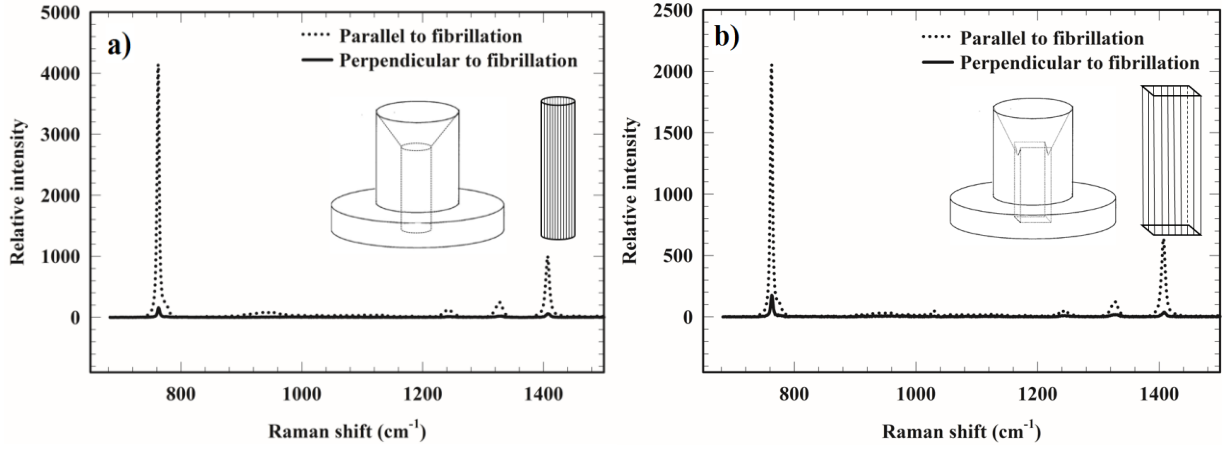


Figure 8.6: Typical depolarized PTFE Raman spectra for a) cylindrical 1-D sample and b) flat 1-D sample extruded from a slit die. The shape of the dies and the corresponding extrudates can be seen in each image

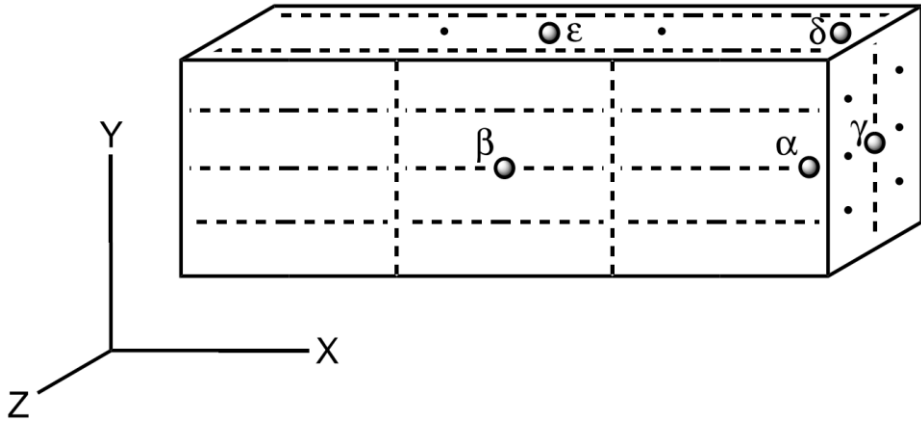


Figure 8.7: PTFE sample cut from the extrudate perpendicular to machine direction (as depicted in Fig 1c), prior to Raman examination on five different spots. X is the transverse direction, Y is the machine (extrusion) direction, and Z is the extrudate's thickness axis. Fibrils are primarily oriented in the transverse direction (along the X-axis) with some oriented in the machine direction (along the Y-axis). Dots in the XZ and YZ planes represent the fibril ends oriented normal to their respective surface

Spectra are recorded in five areas for each 2D sample, as shown in Fig. 8.7, denoted by the Greek letters α , β , γ , δ , ϵ . The Raman Intensity vector for each point can be defined by

$$\mathbf{I} \equiv [I_1, I_2, I_3] = [I_X, I_Y, I_Z]$$

and the relative vector ratio for each case:

$$I_{ij} \equiv I_j / I_i = (I_{\text{perpendicular-to-fibrillation}} / I_{\text{parallel-to-fibrillation}}) \quad (8.2)$$

The depolarization ratio provides information about the relative orientation of the fibrils in different regions of the extrudate:

ρ_α	ρ_β	ρ_γ	ρ_δ	ρ_ϵ
$\frac{Z(XY)Z}{Z(XX)Z}$	$\frac{Z(XY)Z}{Z(XX)Z}$	$\frac{X(ZY)X}{X(ZZ)X}$	$\frac{Y(XZ)Y}{Y(XX)Y}$	$\frac{Y(XZ)Y}{Y(XX)Y}$
$\frac{I_Y}{I_X}$	$\frac{I_Y}{I_X}$	$\frac{I_Y}{I_Z}$	$\frac{I_Z}{I_X}$	$\frac{I_Z}{I_X}$

The Raman spectra in Fig. 8.8, acquired from point ‘ α ’ of the extrudate, provides evidence for 2-D structure. The depolarization ratio at point ‘ α ’ is less than “1”, however greater than zero. This suggests that the preferred direction of fibrils is along the X-axis (transverse direction) more compared to that in the Y-axis (machine direction).

Fig. 8.9 highlights the depolarization ratio at 1407 cm^{-1} in five regions on the extrudate. The ratio of I_Y/I_X for points ‘ α ’ and ‘ β ’ are less than "1". This suggests that the degree of fibrillation is dominantly perpendicular to the machine (extrusion) direction. The ratios of I_Z/I_X for points ‘ δ ’ and ‘ ϵ ’ are also less than "1". Because fibrils oriented along the machine direction are normal to the XZ plane, they have a smaller scattering cross-section. This suggests the dominant orientation in the XZ plane runs perpendicular to the machine direction. The ratio of I_Y/I_Z for point ‘ γ ’ is greater than one. Because fibrils oriented along the transverse direction are normal to the YZ plane, they have a smaller scattering cross-section. This suggests the dominant orientation in the YZ plane runs in parallel with the machine direction.

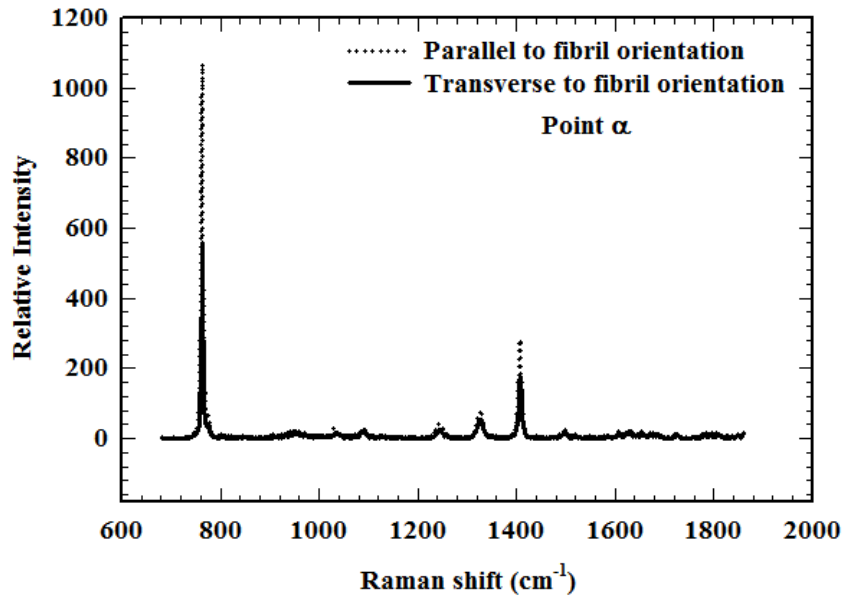


Figure 8.8: Depolarized PTFE Raman spectrum for point (α) on the extrudate

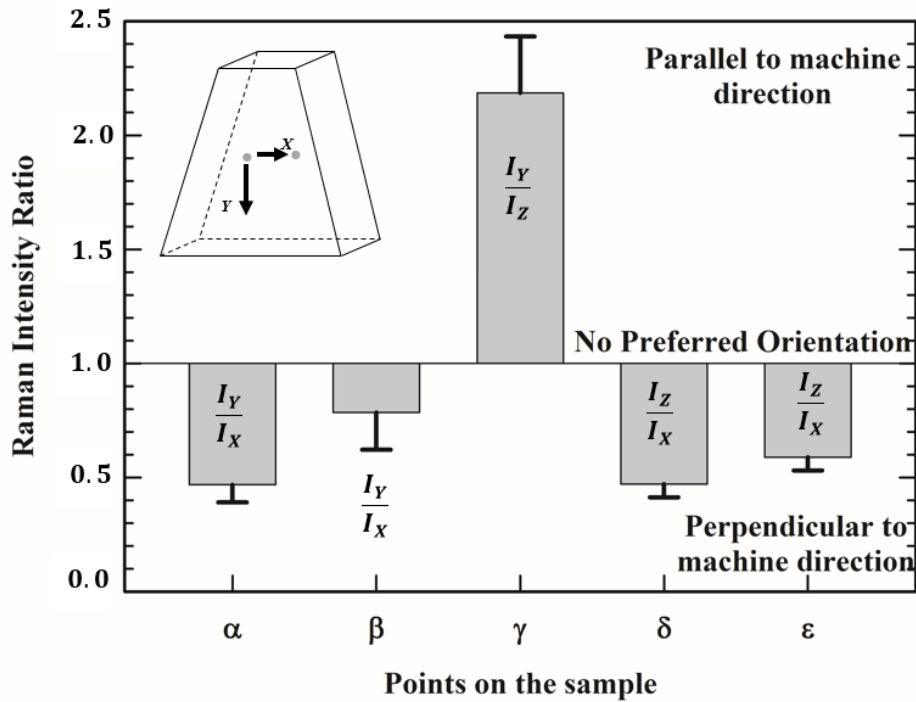


Figure 8.9: Preferred orientation of the extrudates according to depolarized Raman spectroscopy

2-D extrudates were tested in tensile at two different strains using the SER fixture and consequently again tested by Raman spectroscopy to detect changes in the relative orientation of fibrils (microstructural changes). The results are summarized in Fig.8.10. The Hencky strain of $\epsilon_H \approx 0.7$ is at a point in the middle of the test which for the sample fails right after at a

Hencky strain of 1.5. Fig.8.10a) shows the intensity of the Raman for points (β) and (ϵ). Up to medium Hencky strains, the intensity remains constant indicating very small microstructural changes. Strains as small as 0.7 do not change the relative orientation of the fibrils. However, at higher strains the intensity increases significantly along the width of the sample. It is surprising that the intensity remains the same throughout the whole test in the thickness direction. This might be due to the bulk scattering cross section area remaining constant in the XZ plane through stretching, while that of the XY plane changes more significantly. Fig. 8.10b) shows a typical stress-strain curve for the 2-D extrudate. The strain at 0.7 is almost in the middle of the graph while that of 1.5 is right after the max, but well before the failure point.

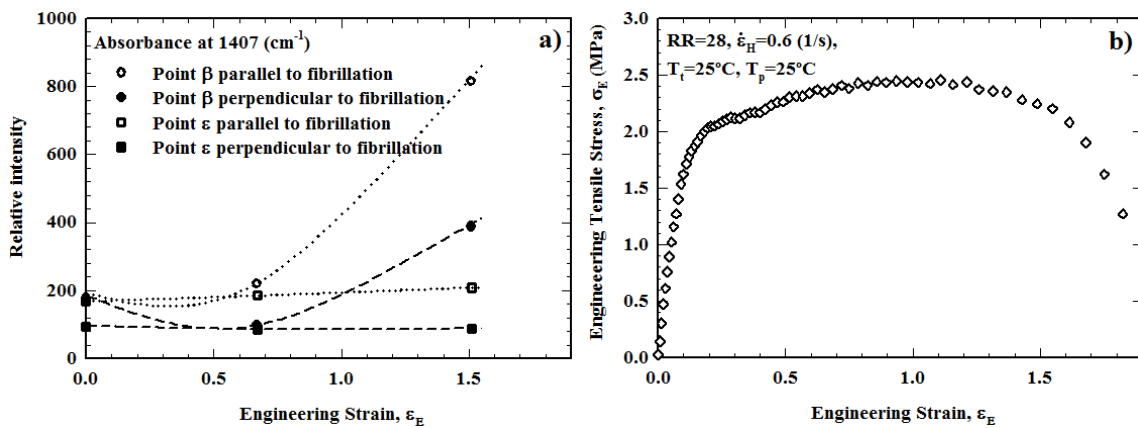


Figure 8.10: a) Raman relative intensity changes for two different levels of strains for the points (β) shown as circles and (ϵ) shown as squares on the 2-D extrudate. Hollow symbols show intensity changes when the laser beam is parallel to fibrillation, while closed symbols for perpendicular to fibrillation b) Typical stress-strain curve justifying the choice of the strains 0.7 and 1.5 correspondingly

8.5 SEM Imaging

Fig.8.11 shows the SEM micrograph at point " β " defined in Fig. 8.7. It should be reminded that X and Y are the transverse and extrusion directions, respectively. As it can be seen in this micrograph most of the fibrillation occurs perpendicular to the extrusion direction, while there are some weak fibrils parallel to the extrusion direction. This observation is in agreement with Raman results where the relative intensity ratio was much higher than 1 indicating the fibrils orientation preference in the transverse direction.

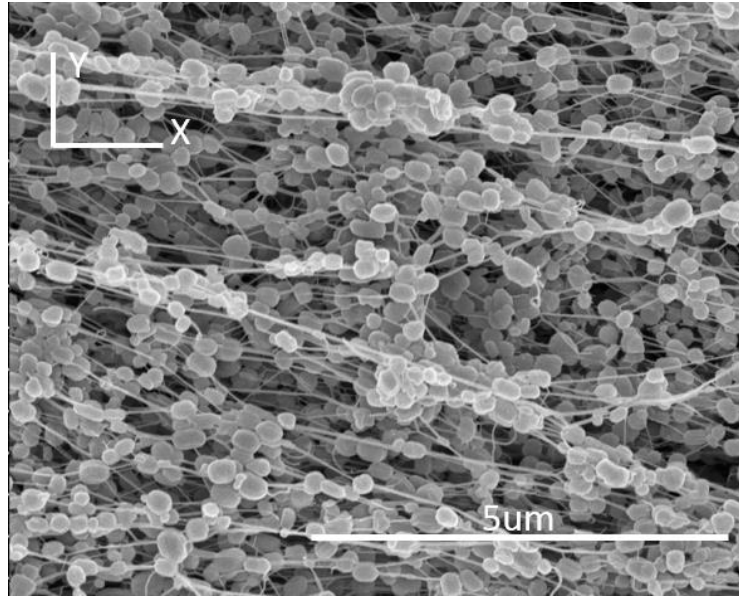


Figure 8.11: SEM micrograph for point beta (β) showing that most of the fibrillation occurs perpendicular to the extrusion direction

8.6 Densitometry

Previous studies have shown that due to the unique fibrillated structure of PTFE extrudates, stretching leads to formation of the voids within the material (US PATENT 3.953.566-Gore R.W. 1976; Kurumada, *et al.* 1998; Huang *et al.* 2008; Choi & Spruiell, 2010; Ranjbarzadeh –Dibazar, *et al.* 2014; Endo, *et al.* 1998), indicating its compressible nature (Caddock & Evans, 1989). In other words, the PTFE samples expand having a Poisson's ratio of nearly zero. Specifically it was reported that the Poisson's ratio is zero for the 1-D samples, possessing fibrils oriented in the extrusion direction (Vavlekas, *et al.* 2016). Therefore, upon stretching one can expect that the density of the PTFE extrudates, which is a function of the elongational strain, would decrease. We repeat the same study here for the 2-D fibrillated samples by considering that the Poisson's ratio is zero for the width of the sample and its thickness. Thus, we can use the following equation to monitor the density changes.

$$RD = \frac{RD_0}{(1 + \kappa \varepsilon_E)^{1 - \nu_{xy} - \nu_{xz}}} \quad (8.3)$$

where RD_0 is the initial relative density before uniaxial extension, ε_E , is the engineering strain, ν_{xy} , ν_{xz} are Poisson's ratio for the width and the thickness of the sample and κ is the recovery factor, respectively. The recovery coefficient κ in Eq. 8.3 was treated as a fitting parameter by noting the Poisson's ratio was zero once again. The physical significance of κ

is a measure of elasticity, related directly to the structure/morphology of fibrils. Moreover, it was reported that the strain recovery coefficient κ , was a function of the RR of the die and the processing temperature T_p . Previous studies (Vavlekas, *et al.* 2016; Ansari, *et al.* 2015) showed that higher RR corresponds to higher values of κ .

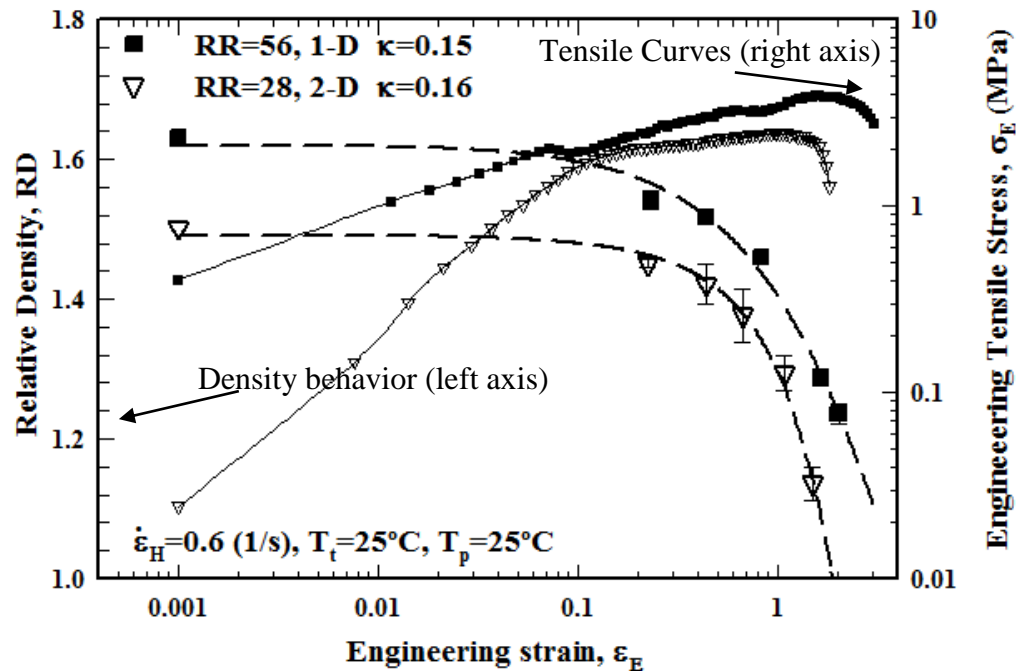


Figure 8.12: The relative density as a function of Hencky strain for extrudates collected at $T_p=25^\circ\text{C}$. The samples were extruded at identical RR dies and a) shows 1-D structure cylindrical sample, while b) shows 2-D structure sample. The fitting of Eq.8.3 is shown as dashed lines

Fig.8.12 shows the comparison of the results using Eq.8.3 for a) 1-D structure cylindrical samples and b) 2-D structure samples. Decreasing the RR value by half gives identical κ values for both sample structures. However, the extensibility of the material is reduced for the 2-D structure. The ultimate strength of the material appears at lower values of engineering strain. The ultimate elongation is a measure of the quality of the fibrils; this result shows fibril crosshatching influences how extensible an extrudate can be. Extrudates produced from a cylindrical die using identical RR dies appeared to be 25% more extensible compared to 2-D structure samples. Moreover, a decrease in the density values of the unstretched sample, appears to be another conclusion drawn out of this graph. The average value for 1-D structure unstretched samples for all the cases that we tested in our recent work (Vavlekas, *et al.* 2016)

was 1.6. However this value dropped for 2-D samples to 1.5, a drop which might be attributed to more voids created during 2-D formation extrudates within the die.

The same trend regarding the extensibility of the samples was observed when using the cylindrical die for producing 1-D samples. For this case the strain where the Ultimate strength appeared (Ultimate strain), was observed to decrease for increasing RR dies. Fig.8.13a) shows a typical result when comparing extrudates produced from three different RR dies (56, 156, 352). After performing numerous experiments on the production of the model equation presented in our recent publication (Vavlekas, *et al.* 2016), using different extrusion (T_p), testing temperatures (T_t), RR die and different Hencky strain rates, it turned out that the overall trend observed for 1-D structure samples regarding their extensibility as a function of the RR, can be described by Fig.8.13b). Normalizing the data according to RR56 where we had the highest values of extensibility for 1-D samples, we notice a drop of 38% in the extensibility of the extrudates from RR56 to RR156 and an additional 23% from RR156 to RR352.

8.7 Summary

A flat die was used for producing extrudates with fibrils oriented in two directions. The tensile mechanical properties of PTFE paste extrudates were studied using uniaxial extension at various Hencky strain rates and temperatures. Poisson's ratio of the material was determined based on these tests. First the transient tensile results were shown to be represented well by the theoretical Matsuoka model (1986) resulting parameters similar to 1-D and 2-D samples tested in the direction that fibrils orient (Vavlekas, *et al.* 2016). The fitted parameters were found to have a physical meaning related to the testing temperature of the extrudates, as well as the rate of stretching. The mechanical properties were found to depend on the testing temperature (Arrhenius dependence) with activation energy similar for both 1-D and 2-D fibrillated samples.

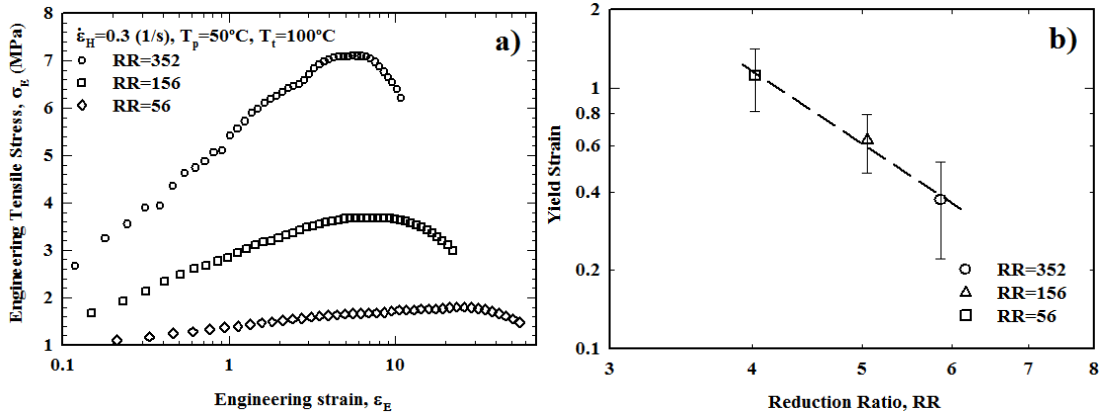


Figure 8.13: Results for cylindrical 1-D structure samples: a) Tensile results at $\dot{\epsilon}_H = 0.3 \text{ s}^{-1}$ and $T_t = 50 \text{ }^\circ\text{C}$ for PTFE samples extruded at $T_p = 100 \text{ }^\circ\text{C}$, through dies with different RR values and b) Overall trend of the ultimate strain versus RR

Raman spectroscopy was used to quantitatively describe the degree of fibril orientation in the extrudates by measuring the polarized Stokes-shifted light in the directions parallel and perpendicular to the extrusion direction. The quality of fibrils was described in terms of their degree of orientation and continuousness within the extrudate at 1407 cm^{-1} , which corresponds to C-C (backbone) stretching, by using the ratio of the Raman scattering intensities between the two polarization geometries.

Finally, as already observed previously (Vavlekas, *et al.* 2016; Ansari *et al.* 2015), due to their compressibility, the relative density of the PTFE extrudates was a decreasing function of Hencky strain. By considering that Poisson's ratio of 2-D structure samples is nearly zero, the density decrease during stretching was modelled using an Equation (Eq.8.3) that takes into account the Poisson's ratio. The strain recovery coefficient κ , appeared to have identical value as the one observed for 1-D structures, extruded from dies with double reduction ratio (RR). However, the ultimate strain of the 2-D fibrillated samples was decreased indicating the influence of 2-D fibril orientation on the extensibility of PTFE samples.

CHAPTER 9: Conclusions, Contributions To Knowledge And Recommendations For Future Work

9.1 Conclusions

This PhD Thesis investigated the role of fibrillation of 1-D and 2-D structured PTFE samples on the Poisson's ratio. The mechanical properties of different resins (homopolymer and copolymer) were initially studied in detail using various capillary dies having different characteristics. One of them (homopolymer) was studied in different extrusion modes (constant shear rate and constant extrusion pressure), testing conditions and strain rates to study the influence of these conditions on the ultimate strength of the produced extrudates. The Matsuoka mechanical property model was used to correlate the Poisson's ratio of the sample with the ultimate strength of the material. The main results from the experimental work can be summarized as follows:

1. Initially the extrusion of two types of PTFE pastes, a homopolymer and a copolymer were studied, using dies with different reduction ratios (RR) and entrance angles. In all cases the transient pressure drop has shown a maximum followed by a plateau (steady-state). The extrusion pressure shows a weak increase with shear rate over a wide range of flow rates and a more significant increase with reduction ratio. Moreover, the extrusion pressure exhibited a minimum for entrance angle around 30° . A previously developed extrusion model was used to model the results which were found compatible with predictions.
2. The extrudates collected at different processing conditions were dried and tested in uniaxial extension to assess their effect on mechanical properties. The tensile mechanical properties of PTFE paste extrudates were also studied. Four different properties were defined and studied, namely the tensile Young modulus, the yield stress, the ultimate tensile strength and the ultimate elongational strain. The tensile modulus, yield stress and ultimate tensile strength of the obtained extrudates were found to be increasing functions of reduction ratio, although the opposite effect was found for the ultimate elongational strain. It has been concluded that the extrudates become stiffer and less extensible by increasing the die reduction ratio. On the other hand, it was shown that the entrance angle has a small effect on the

extrudate stiffness although a maximum has been obtained at the contraction angle of 60° for the ultimate elongational strain. This is confirmed by previous studies where it was also reported that the increasing reduction ratio was found to increase the amount of fibrils formed (Ariawan, PhD thesis, 2001).

3. The tensile mechanical properties of PTFE paste cylindrical 1-D extrudates collected at different processing conditions (extrusion temperature and reduction ratio) were studied using the SER fixture at various Hencky strain rates and temperatures. First the transient tensile results were shown to be described by a theoretical model developed by Matsuoka (1986). The fitted parameter were found to have a physical meaning related to the temperature of the extrusion at which the tested samples were produced, the testing temperature as well as the rate of stretching. A steady-state phenomenological tensile stress model was developed to predict the ultimate strength as a function of these parameters. The model was tested successfully for another die with completely different geometrical characteristics. It was found that the ultimate strength increases with Hencky strain rate following a power-law behavior, while decreases with the tensile testing temperature. The extrusion temperature has also shown an increasing effect on the ultimate strength. Both these temperature effects can be described with Arrhenius equations whose activations energies were calculated. The tensile temperature activation energy was found to be constant and independent of the processing conditions, although the activation energy of processing temperature was an increasing function of the reduction ratio. The fibrillation microstructure appeared in SEM micrographs were used to substantiate these results.
4. A 2-D flat die was used for producing extrudates with fibrils oriented in two directions. The tensile mechanical properties of PTFE paste extrudates were studied using uniaxial extension at various Hencky strain rates and temperatures. Poisson's ratio of the material was determined based on these tests. First the transient tensile results were shown to be represented well by the theoretical Matsuoka model, resulting in parameters similar for 1-D and 2-D samples tested in the direction that fibrils orient. The fitted parameters were found to have a physical meaning related to the testing temperature of the extrudates, as well as the rate of stretching. The mechanical properties were found to depend on the testing

temperature (Arrhenius dependence) with activation energy similar for both 1-D and 2-D fibrillated samples.

5. To produce commercially acceptable extrudates, an acceptable amount of fibrils is required of reasonable quality (strength). The quality of the fibres can be described in terms of their degree of orientation and continuity within the extrudate. Raman spectroscopy was used to quantitatively describe the degree of fibril orientation in the extrudates by measuring the polarized Stokes-shifted light in the directions parallel and perpendicular to the extrusion direction. The quality of fibrils was described in terms of their degree of orientation and continuousness within the extrudate at 1407 cm^{-1} , which corresponds to C-C (backbone) stretching, by using the ratio of the Raman scattering intensities between the two polarization geometries.
6. Due to the compressible nature of PTFE, the relative density of the extrudates decreases in uniaxial extension. The PTFE paste cylindrical extrudates show a Poisson's ratio equal to zero in tensile experiments, thus exhibiting significant density reduction with stretching. Moreover, the effect of tensile strain on the specific gravity was modeled simply by taking into the account the Poisson's ratio and the strain recovery coefficient. The ultimate strain of the 2-D fibrillated samples was decreased indicating the influence of 2-D fibril orientation on the extensibility of PTFE samples.

9.1 Contributions To Knowledge

9.1.1 Ultimate Strength As A Function Of Processing And Testing Conditions

In this PhD a novel steady-state phenomenological tensile stress model was developed to predict the ultimate strength as a function of different processing and testing parameters. This model was tested successfully for another die with completely different geometrical characteristics than those used to develop the model. It was found that the ultimate strength increases with Hencky strain rate following a power-law behavior, while decreases with the tensile testing temperature. The extrusion temperature has also shown an increasing effect on the ultimate strength. Both these temperature effects can be described with Arrhenius equations. The tensile temperature activation energy was found to be constant and independent

of the processing conditions, although the activation energy of processing temperature was an increasing function of the reduction ratio.

9.1.2 *Ultimate Strength Correlated With Poisson's Ratio For 1-D And 2-D Samples*

The transient tensile results were presented to be described by a theoretical model developed by Matsuoka (1986) with resulting parameters similar to 1-D and 2-D samples tested in the direction that fibrils orient. The fitted parameters were found to have a physical meaning related to T_p , T_t , as well as the rate of stretching. The tensile mechanical properties of PTFE paste extrudates were studied using uniaxial extension at various Hencky strain rates and temperatures and the Poisson's ratio of the material was determined based on these tests. The mechanical properties were found to depend on the testing temperature (Arrhenius dependence) with activation energy similar for both 1-D and 2-D fibrillated samples.

9.1.3 *Relative Density Of A Compressible Material In Uniaxial Extension*

Finally, it was found that the relative density of the PTFE extrudates decreases in uniaxial extension due to its compressibility. The PTFE paste extrudates for this fibril orientation show a Poisson's ratio equal to zero in tensile experiments, thus exhibiting expansion (significant density reduction with stretching). It was also shown that the effect of tensile strain on the relative density can be modeled simply by taking into account the Poisson's ratio which was found to be zero for the specific fibrillation of this material and the strain recovery that is the portion of the imposed strain that is recovered upon removal of the imposed tensile stress. The strain recovery coefficient κ , for the 2-D samples appeared to have an identical value as the one observed for 1-D structures, extruded from dies with double reduction ratio (RR). This relative density prediction again is of great interest since PTFE has been used for years in the production of filter membranes. By controlling the strain imposed on the sample, the porosity of the sample can be controlled as well, leading to the manufacture of a product with desired porosity.

9.2 *Recommendations For Future Work*

Overall this work has contributed to the fundamental knowledge of the role of fibrillation on PTFE extrudates. Undeniably, more in depth studies have to be performed in the future to completely unravel the science behind the process. However, many of the results of this work can provide significant initial stages towards a better macroscopic and microscopic understanding of the process to have more predictable results of the Poisson's ratio of PTFE

according to its fibrillation, so that this prediction can be carried out with greater confidence. To complement the above studies on the effect of fibrils of PTFE on Poisson's ratio, the following suggestions can be considered for future work:

1. The effects of various operating variables on the quality of PTFE paste extrudates have been analyzed. The results provide an understanding of the role of the fibres in defining the final product properties. With such understanding it is possible to optimize the extrusion operating variables to produce extrudates that are commercially available with the critical objective to reduce the amount of the process rejects.
2. It would be of interest to check under which geometrical parameters of the flat die we can have an extrudate with the same fibrillation for both machine and longitudinal direction and compare with data that are available so far.
3. It would also be a good idea to see under which of the two modes of operation density and diameter of the extrudates vary to produce products of high consistency in terms of mechanical properties.
4. Moreover, modelling the extensional behaviour of PTFE through a strain energy function W , would also be of great interest. A strain energy function W can be found experimentally keeping in mind that PTFE behaves as a compressible material and therefore the product of the principal extension ratios will be a function of the volume ratio or density ratio. Ogden (1972) in the past determined an strain energy function which is a linear combination of strain invariants, discarding the requirement that W shall be an even powered function of the extensional ratios (proposed in the past by previous researchers), suggesting that:

$$W = \sum_i \frac{m_i}{n_i} (a_1^{n_i} + a_2^{n_i} + a_3^{n_i} - 3) \quad (9.1)$$

5. It would also be of interest to identify the rest of the parameters for the stress components, since some of them are already found (σ_{11} E_1 , E_2 , ν_{12} , ν_{13}).

$$\begin{bmatrix} \varepsilon_{11} \\ \varepsilon_{22} \\ \varepsilon_{33} \end{bmatrix} = \begin{bmatrix} \frac{1}{E_1} & \frac{-\nu_{12}}{E_2} & \frac{-\nu_{31}}{E_3} \\ \frac{-\nu_{21}}{E_1} & \frac{1}{E_2} & \frac{-\nu_{32}}{E_3} \\ \frac{-\nu_{13}}{E_1} & \frac{-\nu_{23}}{E_2} & \frac{1}{E_3} \end{bmatrix} \begin{bmatrix} \sigma_{11} \\ \sigma_{22} \\ \sigma_{33} \end{bmatrix} \quad (9.2)$$

Bibliography

- Alderson, A., Evans, K. E. Deformation mechanisms leading to auxetic behaviour in the α -cristobalite and α -quartz structures of both silica and Germania, *Journal of Physics: Condensed Matter*, (21), 2009.
- Ansari, M., Vavlekas, D., McCoy, J.L., Hatzikiriakos, S.G., Paste extrusion and Mechanical Properties of PTFE, *International Polymer Processing*, (5), 603, 2015.
- Ansari, M., Zisis, T., Hatzikiriakos, S.G., Mitsoulis, E. Capillary flow of low-density polyethylene. *Polymer Eng & Sci.* (52), 649, 2012.
- Ardakani, H. A. Mitsoulis, E. Hatzikiriakos, S.G., Rheology of Pastes: Effects of Fibrillation, Thixotropy and Structure PhD thesis, The University of British Columbia, Vancouver, 2014.
- Ardakani, H.A., Mitsoulis, E. and Hatzikiriakos, S.G. "A simple improved mathematical model for polytetrafluoroethylene (PTFE) paste extrusion," *Chem. Eng. Sci.* (89), 216, 2013a.
- Ardakani, H.A. Mitsoulis, E. and Hatzikiriakos, S.G. "Polytetrafluoroethylene paste extrusion: a fibrillation model and its relation to mechanical properties," *Intern. Polym. Proc.* (3), 306, 2013b.
- Ariawan, A.B., Paste extrusion of polytetrafluoroethylene fine powder resins, PhD thesis, The University of British Columbia, Vancouver, 2001.
- Ariawan, A.B. Ebnesajjad, S., Hatzikiriakos, S.G. Preforming Behavior of Polytetrafluoroethylene Paste, *Powder Technology*, (121), 249, 2001.
- Ariawan, A.B. Ebnesajjad, S., Hatzikiriakos, S.G. "Paste Extrusion of Polytetrafluoroethylene (PTFE) Fine Powder Resins," *Can. Chem. Eng. J.*, (80), 1153, 2002a.
- Ariawan, A.B., Ebnesajjad, S., Hatzikiriakos, S.G. Properties of PTFE paste extrudates, *Polymer Engineering Science*, (42), 1247, 2002b.
- Aho, J., Rolon-Garrido, V.H., Syrjala, S. Wagner, M.H. "Measurement technique and data analysis of extensional viscosity for polymer melts by Sentmanat extensional rheometer (SER)". *Rheol Acta*, (49), 359, 2010.
- Bagher, M., Reza, B. M. Polymer Optic Technology *Optics.* (4), 1, 2015.
- Baughman, R. H., Shacklette, J. M., Zakhidov, A. A., Stafstroem, S. Negative Poisson's ratios as a common feature of cubic metals, *Nature*, (392), 362, 1998.
- Benbow, J.J., J. Bridgwater, Paste Flow and Extrusion, Oxford University Press, Oxford, 1993.
- Blanchet, T.A., Polytetrafluoroethylene, in Handbook of Thermoplastics, (O.Olabisi. ed), 1st ed., Marcel Dekker, Inc. New York, 981-1000, 1997.

Bowick, M., Cacciuto, A., Thorleifsson, G., Travesset, A. The Universal Negative Poisson Ratio of Self-Avoiding Fixed-Connectivity Membranes, *Physical Review Letters*, (87), 148103, 2001.

Caddock, B. D., Evans, K. E. Microporous materials with negative Poisson's ratios. I: Microstructure and mechanical properties. *Journal of Physics*, (D. 22), 1877, 1989.

Caddock B.D. & Evans K.E., Negative Poisson ratios and strain dependent mechanical properties in arterial prostheses, *Biomaterials*, (16), 1109, 1195.

Carta, G., Brun, M., Baldi, A. Design of a porous material with isotropic negative Poisson's ratio, *Mechanics of materials*, (97), 67, 2016.

Chandler-Temple A.F., and Wentrup-Byrne, E., Grondahl, L. Expanded Polytetrafluoroethylene: from conception to biomedical device. *Chemistry in Australia*, (75), 3-6, 2008.

Choi K.J., Spruiell, J. Structure Development in Multistage Stretching of PTFE Films, *Journal of Polymer Science, Part B: Polymer Physics*, (48), 2248, 2010.

Christy, A., Tavassoli, N., Bain, A., Melo, L., Grant, E. R. Wide-Field Confocal Interferometric Backscattering (iSCAT)-Raman Microscopy. In *Optics in the Life Sciences; Optical Society of America*, p. NM4C.4, 2015.

Clark, E.S., Muus, L.T.Z., Krist, Partial disordering and crystal transitions in polytetrafluoroethylene, *Zeitschrift für Kristallographie*, (117), 119-127, 1962.

Clough N.E. (visited on 30/09/2014) Innovations in ePTFE fibre technology. New capabilities, new applications, New opportunities
https://www.gore.com/MungoBlobs/168/901/ePTFE_INNOVATIONS_PAPER.pdf

Coleman, C.J. The Effect of Extrusion on the Mechanical Properties of Polytetrafluoroethylene Paste, *Pol Eng & Sci*. (18), 260, 1978.

Cotrell, T.L. The strength of chemical Bonds, 2nd Ed., Butterworths, Washington D.C., 1958.

Cumming R.D., Philips P.A., Singh P.I. Surface Chemistry and Blood-Material Interactions, *Transactions-American Society for Artificial Internal Organs*, (29), 163, 1983.

Daikin Industries Ltd., Daikin PTFE fine powder, Technical Bulletin, 2003.

Daikin polyflon PTFE molding powder www.daikinchem.de/downloads/PTFE-M.pdf (visited on 01/05/2017).

Daikin SKMBT_C35311062311480.pdf visited on 30/04/2017.

Dealy, J.M., Wissbrun, K.F. Melt Rheology and Its Role in Plastics Processing Theory and Applications, Van Nostrand Reinhold, New York, 1990.

DermnetNZ (visited on 13/06/2014) <http://dermnetnz.org/procedures/polytetrafluoroethylene.html>

Delgadillo-Velazquez, O., Hatzikiriakos, S.G., Sentmanat, M.L. Thermorheological Properties of LLDPE/LDPE Blends, *Rheol Acta*, (47), 19, 2008.

Douglas, B.R., Design of Stent Expansion Mechanisms, MSc Thesis, University of British Columbia, 2012.

Dominghaus, H. Plastics for Engineers. Hanser Publishers Inc. 1993.

DuPont, Teflon PTFE Fluoropolymer resin, Properties Handbook (visited on 30/12/2014) www.rjchase.com/ptfe_handbook.pdf

Dupont Fluoroproducts , Teflon PTFE Fluoropolymer Resin-Processing Guide for Fine Powder Resins, Technical Bulletin, Wilmington, Delaware, 1994.

Ebnesajjad, S., Fluoroplastics, Non – Melt Processible Fluoroplastics, The Definitive User's Guide and Databank, William Andrew, 2000.

Ebnesajjad, S., Expanded PTFE applications Handbook, Technology Manufacturing and Applications, William Andrew, Oxford, 2017.

Endo, R., Jounai, K., Uehara, H. Kanamoto, T., Porter, R.S. Uniaxial Drawing of Polytetrafluoroethylene Virgin Powder by Extrusion Plus Cold Tensile Draw. *J of Polym Sci: Part B: Polym Phys*, (36), 2551, 1998.

Evans, K.E., Caddock, B.D. Microporous materials with negative Poissons ratio II, Mechanisms and Interpretation, *J. Physics D App. Physics*, (22), 1883-1889, 1989.

Evans, K.E. Tensile network microstructures exhibiting negative Poisson's ratios, *J. Physics D App. Physics* (22), 1870-1876, 1990.

Evans, K. E., Nkansah, M. A., Hutchinson, I. J., Rogers, S. C. Molecular network design, *Nature*, (353), 124, 1991.

Exxon Mobile Isopar H: Exxon%20Isopar%20H.pdf (visited on 25/10/2014)

Frick, D., Sich, G., Heinrich, C., Stern, M., Gossi, T.A., Relationship between Structure and Mechanical Properties of Melt Processable PTFE: Influence of Molecular Weight and Comonomer Content, *Macromol Mater Eng.* (298), 954, 2013.

Friis E.A., Lakes, R.S., Park, J.B. Negative Poisson's ratio polymeric and metallic foams, *Journal of Materials Science*, (23), 4406-4414, 1988.

- Gangal, S.V., Kroschwitz, J.I. ed. Encyclopedia of Chemical Technology. 4th ed. John Wiley and Sons, v. 11 p. 657-671, 1994.
- Gangal, S.V., Grot, W., Mark, H.F., Bikales, N.M., Overberger, C.G., Menges, G., Encyclopedia of Polymer Science and Engineering. 2nd ed. John Wiley and Sons. 1989.
- Gibson, L.J., Ashby, M.F., Cellular solids: Structure and Properties, 70-82, Pergamon, Oxford, 1988.
- Galloway, C. M., Le Ru, E. C., Etchegoin, P. G. An Iterative Algorithm for Background Removal in Spectroscopy by Wavelet Transforms. *Appl. Spectrosc.* (63), 1370, 2009.
- Geissler, E., Hecht, A.M., The Poisson Ratio in Polymer Gels, *Macromolecules*, (13), 1276, 1980.
- Greaves, G. N., Greer, A. L., Lakes, R. S., Rouxel, T. Poisson's ratio and modern materials. *Nature Materials* (10), 823, 2011.
- Guo, Y.H., Chen, J.Y., Gao, J.X., Zhang, H.P., Feng, X.X. A Study on the Nonuniform Deformation of PTFE Membrane During its Tenting Transverse Stretching, *J. of Appl. Polym. Sci.*, (116), 1124–1130, 2010.
- Grima, J. N., Gatt, R., Alderson, A., Evans, K. E. On the origin of auxetic behaviour in the silicate α -cristobalite, *Journal of Materials Chemistry*, (15), 4003, 2005.
- Grima, J. N., Attard, D. Molecular networks with a near zero Poisson's ratio, *Phys. Status Solidi B*, (248), 111, 2011.
- Haw, M.D. Jamming, Two-Fluid Behavior, and Self-Filtration in Concentrated Particulate Suspensions, *Phys. Rev. Lett.*, (92), 18506, 2004.
- Heydorn W.H., Col, M.C., Zajtchuk R., Miller J., Schuchmann G.F., Gore-Tex Grafts for Replacement of the Superior Vena Cava, *The Annals of Thoracic Surgery*, (6), 539, 1977.
- Horrobin, D.J., Nedderman, R.M. Die entry pressure drops in paste extrusion, *Chem. Eng. Sci.*, (53), 3215, 1998.
- Hooper, R., Macosko, C.W., Derby, R.J. Assessing a flow based-finite element model for the sintering of viscoelastic particles, *Chemical Engineering Science*, (55), 733, 2000.
- Huang J., Zhang J., Hao X., Guo Y., Study of a novel process for preparing and co-stretching PTFE membrane and its properties. *European Polymer Journal*, (40), 667, 2004.

Huang, L. T., Hsu, P. S., Kuo, C. Y., Chena, C. S., Lai, J. Y., Pore Size Control of PTFE Membranes by Stretch Operation with Asymmetric Heating System, *Desalination*, (233), 64, 2008.

Huang, R., Hsu, P.S., Kuo, C.Y., Chen, S.C., Lai, J.Y., Lee, L.J. Paste Extrusion Control and Its Influence on Pore Size Properties of PTFE Membranes. *Adv. in Polym Tech.* (26), 163, 2007.

Jin, T., Goo, N. S., Woo, S. C., Park, H. C, Finite Element Modeling of a Beetle Wing, *Journal of Bionic Engineering*, (6), 224, 2009.

Kitamura, T., Kurumada, K. I., Tanigaki, M., Ohshima, M. and Kanazawa, S. I., Formation Mechanism of Porous Structure in Polytetrafluoroethylene (PTFE) Porous Membrane through Mechanical Operations, *Polymer Engineering Science*, (39), 2256, 1999.

Koo, G.P., Andrews, R.D. Mechanical Behavior of Polytetrafluoroethylene Around the Room-Temperature First-Order Transition. *Pol Eng & Sci.* (9), 268, 1969.

Kurumada, K., Kitamura, T., Fukumoto, N., Oshima, M., Tanigaki, M., Kanazawa, S., Structure Generation in PTFE Porous Membranes induced by the Uniaxial and Biaxial Stretching Operations, *Journal of Membrane Science*, (149), 51, 1998.

Lakes R., A broader view of membranes, *Nature*, (414), 503, 2001.

Lakes, R. S. Foam structures with a negative Poisson's ratio, *Science*, (235), 1038, 1987.

Lalia, B. S., Kochkodan, V., Hashaikeh, R. and Hilal, N., A Review on Membrane Fabrication: Structure, Properties and Performance Relationship, *Desalination*, (326), 77, 2013.

Li, M., Zhang, W., Wang, C., Wang, H. Melt processability of polytetrafluoroethylene: Effect of melt treatment on tensile deformation mechanism. *J Appl Polym Sci.* (123), 1667, 2012.

Lira, C., Scarpa, F., Olszewska, M., Celuch, M. The Silicomb cellular structure: Mechanical and dielectric properties, *Phys. Status Solidi*, (B 246), 2055, 2009.

Liu, Q. (visited on 12/01/2016) Literature Review: Materials with Negative Poisson's Ratios and Potential Applications to Aerospace and Defence DSTO-GD-0472 www.dtic.mil/dtic/tr/fulltext/u2/a460791.pdf

Liu, G., Gao, C., Li, X., Guo, C., Chen, Y., Preparation and properties of porous polytetrafluoroethylene hollow fibre membrane through mechanical operations. *J Appl Polym Sci.* (132), 42696, 2015.

Matsuoka, S., Brostow, W., Corneliussen, R. eds., *Failure of Plastics*, Hanser, New York, 1986.

- Mazur, S., Paste Extrusion of Poly(tetrafluoroethylene) Fine Powders in Polymer Powder technology, 441-481, Narks, M., Rosenzweig, N., Ed. John Wiley & Sons, 1995.
- Mc Gee, R.L., Collier, J.R. Solid State Extrusion of Polytetrafluoroethylene Fibres, *Pol Eng & Sci.* (26), 239, 1986.
- Nelson, O. Density Dependence of the Dielectric Properties of Particulate Materials Stuart, Transactions of the ASAE, 1823, 1983.
- Ochoa, I., Hatzikiriakos, S.G. PTFE Paste Preforming: Viscosity and Surface Tension Effects, *Powder Technology*, (146), 73, 2004.
- Ochoa, I., Hatzikiriakos, S.G. Paste extrusion of polytetrafluoroethylene (PTFE): Surface tension and viscosity effects, *Powder Technology*, (153), 108, 2005.
- Ochoa, I., Hatzikiriakos, S.G. Soc Plast Eng Tech Papers. CD-ROM: 2003:49.
- Ochoa, I., Paste extrusion of polytetrafluoroethylene fine powder resins: The effects of processing aid physical properties, PhD thesis, The University of British Columbia, Vancouver, 2006.
- Ochoa, I., Hatzikiriakos, S.G., Mitsoulis, E. Paste Extrusion of Polytetrafluoroethylene (PTFE): Temperature, Blending and Processing Aid Effects, *Intern. Polym. Proc.* (21), 497-503, 2006.
- Ogden, R.W. Large deformation isotropic elasticity - on the correlation of theory and experiment for incompressible rubberlike solids, *Proc. R. Soc. London, Ser.* (326), 565, 1972.
- Olympio K.R., Gandhi, F. Zero- ν Cellular Honeycomb Flexible Skins for One-Dimensional Wing Morphing, in: 48th AIAA/ASME/ASCE/ AHS/ASC Structures, Structural Dynamics, and Materials Conference, Honolulu, Hawaii, 23–26 April, 2007.
- O'Leary, K., Geil, P.H. Polytetrafluoroethylene Fibril Structure, *J. Appl. Phys.* (38), 4169-4181, 1967.
- Patil, P.D., Feng, J.J., Hatzikiriakos, S.G. Constitutive modeling and flow simulation of polytetrafluoroethylene (PTFE) paste extrusion. *J Non-Newtonian Fluid Mech.* (139), 44, 2006.
- Quarti, C., Milani, A., Castiglioni, C. Ab Initio Calculation of the IR Spectrum of PTFE: Helical Symmetry and Defects, *J. of Phys. Chem.* (117), 706, 2013.
- Rae, P.J., Dattelbaum, D.M. The properties of poly(tetrafluoroethylene) (PTFE) in compression, *Polymer*, (45), 7615, 2004.

Ranjbarzadeh-Dibazar, A., Shokrollahi, P., Barzin, J., Rahimi, A., Lubricant facilitated thermo-mechanical stretching of PTFE and morphology of the resulting membranes, *Journal of Membrane Science*, (470), 458, 2014.

Reis, J.M.L. Pacheco, L.J. Mattos, H.S. da Costa, Influence of the temperature and strain rate on the tensile behavior of post-consumer recycled high-density polyethylene, *Polymer Testing*, (32), 1576, 2013.

Sanchez-Valle, C., Sinogeikin, S. V., Lethbridge, Z. A. D., Walton, R. I., Smith, C. W., Evans, K. E., Bass, Brillouin scattering study on the single-crystal elastic properties of natrolite and analcime zeolites, *Journal of Applied Physics*, (98), 053508, 2005.

Sheppard, W.A., Sharts, C.M. Organic Fluorine Chemistry, W.A.Benjamin, Inc., New York, 1969.

Sperati, C.A., Brandrup, J., Immergut, E.H., Polymer Handbook, 3rd edition, John Wiley and Sons. New York, 1989.

Snelling, G.R., Lontz, J.F. Mechanism of lubricant-extrusion of Teflon TFE-Tetrafluoroethylene resins, *J. Appl. Polym. Sci.*, (3), 257, 1960.

Sentmanat M., Wang, B. N., McKinley, G.H., Measuring the Transient Extensional Rheology of Polyethylene Melts Using the SER Universal Testing Platform, *Journal of Rheology*, 2005.

M.L. Sentmanat. US Patent. 6.578.413.

Sentmanat, M.L. Miniature Universal Testing Platform: from Extensional Melt Rheology to Solid-State Deformation Behavior. *Rheol Acta*, (43), 657, 2004.

Speerschneider, C.J., Li, C.H., A Correlation of Mechanical Properties and Microstructure of Polytetrafluoroethylene at Various Temperatures, *J of Appl Phys.* (34), 3004, 1963.

Snelling, G.R., Lontz, J.F. Mechanism of Lubricant-Extrusion of Teflon[®] TFE-Tetrafluoroethylene Resins, *J. Appl. Polym. Sci.* (3), 257, 1960.

Soman, P., Fozdar, D.Y., Lee, J.W., Varghese, A.P.S., Chen, S., A three-dimensional polymer scaffolding material exhibiting a zero Poisson's ratio. *Royal Society of Chemistry*, (8), 4946, 2012.

US Patents: 3.664.915-3.953.566-3.962.153

Vavlekas, D., Ansari, M., Hao, H., Fremy, F. McCoy, J. L. Hatzikiriakos, S. G. Zero Poisson's ratio PTFE in uniaxial extension, *Pol. Testing*, (55), 143, 2016.

Wang, Z., Zhou, Y., Mallick, P.K. Effects of Temperature and Strain Rate on the Tensile Behavior of Short Fibre Reinforced Polyamide-6, *Polymer Composites*, (23), 858, 2002.

Wang, H., Ding, S., Zhu, H., Wang, F., Gu, Y., Zhang, H. and Chen, J., Effect of Stretching Ratio and Heating Temperature on Structure and Performance of PTFE Hollow Fibre Membrane in VMD for RO Brine", *Purif. Technol.* (126), 82, 2014.

Wang, Y., Wang, S.Q. From elastic deformation to terminal flow of a monodisperse entangled melt in uniaxial extension. *J Rheol.* (52), 1290, 2008.

Wang, X., Lou, K., Zhang, X., Sun, Z., Cao, G., Xia, Z. Mechanical and Electrical Properties of Laminated Polytetrafluoroethylene Films. *IEEE Trans on Dielec & Elec Insul.* (18), 57, 2011.

Wlochowicz, R. Scigala. Effect of Molecular Weight on the Mechanical Properties of Polytetrafluoroethylene (PTFE). *Brit Polym J.* (21), 205, 1989.

Yu, A.B., Bridgwater, A.S., Burbidge, Saracevic, Z. Liquid maldistribution in particle paste extrusion, *Powder Technology*, (103), 103, 1999.